LARA HARRISON

Clinical Applicability of MRI Texture Analysis

ACADEMIC DISSERTATION
To be presented, with the permission of
the board of the School of Medicine of the University of Tampere,
for public discussion in the Main Auditorium of Building M,
Pirkanmaa Hospital District, Teiskontie 35,
Tampere, on September 23rd, 2011, at 12 o'clock.

UNIVERSITY OF TAMPERE

UNIVERSITY OF TAMPERE

ACADEMIC DISSERTATION
University of Tampere, School of Medicine
Tampere University Hospital, Department of Radiology
Pirkanmaa Hospital District, Medical Imaging Centre
Tampere University of Technology, Department of Biomedical Engineering
Finland

Supervised by
Professor Seppo Soimakallio
University of Tampere
Finland
Docent Prasun Dastidar
University of Tampere
Finland

Reviewed by
Professor Andrzej Materka
Technical University of Lodz
Poland
Professor Ritva Vanninen
University of Eastern Finland
Finland

Distribution
Bookshop TAJU
P.O. Box 617
33014 University of Tampere
Finland

Tel. +358 40 190 9800
Fax +358 3 3551 7685
taju@uta.fi
www.uta.fi/taju
http://granum.uta.fi

Cover design by
Mikko Reinikka

Acta Universitatis Tamperensis 1640
ISBN 978-951-44-8526-8 (print)
ISSN-L 1455-1616
ISSN 1455-1616

Acta Electronica Universitatis Tamperensis 1102
ISBN 978-951-44-8527-5 (pdf)
ISSN 1456-954X
http://acta.uta.fi

Tampereen Yliopistopaino Oy – Juvenes Print
Tampere 2011

To Ronja and Sorje

What is essential is invisible to the eye.

—The Little Prince, Antoine De Saint-Exupéry, 1943

ABSTRACT

The usage of computerised methods in radiological image interpretation is becoming more common. Texture analysis has shown promising results as an image analysis method for detecting non-visible and visible lesions, with a number of applications in magnetic resonance imaging (MRI). Although several recent studies have investigated this topic, there remains a need for further analyses incorporating different clinical materials and taking protocol planning for clinical analyses into account. The purpose of this thesis was to determine the clinical applicability of MRI texture analysis from different viewpoints.

This study is based on three patient materials and one collection of healthy athletes and their referents. A total of 220 participants in wider on-going study projects at Tampere University Hospital were included in this thesis. The materials include a study on non-Hodgkin lymphoma, representing soft tissue imaging with malignant disease treatment monitoring; and two studies on central nervous system diseases, mild traumatic brain injury and multiple sclerosis. A musculoskeletal imaging study investigated load-associated physiological changes in healthy participants' bones. Furthermore, manual Region of Interest (ROI) definition methods and the selection of MRI sequences for analyses of visible and non-visible lesions were evaluated.

In summary, this study showed that non-visible lesions and physiological changes as well as visible focal lesions of different aetiologies could be detected and characterised by texture analysis of routine clinical 1.5 T scans. The details of MRI sequence selection and ROI definition in this study may serve as guidelines for the development of clinical protocols. However, these studies are partly experimental and need to be validated with larger sample sizes.

TIIVISTELMÄ

Tietokoneavusteisten menetelmien käyttö lisääntyy radiologisessa diagnostiikassa. Tekstuurianalyysi on antanut lupaavia tuloksia magneettikuvien tarkastelussa. Sen avulla on voitu määrittää sekä pieniä hajanaisia että suurempia paikallisia muutoksia. Menetelmää tulisi tutkia edelleen, koska kliinisen menetelmän kehittämistä varten tarvitaan lisätietoa sen soveltuvuudesta erilaisille aineistoille sekä analyysimenetelmän eri vaiheiden optimoimisesta. Tämän väitöstutkimuksen tavoite oli selvittää magneettikuvauksen (MRI) tekstuurianalyysin kliinistä käytettävyyttä eri kannoilta.

Tutkimusaineisto koostui kolmesta potilasmateriaalista ja yhdestä terveiden urheilijoiden joukosta sekä heidän verrokeistaan. Aineisto kerättiin osina Tampereen yliopistollisessa sairaalassa toteutettuja laajempia tutkimusprojekteja, ja mukaan otettiin yhteensä 220 osallistujaa. Ensimmäisessä osatyössä tarkasteltiin pehmytkudoskuvantamista, non-Hodgkin-lymfooman hoitovasteen arviointia tekstuurianalyysilla. Kaksi seuraavaa osatyötä käsitteli keskushermoston kuvantamista: lieviä aivovammoja sekä MS-tautia. Viimeisessä osatyössä arvioitiin liikunnan vaikutusta urheilijoiden ja verrokkien reisiluun kaulan luurakenteeseen. Kudosten ja muutosten vertailuissa oli edustettuna sekä ympäröivästä kudoksesta visuaalisella tarkastelulla erottumattomia että selkeästi erottuvia rakenteita. Lisäksi tutkimuksessa selvitettiin mielenkiintoalueen käsityönä tehtävän rajaamisen ja MRI- kuvaussekvenssin valinnan vaikutusta analyysiin.

Yhteenvetona todetaan, että tekstuurimenetelmällä on mahdollista havaita ja karakterisoida tutkimukseen valikoidun aineiston edustamia etiologialtaan erilaisia muutoksia kliinisistä 1.5 Teslan magneettikuvista. Tutkimuksessa käsitellyt yksityiskohdat MRI-kuvasarjojen valinnasta sekä mielenkiintoalueiden piirtämisestä antavat pohjaa kliinisen protokollan kehittämiseen. Osa tutkimusaineistoista oli kokeellisia, ja niiden tulokset tulisi vahvistaa laajemmilla kliinisillä tutkimuksilla.

TABLE OF CONTENTS

LIST OF SYMBOLS AND ABBREVIATIONS

ACC	Average correlation coefficients
ADC	Apparent diffusion coefficient
ANN	Artificial neural network
AR, ARM	Autoregressive model
BMD	Bone mineral density
BV/TV	Bone volume fraction (bone volume/total volume)
CAD	Computer-aided diagnosis
CIS	Clinically isolated syndrome
CNS	Central nervous system
COST	European Cooperation in Science and Technology
CSF	Cerebrospinal fluid
CT	Computed tomography
DCE	Dynamic contrast enhanced
DICOM	Digital imaging and communications in medicine
DTI	Diffusion tensor imaging
DXA	Dual energy x-ray absorptiometry
FAT SAT	Fat saturation
FDG-PET	^{18}F-fluorodeoxyglucose positron emission tomography
FISP	Fast imaging with steady state precession
FLAIR	Fluid attenuation inversion recovery
FLASH	Fast low angle shot
FLT-PET	^{18}F-fluoro-thymidine positron emission tomography
FSE	Fast spin echo/Turbo spin echo (TSE)
FSPGR	Fast spoiled gradient recalled echo
GCS	Glasgow Coma Scale
GDM	Gradient density matrix
GE	General Electric
GLCM	Grey level co-occurrence matrix
GRE	Gradient echo
k-NN	k-Nearest neighbour classification
LDA	Linear discriminant analysis
MDF	Most discriminative features
MEDIC	T2* weighted spoiled gradient echo with multiple echoes
MEF	Most expressive features
MPGR	Multiplanar gradient-recalled acquisition in steady state

MPR	Magnetization prepared gradient echo/Multi-Planar Reconstruction
MRI	Magnetic resonance imaging
MRF	Markov random fields
MS	Multiple sclerosis
MTBI	Mild traumatic brain injury
NA	Number of averages
NAGM	Normal-appearing grey matter
NAWM	Normal-appearing white matter
NDA	Non-linear discriminant analysis
NHL	Non-Hodgkin lymphoma
NYHA	New York Heart Association classification
PCA	Principal component analysis
PET	Positron emission tomography
PET-CT	Positron emission tomography – computed tomography
PNN	Probabilistic neural network
POE	Classification error probability
PPMS	Primary progressive MS
PRMS	Progressive-relapsing MS
PST	Polar Stockwell Transform
QCT	Quantitative CT
rCBV	Relative cerebral blood volume
RDA	Raw data analysis
RECIST	Response evaluation criteria in solid tumors
RF	Radio frequency
ROI	Region of interest
RRMS	Relapsing-remitting MS
SE	Spin echo
SD	Standard deviation
SPGR	Spoiled gradient echo
SPMS	Secondary progressive MS
STIR	Short T1 inversion recovery
SVM	Support vector machine
T	Tesla
TA	Texture analysis
TAUH	Tampere University Hospital
Tb.N	Trabecular number
Tb.Th	Trabecular thickness
Tb.Sp	Trabecular separation
TE	Echo time

TI	Inversion time
TIRM	Inversion recovery turbo spin echo
TR	Time to repetition
TSE	Turbo spin echo/Fast spin echo
TUVA	Tumor response evaluation
T1	Longitudinal relaxation time
T2	Transverse relaxation time
T2*	Effective transverse relaxation time
WHO	World Health Organization
WM	White matter
1-NN	Nearest-neighbour classification
2D	Two-dimensional
3D	Three-dimensional

LIST OF ORIGINAL PUBLICATIONS

This thesis is based on the following original articles, referred to in the text by their Roman numerals (I–IV):

I Harrison LC, Luukkaala T, Pertovaara H, Saarinen TO, Heinonen TT, Järvenpää R, Soimakallio S, Kellokumpu-Lehtinen PL, Eskola HJ, Dastidar P. *Non-Hodgkin Lymphoma response evaluation with MRI Texture Classification.* Journal of Experimental and Clinical Cancer Research. 2009 Jun 22;28:87.

II Holli KK, Harrison L, Dastidar P, Wäljas M, Liimatainen S, Luukkaala T, Öhman J, Soimakallio S, Eskola H. *Texture analysis of MR images of patients with mild traumatic brain injury.* BMC Medical Imaging. 2010 May 12;10:8.

III Harrison LC, Raunio M, Holli KK, Luukkaala T, Savio S, Elovaara I, Soimakallio S, Eskola HJ, Dastidar P. *MRI texture analysis in multiple sclerosis: toward a clinical analysis protocol.* Academic Radiology 2010; 17:696-707.

IV Harrison LCV, Nikander R, Sikiö M, Luukkaala T, Helminen M, Ryymin P, Soimakallio S, Eskola HJ, Dastidar P, Sievänen H. *MRI Texture Analysis of Femoral Neck: Detection of Exercise Load-Associated Differences in Trabecular Bone*. Accepted for publication in Journal of Magnetic Resonance Imaging on 8. Feb.2011.

1. INTRODUCTION

A number of computer aided visualisation methods, in addition to qualitative and quantitative analysis techniques, are available in clinical radiology. These methods provide clinicians with a comprehensive view of the imaged object from the macroscopic to the microscopic or even to the molecular level of the imaged object. This thesis focuses on non-ionising imaging method magnetic resonance imaging (MRI) as a promising imaging modality for quantitative texture analysis.

Research groups led by F. Bloch and E.M. Purcell in the 1940s discovered methods for measuring nuclear magnetic resonance in organic materials, leading to their receipt of the Nobel Prize in Physics in 1952 (Purcell, 1952; Bloch, 1952). Five decades later, the 2003 Nobel Prize in Physiology or Medicine was awarded to P. Lauterbur and P. Mansfield for their discoveries concerning "magnetic resonance imaging" (Mansfield, 2003; Lauterbur, 2003). Apart from these eminent scientists' discoveries, other fundamental inventions in the fields of medicine, physics, electronics, signal processing and image analysis find their uses in MRI devices and applications.

MRI analysis methods constitutes a wide field of interest from visualisation in two (2D) and three dimensions (3D); volumetric, shape and texture analyses of specific tissues and abnormalities; and functional measures of cell activity, blood perfusion and oxygen concentration. Different segmentation methods and 3D visualisation of magnetic resonance images have provided not only advanced diagnostic tools for radiologists but offer clinicians new insights and powerful tools for treatment planning in operative specialities and in oncology. Specific imaging sequences highlighting the diffusion properties of water have opened unforeseen levels of detail, especially in brain imaging. Now, when viewing the imaged object at the level of individual pixels, the smallest elements in a digital image; the grey level values of the pixels may be investigated with histogram analyses and more advanced methods, and the relationships between the grey levels of pixels are used to describe the texture of the tissues. Texture analysis (TA) based on MRI is an emerging field of research, with applications in a wide variety of radiological topics, including the detection of lesions and characterisation of and differentiation between pathological and healthy tissues in different organs (Castellano et al., 2004; Kassner and Thornhill, 2010).

The most significant objective in quantitative image analysis is to find tissue-specific features that have biological significance and are correlated with pathophysiologies that may be detected by other methods, i.e., clinical examination, other imaging modalities or histopathological diagnosis, and secondly to provide this new tissue property information to be used alone or in combination with other clinical information to allow more reliable detection and characterisation of disease.

The present thesis aims to increase our knowledge of magnetic resonance imaging-based texture analysis for clinical use. Texture analysis based mostly on statistical parameters was applied to a selection of clinical materials as a step towards the development of a tissue classification method as a clinical diagnostic and follow-up tool.

2. BACKGROUND AND LITERATURE REVIEW

2.1 Introduction to texture analysis

Texture is an important pattern property of the two-dimensional pictorial and three-dimensional volumetric descriptions of an object. Texture is present everywhere, both in nature and in man-made objects. Textures may be detected qualitatively by the different senses; one may feel the texture of different surfaces (for example, textiles or tree bark). Visually, one may detect the same texture with new features. There is no precise definition of texture in the literature. It may be described by many adjectives: fine, coarse, smooth, irregular, or lineated, to mention only a few (Haralick et al., 1973). The ability of human vision to detect and discriminate between complex textures is limited (Julesz et al., 1973). Image1 presents several examples of textures. Quantitatively, texture may be defined and analysed according to numerous parameters through different methods of calculation (Tuceryan and Jain, 1998). These methods are able to detect textural differences below the limits of human visual perception.

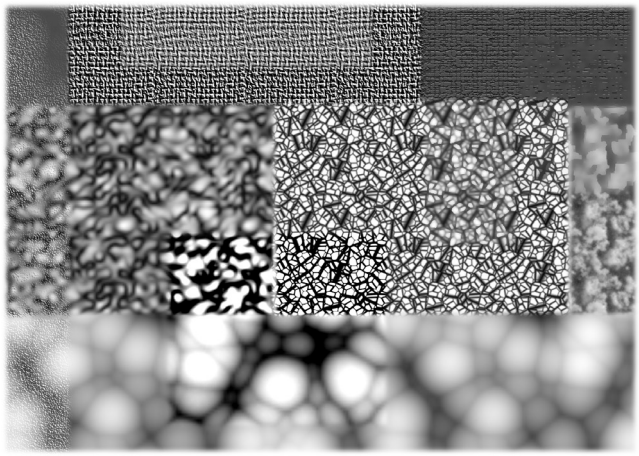

FIGURE 1. *Examples of textures.*

Texture has long been used as a parameter for the qualitative and quantitative classification and analysis of materials in industry and medicine. Kaizer used autocorrelation function-based TA for aerial photographs in the 1950s (Kaizer, 1955). Haralick tested texture features based on grey tone spatial dependencies on three different scale images: photomicrographs, aerial photographs and multispectral scanner satellite image, with good classification results (Haralick et al., 1973). These two approaches to texture were among the first examples of statistical TA. Statistical TA is also important for machine vision, which is used in different industries for automated inspection to classify objects, detect defects and control quality. An overview of texture analysis methods is presented in the next Chapter, and the methods used in this study are reviewed in more detail in Chapter 2.3.

Medical applications of texture analysis provide a quantitative means of identifying anatomical and pathological structures. In 1974, Chien and Fu published their application of co-occurrence matrix for automated chest X-ray analysis (Chien and Fu, 1974). In radiology, applications based on radiograph, ultrasound, computed tomography and magnetic resonance image data have proven able to provide advanced non-visible information about tissues of interest. A detailed review of recent publications on MRI TA with study settings possible to repeat in clinical imaging, is presented in Chapter 2.4.

2.2 Texture analysis methods

The wide variety of texture methods proposed in the literature can be divided into four major categories, referred to by Tuceryan and Jain as statistical, geometrical, model-based and signal-processing methods (Tuceryan and Jain, 1998). In reviews of medical TA, Materka and Castellano term the geometrical methods group structural, and the signal-processing methods transform methods (Castellano et al., 2004; Materka and Strzelecki, 1998). Both of these nomenclatures are commonly used, and the contents of the groups are analogous.

Statistical methods comprise the oldest approach in texture analysis. They describe texture by computing the local features of spatial grey level distribution and relationships between pixels. These features can be classified into first-order and second-order statistics. First-order statistics describe image properties that depend solely on individual pixel values, whereas second-order statistics describe the properties of pixel pairs (Tuceryan and Jain, 1998). Statistical methods include features derived from the histogram, gradient, autocorrelation function, run-length matrix and co-occurrence matrix. The run-length matrix approach and the co-occurrence matrix approach were introduced in the 1970s by Galloway and Haralick, respectively (Galloway, 1975; Haralick et al., 1973; Haralick, 1979).

Model-based TA involves fractal features (Mandelbrot, 1977; Pentland, 1984), Markov random fields (MRF) (Jain, 1989) and autoregressive (AR) models (Haralick, 1979; Jain, 1989). A fractal is a geometric shape or object that is made up of smaller copies of itself. Mandelbrot's fractal geometry provides a mathematical model for many complex forms found in nature. Fractals are generally self-similar and independent of scale. In MRF models the pixel intensity value depends on the neighbouring pixel intensities. Autoregressive models assume that pixel intensity is the weighted sum of neighbouring pixel intensities.

Geometrical or structural TA techniques define texture with local primitive elements, such as lines or shapes, which are replicated at other locations in the image (Goutsias et al., 2000; Allen and Mills, 2004). These techniques are not used as widely as other texture analysis methods, but they provide a good symbolic description of the image and are more useful for texture synthesis.

Signal-processing methods describe the textural properties of the object as parameters derived from transformations used in signal processing, e.g., Fourier, Gabor, Wavelet and Stockwell transforms (Tuceryan and Jain, 1998; Allen and Mills, 2004; Qian and Chen, 1993; Russ, 2002; Stockwell et al., 1996).

The textural properties of objects vary greatly, and the best discriminating textural features vary even within the same material. Among the wide range of texture parameters that may be calculated, researchers must define and select the features that provide the best discrimination properties for their data of interest. Limiting the feature set is an important step towards reducing the processing time and optimising classification. Several texture analysis methods may be used in combination to obtain better classification results. Different classification methods have been used to attain accurate classification.

2.3 Texture analysis software (MaZda package)

The texture analysis application used in this thesis is introduced here, along with a more detailed discussion about the nature of the parameters calculated. The parameters introduced in this section are also commonly used in many of the studies referred to in the literature review; however, the parameter calculation is performed by different applications in some of those studies.

Recently, two European cooperation projects on coordinating and developing quantitative MRI were established. These projects were coordinated by the European Cooperation in Science and Technology (COST), which is one of the longest-running instruments supporting cooperation among scientists and researchers across Europe. COST action B11, namely the Quantitation of Magnetic Resonance Image Texture project (1998-2002), focused on recent

developments in quantitative MRI, in particular texture analysis, to maximise the amount of clinical diagnostic information that could be extracted from this technique (Materka and Strzelecki, 1998; COST B11, 2001). The MaZda MRI texture analysis software package was developed at The Institute of Electronics in the Technical University of Lodz, Poland, in cooperation with the B11 project. MaZda and an integrated B11 software package became the official tool for MR-image analysis within the framework of the project (Materka et al., 2006; Szczypiński et al., 2009). Similar work continued in 2003-2008 with COST action B21, Physiological Modelling of MR Image Formation (COST B21, 2008), and a book on the topic of TA was published in 2006 (Hájek et al., 2006).

MaZda and integrated B11 software is run under *Microsoft Windows 9x/NT/2k/XP* operating systems. MaZda (3.20) calculates almost 300 texture parameters, divided into histogram, gradient, run-length matrix, co-occurrence matrix, autoregressive model and wavelet-derived parameter feature sets. Regions of interest (ROI) are set manually or semi-automatically by drawing on a layer on the image. (Materka et al. 2006; MaZda)

The texture features calculated by MaZda (3.20) (Table 1) and some other functions of the software package are presented in the following sections of this chapter. Mathematical notations for the TA parameters are presented in Appendix.

TABLE 1. *Texture features calculated by MaZda (3.20)*

Histogram
Mean, variance, skewness, kurtosis, percentiles 1-%, 10-%, 50-%, 90-% and 99-%
Absolute gradient
Mean, variance, skewness, kurtosis, percentage of pixels with a nonzero gradient
Run-length matrix
Run-length nonuniformity, grey level nonuniformity, long run emphasis, short run emphasis, fraction of image in runs
Co-occurrence matrix
Angular second moment, contrast, correlation, sum of squares, inverse difference moment, sum average, sum variance, sum entropy, entropy, difference variance, difference entropy
Autoregressive (AR) model
Theta (θ): model parameter vector, 4 parameters;
Sigma (σ): standard deviation of the driving noise
Wavelet
Energy of wavelet coefficients in sub-bands at successive scales;
Maximum 4 scales each with 4 parameters

2.3.1 Histogram-based parameters

The number of distinct grey tones that can be represented by a digital image depends on the number of bits per pixel. For example, if information in a single pixel is represented by 8 bits, then 256 grey tones are available, while 16 bits per pixel can encode 65,536 tones.

Grey level intensity histogram is a function that counts the number of observed pixels with specific grey level tones. It counts the frequencies of discrete intervals; in this application, the number of intervals equals the number of possible grey level tones in the image. Histograms can be easily calculated from images, and the results are plotted on a graph. Several statistical properties of the image can be calculated from the histogram; in MaZda (3.20), the following histogram parameters can be calculated. Mean is the average intensity level of the image. Variance describes how far values lie from the mean, i.e., the roughness of the image. Skewness describes the histogram symmetry about the mean, i.e., whether there is a wider range of darker or lighter pixels than average; positive skewness indicates that there are more pixels below the mean than above, and a negative skewness indicates the opposite. Kurtosis describes the relative flatness of the histogram, i.e., how uniform the grey level distribution is compared to a normal distribution; negative kurtosis describes a flat distribution, and positive kurtosis describes a peaked distribution. Percentiles give the highest grey level value under which a given percentage of the pixels are contained. These parameters are first-order statistical parameters because their calculation is based on single pixel values, not relationships between pixel pairs. (Materka et al., 2006; Lahtinen, 2009)

2.3.2 Gradient-based parameters

A gradient is a directional change in grey level intensity in an image. High gradient values represent dramatic changes in grey level between light and dark tones; low gradient values are produced when the change in tone is smooth. The measure of mean grey level variation across the image is represented by the mean absolute gradient. Gradient variance describes the how far the values are from the mean. Gradient skewness and kurtosis are functions of gradient asymmetry. (Materka et al., 2006; Lahtinen, 2009)

2.3.3 Run-length matrix-based parameters

The run-length matrix contains information about the number of runs with pixels of defined grey levels and run lengths in an image. These matrices can be calculated for different run angles. In this application, the orientations of horizontal, vertical and two diagonals are calculated. Long and short run emphasis parameters give measures of proportions of runs with long and short lengths. Short run emphasis is expected to be larger in coarser images, and long run emphasis is larger in smoother images. Grey level nonuniformity calculates how uniformly runs are distributed among the grey levels; it takes small values when the distribution of runs is uniform. Similarly, run length nonuniformity measures the distribution of grey levels among the run lengths. The fraction of image in runs describes the fraction of image pixels that are part of any run available in the defined matrix. (Materka et al., 2006; Lahtinen, 2009)

2.3.4 Co-occurrence matrix-based parameters

The grey level co-occurrence matrix (GLCM), also called the grey tone spatial dependency matrix, describes how often different combinations of pixel grey level values occur in an ROI or image. The relationships of pixel pairs, i.e., with different angles and separation between the reference and neighbour pixels, are calculated in separate matrices. Several parameters are calculated from these matrices. The angular second moment, also known as energy, is a measure of the homogeneity of the image, and homogenous images give high values. Contrast is a measure of the local variation present in the image. Correlation measures the linear dependencies of the grey level in the image. The sum of squares defines the variance in the co-occurrence matrix. The inverse difference moment measures image homogeneity such that a smooth image gives a high value. The sum average gives the average of sums of two pixel values in the original image of interest. The sum variance is calculated based on the sum average. Entropy measures the disorder of the image. The highest value for entropy is reached when all probabilities are equal. The sum entropy is calculated in a similar way as the other sum parameters. Difference variance and difference entropy are based on differences calculated between two pixel values. (Materka et al., 2006; Lahtinen, 2009)

2.3.5 Autoregressive model-based parameters

Autoregressive models assume a local interaction between image pixels and describe each pixel grey level value as a weighted sum of the values of the neighbouring

pixels. For coarse textures, the coefficients of neighbouring pixels will be similar each other, while for fine textures, the coefficients vary more widely. In MaZda, five parameters are given for each ROI: the coefficients for the four neighbouring pixels (Theta, θ), and the standard error of noise (Sigma, σ). (Materka et al. 2006; Lahtinen, 2009)

2.3.6 Wavelet-based parameters

Wavelet analysis presents the image as a set of independent spatially-oriented frequency channels. In wavelet transformations the image signal is put through a low-pass and high-pass filter cascade, where the signal is down-sampled and decomposed simultaneously to increase the frequency resolution. The outputs give detail and approximation coefficients for the original signal. In MaZda, the energy of Haar wavelet sub-bands are calculated. (Materka et al., 2006)

2.3.7 Grey level intensity normalisation

MaZda (3.20) provides three methods for image grey level intensity normalisation: analysis of the original image without normalisation; analysis for an image grey scale range between 1% and 99% of the cumulated image histogram; and analysis for image intensities in the range $[\mu-3\sigma, \mu+3\sigma]$, where μ is the mean grey level value and σ is the standard deviation. (Materka et al., 2006)

2.3.8 Feature selection methods

MaZda (3.20) provides two automated methods for the selection of up to ten texture features that show the best discrimination between texture categories or ROIs. The Fisher coefficient (Fisher) method uses a ratio of between-class variance to within-class variance. The other method uses classification error probability (POE) combined with average correlation coefficients (ACC). Alternatively, the user may manually select up to 30 features for further analysis and classification in the B11 application. (Materka et al., 2006)

2.3.9 Analysis and classification

The B11 application integrated in MaZda is used for data analysis and classification. B11 investigates how well input-data texture features can distinguish texture

categories by principal component analysis (PCA), linear discriminant analysis (LDA) and nonlinear discriminant analysis (NDA). Classification tests on input data may also be performed with nearest neighbour (k-NN) and artificial neural network n-class (ANN n-class) classifiers. Details of these analyses are given in Szczypiński et al. (2009) and Materka et al. (2006).

2.4 Literature review on MRI texture analysis

In radiology, there are several types of diagnostic and other clinical questions to be answered about the images. For example: are focal or diffuse lesions and abnormalities detected? What are the probable differential diagnostic aetiologies of the findings? Have previously detected lesions recovered or worsened over time and/or due to treatment procedures performed? Recent studies on MRI texture analysis on the fields of soft tissue imaging, neuroradiology and skeletal imaging as well as some technical considerations and phantom studies are discussed below.

2.4.1 Soft tissue tumour and abdominal imaging

MRI is commonly used as a diagnostic imaging modality in soft tissue tumours. In addition to conventional expertise-driven visual analysis of images in the clinical environment, several studies on efficiency in TA have been applied for the diagnosis of abdominal organ diseases and soft tissue lesions with promising results.

Signal intensity and homogeneity characteristics have been evaluated to find differences in benign and malignant soft tissue masses (Mayerhoefer et al., 2008). The image data consisted of 1.0 T T1-weighted, T2-weighted and short T1 inversion recovery (STIR) series with variations in the acquisition parameters. Texture analysis was run with MaZda (3.20), Fisher and POE+ACC methods were used for feature selection and k-NN and ANN were used for classification. There was no clear difference in the performance of parameters selected by Fisher compared to POE+ACC. The ANN classifier performed better to separate benign and malignant lesions. Differences detected between groups were small, and in general, the data based on STIR images led to the most successful classification.

Several machine learning systems have been tested in a study of diverse group of histologically confirmed soft-tissue tumours in an attempt to automatically discriminate between malignant and benign tumours (Juntu et al., 2010). T1-images were included in the analysis and fixed size ROIs were used to define tumour area for texture parameter calculation in MaZda (3.20). Eight feature selection

methods were tested to select optimal features for classification. These methods belong to three feature selection families: 1) subset feature selection methods (forward search, backward search, bidirectional search, and greedy stepwise method), 2) feature ranking methods (chi-squares statistics and information gain methods) and 3) embedded methods in which feature selection is combined with a classifier [C4.5 decision trees and Vapnik's support vector machine (SVM)]. The forward search method was found to identify the best discriminating feature subset. Vapnik's nonlinear SVM classifier performed the classification task better than a neural network or Quinlan's C4.5 decision tree classifier. The SVM had better classification accuracy [93%; (91% specificity; 94% sensitivity)] than the radiologists [classification accuracy of 90% (92% specificity; 81% sensitivity)]. The overall results of this study were highly promising, particularly taking into account the diverse aetiologies of the tumours and some variations in MR acquisition.

Healthy and cirrhotic livers were investigated in a study of 1.5 T T2-weighted images (Jirák et al., 2002). MaZda was used to calculate textural features. The Fisher method, POE, and multidimensional discrimination measure in addition to manual parameter selection were used to describe the feature sets for the classification procedure. K-NN and ANN were successfully used to classify healthy and diseased livers, but these methods were unable to distinguish between three sub-groups of liver cirrhosis, which are clinically characterised by different Child-Pugh scores.

In a similar study, a computer-aided diagnosis (CAD) system including ANN based on texture analysis was implemented to diagnose hepatic fibrosis based on MRI images (Kato et al., 2007). A series of respiratory-triggered T2-weighted fast spin echo (FSE) and T1-weighted spoiled gradient echo (GRE) with contrast enhancement were obtained with a 1.5 T scanner. Histogram features (mean grey scale value and SD) and co-occurrence matrix features (contrast, angular second moment, entropy, mean, and inverse difference moment) were used as input for ANN. The analysis method reflected the degree of hepatic fibrosis, and contrast enhanced images at the equilibrium phase gave the best performance.

Focal liver lesion classification was performed in a recent study by Mayerhoefer and colleagues (2010) on 3.0 T standard clinical acquisition protocols of T1- and T2-weighted images without contrast enhancement. The apparent spatial resolution of the images was increased by zero-fill interpolation. MaZda (4.60) was used for texture parameter calculation. Fisher, POE+ACC and mutual information methods were used to select texture feature subsets for further classification by LDA in combination of k-NN and k-means clustering. Classification was feasible for two types of focal liver lesions, cysts and haemangioma. Co-occurrence matrix features were selected more frequently by automated feature selection methods

than parameters originating from other categories. The T2-weighted image data produced slightly better overall classification results than the T1-weighted data. The LDA/k-NN classifier approach was superior to the k-means classifier.

In breast imaging, dynamic contrast-enhanced (DCE) MRI has emerged as an alternative method for diagnosing breast cancer. In clinical radiology, tumour diagnostics is based on morphology and enhancement kinetics, but researchers have shown interest in texture-based quantitative methods as well. These methods have been able to discriminate breast tissue and lesion types with promising results (Gibbs and Turnbull, 2003; Holli et al., 2010; Nie et al., 2008).

2.4.2 Neuroradiology

Texture analysis has been viewed as a potential method for the quantitative evaluation of diseases in neuroimaging, and Kassner and Thornhill recently published an excellent review article on its applications (Kassner and Thornhill, 2010).

TA as a qualitative means of representing fine changes in tissues was reportedly successful in epilepsy related studies. Hippocampal abnormalities were detected by texture features calculated by MaZda from temporal lobe epilepsy or hippocampal sclerosis patients compared to healthy referents (Yu et al., 2001; Bonilha et al., 2003).

Focal cortical dysplasia has also been identified in patients with the disease compared to normal controls by evaluating grey matter thickening by relative signal intensity, run-length coding and the transition between grey and white matter by absolute gradient in a study of 1.5 T T1-weighted GRE images (Bernasconi et al., 2001). The previous study setting was extended with co-occurrence matrix-derived parameters (Antel et al., 2003), which showed that angular second moment, contrast and difference entropy values exhibited statistically significant differences between patients and healthy controls.

Sankar et al. evaluated structural changes in the temporopolar cortex and its white matter in patients with temporal lobe epilepsy. These analyses were based on volumetric and texture (entropy and gradient) means in 1.5 T T1-weighted GRE images (Sankar et al., 2008). Cortical and white matter atrophy, as well as decreased texture values, were detected in temporopolar locations ipsilateral to the seizure focus.

Hippocampus volume, signal intensity and wavelet texture appearance were investigated in a recent study (Jafari-Khouzani et al., 2010) of 1.5 T fluid attenuation inversion recovery (FLAIR) images from patients with lateralising mesial temporal lobe epilepsy. Mean and standard deviation signal intensities

successfully lateralised the site of epileptogenicity with an accuracy of 98%. Wavelet texture features were successful in 94% of cases, and hippocampal volumetry was successful in 83% of cases.

The manifestation of multiple sclerosis (MS) in MRI images has been investigated in several studies. Spinal cord images of four clinical subgroups of MS and healthy referents were obtained with a 1.5 T volumetric inversion-prepared fast spoiled gradient echo (FSPGR) sequence (Mathias et al., 1999). Texture analysis was applied with first order statistical and co-occurrence matrix-based features. There were statistically significant differences in texture between controls and patients, whereas disease subgroups were not distinguishable at a statistically significant level.

Another recent study investigated the discrimination of MS from cerebral microangiopathy lesions based on 1.5 T FLAIR images with pattern recognition methods based on four classifiers (minimum distance, LDA, logistic regression and probabilistic neural network (PNN)) using histogram, co-occurrence matrix and run-length matrix-based features (Theocharakis et al., 2009). All texture features other than skewness and grey-level nonuniformity exhibited statistically significant differences between groups. The PNN classifier outperformed other classifiers with an overall accuracy of 88.46%.

A comparison of different texture feature sets' abilities to classify MS lesions vs. normal-appearing white matter (NAWM), MS lesions vs. white matter (WM) and NAWM vs. WM from 1.5 T T2-weighted turbo spin echo (TSE) images was performed with MaZda 3.20 (Zhang et al., 2008). Two feature sets were used; one that consisted of co-occurrence matrix-based features only, and another made up of features that emerged from different parameter categories calculated by MaZda. Classification by 1-NN and ANN was successful for MS vs. NAWM and MS vs. WM with both feature sets. However, the combined set of features showed higher discrimination power as evaluated by the Fisher coefficient. The classification was unsuccessful for tissue pair WM-NAWM.

In a recent longitudinal study (Zhang et al., 2009), texture analysis based on the polar Stockwell Transform (PST) was performed on new acute MS lesions. The lesions included in the study showed new gadolinium-enhancement on 1.5 T T1-weighted spin-echo (SE) post-contrast sequences of patients imaged every two months. The TA was based on T2-weighted FSE images acquired 2 months before new lesion detection, images at the time of detection and 2, 4, 6 and 8 months after detection. PST texture changes appeared to be independent from the changes in signal intensity and volume. PST was able to identify abnormalities in pre-lesional NAWM and to measure tissue injury in acute lesions as well during lesion recovery.

Herlidou-Même et al. (2003) investigated the robustness of texture analysis based on histogram, co-occurrence, gradient and run-length matrix parameters in a multicentre study. These authors used scans of test objects, patients with intracranial tumours and healthy referents. Images were acquired in three sites with 1.5 T scanners using centre-specific routine acquisition parameters for T2-weighted FSE and T1-weighted spoiled grass sequences. Correspondence factorial analysis was used to select the best discriminating texture features, and a hierarchical ascending classification and Mann-Whitney test were used to evaluate the discrimination between tested tissues. No significant differences were observed between data originating from different centres, and texture features suitable for tissue discrimination were found in these data.

The performance of 2D and 3D co-occurrence matrix parameters in the discrimination of solid tumour, necrosis, edema and white matter was evaluated in glioma data (Mahmoud-Ghoneim et al., 2003). The analysis was based on 1.5 T T1-weighted GRE images. The classification based on the 3D data by LDA produced better discrimination between necrosis vs. solid tumour and edema vs. solid tumour than the 2D data classification results.

Another recent study (Georgiadis et al., 2009) also compared the discrimination power of 2D versus 3D analyses. In this study, textural features of co-occurrence and run-length matrices on 1.5 T T1-weighted contrast enhanced series of intracranial tumours were classified by a linear least squares mapping technique SVM. Classification by 3D features outperformed that by 2D features when discriminating primary tumours from metastatic tumours, whereas discrimination of benign from malignant tumours resulted in exact classification with both 2D and 3D feature types.

Zacharaki et al. reported the classification of brain tumour types and grades based on 3.0 T data acquired from four fixed sequences and relative cerebral blood volume (rCBV) maps (Zacharaki et al., 2009). Tumour shape features, image intensity characteristics and texture features based on a Gabor filter were calculated. Optimal feature subsets selected by *t* test and constrained LDA were classified with three methods: LDA with Fisher discriminant rule, k-NN and nonlinear SVM. The accuracy of classification by SVM was higher than that achieved by the other classifiers. The most accurate discrimination was achieved when distinguishing grade II glioma from metastases (97.8% accurate) and the least accurate when distinguishing grade II from grade III glioma (75%).

De Nunzio et al. (2011) investigated whether 3D texture analysis could be used to characterise glioma-related pathological vs. healthy tissue in 3 T diffusion tensor imaging (DTI), an MRI technique that highlights tissue diffusion properties. These preliminary studies aimed for the automatic detection of cerebral glioma

by means of statistical TA features calculated by MaZda, and the use of an ANN showed promising results in discriminating tissues.

Textural differences between Alzheimer's disease and controls were found in a study by Freeborough and Fox (1998), in which 1.5 T T1-weighted images were examined with co-occurrence matrix textural parameters. Additionally, Torabi (2006) investigated co-occurrence matrix features in Alzheimer's disease and in normal brains and were able to achieve accurate classifications using PCA for feature reduction and an ANN classifier.

Brown et al. discovered a non-invasive method for detecting genetic signatures in oligodentroglioma using texture analysis based on S-transformation (Brown et al., 2008). The analysis was performed on 1.5 T T1-weighted contrast enhanced, T2-weighted and FLAIR sequences with variable acquisition parameters. The textural appearance of tumours originating from patients with clinically relevant coincident allelic loss of specific chromosomal arms was different from those in patients with the alleles in question intact. Especially the analysis based on T2-weighed images performed with high sensitivity and specificity.

Kassner et al. (2009) evaluated acute ischemic stroke patients' T1-weighted SE post-contrast images obtained with a 1.5 T scanner and detected co-occurrence matrix-based texture changes. These changes may be superior to visual evidence of enhancement for the prediction of haemorrhagic transformation.

2.4.3 Skeletal imaging

Texture is recognised as an important pattern property of bones and has been quantitatively analysed with different imaging modalities. Radiography and computed tomography (CT) are the most commonly used techniques, but magnetic resonance imaging has also been used. Here, a pair of recent studies is presented; microimaging studies are not discussed.

Osteoporotic patients and their healthy referents were imaged with a 1.5 T scanner. MaZda was used to calculate trabecular bone texture parameters from spoiled gradient recalled (SPGR) and fast spoiled gradient echo (FSPGR) gradient sequences of the calcaneus (Herlidou et al., 2004). Correspondence factorial analysis was used to select the most significant texture parameters for hierarchical ascending classification. In this study, Herlidou et al. showed that statistical 2D texture information from trabecular tissue characterize osteoporosis and age effects on the bone.

Wrists were imaged with a 3.0 T scanner using a true fast imaging with a steady precession (FISP) sequence to investigate whether bone structural parameters were correlated with texture parameters (Tameem et al., 2007). Structural parameters

were extracted from high-resolution MR images. 3D co-occurrence matrix-based texture values were calculated from MR images, and lower resolution images were sub-sampled from the original images. The results indicate that images with clinically applicable resolution provide textural information about trabecular bone architecture. This study highlights the potential of using clinical MRI to quantify bone architecture.

2.4.4 Phantom studies and technical evaluations

Mayerhoefer et al. (2009b) recently published a systematic study on MRI acquisition parameter variations and protocol heterogeneity effects on texture analysis. In this study, phantoms originally designed as models for liver cirrhosis and with relaxation times in the range of biological tissues were imaged on a 3.0 T scanner with a T2-weighted multislice multiecho sequence. Acquisition parameters TR, TE, number of averages (NA) and sampling bandwidth were used as independent variables, and three spatial resolutions were used. Texture parameters were calculated by MaZda 3.30. LDA and k-NN classifier were used for pattern discrimination. All categories of calculated texture features (co-occurrence matrix, run-length matrix, gradient, autoregressive model and wavelet) were sensitive to variations in acquisition parameters, but as long as the spatial resolution was sufficiently high, clinically feasible variations in acquisition parameters had little effect on the classification results. The discriminatory power of co-occurrence matrix-based features was superior to the other features at lower resolutions with data sets containing spatial resolution heterogeneity.

Image interpolation effects on texture-based classification were investigated on another study on polystyrene spheres and agar gel phantoms with a 3.0 T T2-weighted multislice multiecho sequence (Mayerhoefer et al., 2009a). Matrix size was increased by three image processing methods: linear and cubic B-spline interpolation operated at the pixel level of images and zero-fill interpolation operated in k-space. Texture features were calculated with MaZda 4.60 from fixed-size ROIs. Texture patterns were classified by k-means clustering. Insufficient original image resolution could not be compensated with interpolation methods. Otherwise, image interpolation was found to improve classification based on, for example, co-occurrence matrix-derived parameters. Zero-filling was superior to the other methods used.

Collewet et al. (2004) evaluated the influence of MRI acquisition protocols and grey level normalisation methods on texture classification. They used soft cheese samples imaged on a 0.2 T MRI scanner with proton density-weighted and T2-weighted SE sequences. They used gradient-, co-occurrence- and run-

length matrix, autoregressive model and wavelet-based texture parameters. Original images and their copies processed with three grey level normalisation methods were tested. Classification was performed with a 1-NN classifier. When no normalisation or normalisation by multiplicative methods preserving the relative variation between two grey levels was performed before the texture calculation, the classification errors depended on the acquisition protocol. The best classification results were obtained when using a method that converts image intensities in the range $[\mu-3\sigma, \mu+3\sigma]$, where μ is the mean grey level value and σ is the standard deviation. The $[\mu-3\sigma, \mu+3\sigma]$ method enhances the variations in grey levels between neighbours, thereby improving classification performance.

2.5 Clinical materials

Four clinical materials covering different topics in radiological imaging were selected for this thesis to demonstrate the performance of texture analysis in a variety of clinical applications, including soft tissue tumours, traumatic injuries, chronic progressive disease and a physiological condition. The clinical questions for MR imaging in these materials focus on the detection of non-visible and visible changes in imaged tissues. In each topic, quantitative image analysis methods, such as texture analysis, can potentially provide new clinically important information, particularly in combination with current clinical imaging practices.

2.5.1 Soft tissue tumours: Non-Hodgkin lymphoma

Non-Hodgkin lymphomas (NHL) are a heterogeneous group of cancers comprising very slow-growing low-grade to aggressive, highly malignant lymphomas. Lymphoma mass lesions are commonly localised to the neck, chest, abdomen and pelvis. A variety of diagnostic tools are used to stage the disease as well as in response assessment; these include biopsies, computed tomography (CT), integrated positron emission tomography-computed tomography (PET-CT), magnetic resonance imaging (MRI), and ^{18}F-fluorodeoxyglucose (FDG) or ^{18}F-fluoro-thymidine (^{18}FLT) PET (Ansell and Armitage, 2005; Hampson and Shaw, 2008). Chemotherapy is the mainstay of therapy.

The Response Evaluation Criteria in Solid Tumors (RECIST) guidelines (Therasse et al., 2000; Eisenhauer et al., 2009) recommend measuring tumour response through one-dimensional measures of radiological images, while the World Health Organization criteria (WHO, 1979) recommends two dimensional analysis, and several research groups uses volumetric three-dimensional analysis

(Therasse et al., 2006). Response evaluation based on PET examinations evaluates malignant lesion activity by measuring its uptake of specific tracers (Ansell and Armitage, 2005; Hampson and Shaw, 2008).

In routine clinical practice, treatment planning is driven by repetitive response evaluations. Response evaluation based on mass lesion dimensions does not take into account the possible appearance of residual non-active-masses, whereas methods measuring mass-lesion activity with tracers have limited capacity to differentiate inflammatory processes from active disease. Integrated PET-CT may outperform both PET and CT alone in diagnostic and response evaluation performance; however, some sub-types of NHL may possibly be FDG negative (Kwee et al., 2008). Diffusion-weighted MRI (DWI) with apparent diffusion coefficient (ADC) mapping (Perrone at al., 2011) and dynamic contrast-enhanced (DCE) MRI (Lee et al., 2011) could be considered as supportive tools for analysing lymph node enlargements. Among these methods, new quantitative methods, such as MRI texture analysis, are important topics to investigate as they may provide additional information about structural changes in mass lesions that may be useful for treatment response monitoring.

2.5.2 Central nervous system: Mild traumatic brain injury

Traumatic brain injury varies from mild to severe. The criteria for mild traumatic brain injury (MTBI), according to the WHO Collaborating Centre for Neurotrauma Task Force on Mild Traumatic Brain Injury (Carroll et al., 2004), include several variables that define the severity of injury: the Glasgow Coma Scale (GCS) score, the occurrence of transient neurological abnormalities, the duration of loss of consciousness and post-traumatic amnesia, and the presence of intracranial lesions not requiring surgery. A working group set up by the Finnish Medical Society Duodecim has published a national Current Care guideline for adult brain injuries including definitions of injury severities (Aikuisiän aivovammat, Current Care Summary, 2008). In mild traumatic brain injury (MTBI), the current clinical routine CT and MRI scans may be normal both in the acute phase and when repeated in the follow-up phase; however, these patients may develop chronic symptoms that interfere with their everyday life. Diffusion tensor imaging has been shown to provide advanced information about conventionally non-visible mild injuries (Rutgers et al., 2008). However, currently there is no clinical method for the detection of subtle changes in cerebral tissues based on conventional MR images. Thus, the performance of texture analysis in detecting non-visible traumatic changes in MTBI should be tested.

2.5.3 Central nervous system: Multiple sclerosis

Multiple sclerosis is a chronic autoimmune disease of the central nervous system. The sub-types of disease are named according to the disease course and progression: relapsing-remitting (RRMS), primary progressive (PPMS), secondary progressive (SPMS), progressive-relapsing (PRMS), and clinically isolated syndrome (CIS) suggestive of MS.

The complex pathophysiology of MS, including inflammation, demyelination, axonal degeneration and neuronal loss, generate visible focal lesions as well as non-visible diffuse changes in the brain and spinal cord MR images. MRI plays an essential role in the diagnosis and follow-up of MS. The current practise in diagnosing MS is based on the McDonald clinical diagnostic criteria (McDonald et al., 2001; Polman et al., 2005; Polman et al., 2011; Galea et al., 2011; Kilsdonk et al., 2011). The McDonald criteria include an evaluation of MS disease attacks, cerebrospinal fluid analysis and MRI findings. With reference to these criteria, the dissemination of lesions in space and in time can be demonstrated by T2 and gadolinium-enhancement of lesions in typical areas of the central nervous system (CNS): periventricular, juxtacortical, infratentorial and spinal cord. In the literature on MS, MRI texture analysis has been applied as a quantitative means to characterise disease-related changes in the central nervous system (Kassner and Thornhill, 2010). In the future, TA may provide additional information for the clinical radiologist. However, before clinical use of TA in MS, the robustness of the analysis protocol needs to be investigated.

2.5.4 Musculoskeletal: Trabecular bone strength and changes caused by physical loading

Osteoporosis is a serious public health problem, and the prevention of this bone fragility as well as related fractures are of interest to bone researchers. Bone strength is commonly estimated by bone mineral density (BMD), as measured by dual energy X-ray absorptiometry (DXA) (Blake and Fogelman, 2010) and quantitative-CT (QCT) (Adams 2009). Bone cortical geometry and trabecular architecture are both essential to bone strength. Bone structural features, such as bone volume fraction (bone volume/total volume; BV/TV), trabecular number (Tb.N), trabecular thickness (Tb.Th) and trabecular separation (Tb.Sp), can be calculated from high-resolution QCT and MRI data (Manske et al., 2010).

It has been demonstrated that different exercises affect bone structure in different ways and that some types of loading exercises have bone-strengthening properties (Nikander et al., 2009). In particular, Nikander et al. evaluated the

cortical bone of athletes using MRI. MRI provides a non-ionising method to assess bone structure from the proximal parts of body, which is important because neither these studies nor population screening could ethically use ionising imaging modalities in healthy study participants of reproductive age. The impact of exercise on trabecular bone is also an interesting topic, and the current repertoire of MRI sequences available for clinical imaging provides suitable alternatives for bone imaging (Bydder and Chung, 2009). Texture, as a measure of structure at different magnitudes, might have the potential to discriminate trabecular bone structures exposed to different loading.

3. AIMS OF THE STUDY

This thesis employed MRI-based texture analyses with histogram, run-length-matrix, co-occurrence-matrix, autoregressive model and wavelet-derived parameters in a clinical environment. Quantitative MRI texture analysis was applied to three clinical medical imaging situations that are conventionally evaluated using qualitative means by experienced radiologists (Study I-III) and one study of a physiological situation (Study IV). The specific aims were the following:

1) To evaluate the effectiveness of texture analysis for the characterisation of visible lesions on normal-appearing tissue (Study III).

2) To evaluate the effectiveness of texture analysis for the detection of non-visible changes in tissues (Study I, II, III, and IV).

3) To compare ROI settings and different imaging sequences for texture analysis protocols (Study I, II, III, and IV).

4) To investigate the applicability of MRI-based texture analysis in clinical imaging settings (Study I, II, III, and IV).

4. MATERIALS AND METHODS

4.1 Study design

In Study I, texture analysis was applied at the diagnostic stage and at two treatment response staging timepoints in patients with non-Hodgkin lymphoma. In this study, the role of MRI TA in providing additional information on subtle under-treatment changes in homogenous mass lesions was investigated. The change in tumour volume is used as a control for therapy response.

Mild traumatic brain injury may not be visually detectable in routine MRI scans during either the diagnostic or follow up phases. In Study II, TA is applied to acute phase images of patients and their referents to determine whether any microstructural traumatic changes can be detected in cerebral tissues that have a homogenous appearance.

Study III concentrates on MRI TA of MS, specifically in the separation of focal and diffuse changes. The robustness of analysis protocol phases is tested in the perspective to development of a clinical protocol.

In Study IV, non-visible physical loading-related changes in the trabecular bone of the femoral neck are investigated by texture analysis.

The main features of the investigated data are given in Table 2.

TABLE 2. *The main features of data from Studies I–IV.*

Data Features	Study I NHL	Study II MTBI	Study III MS	Study IV Bone
Focal lesions			●	
Diffuse changes	●	●	●	●
Malignancy	●			
Treatment response monitoring	●			
Traumatic lesions		●		
Long-term disease			●	
Physiological changes				●

4.2 Study populations

Study patient materials (I–III) were selected from several prospective clinical research projects ongoing at Tampere University Hospital. Patients included participants in a tumour response evaluation project, neuroinflammatory diseases project, mild traumatic brain injury project and healthy referents of the MTBI project. The participants in the bone study were healthy athletes and nonathlete referents participating in a study project on bone strength evaluation. The Ethics Committee of the Tampere University Hospital approved these studies, and participants provided written informed consent.

4.2.1 Non-Hodgkin lymphoma

Nineteen Non-Hodgkin lymphoma (NHL) patients participating in the Tumor Response Evaluation project were included this study (14 males, 5 females; mean age ± SD, 61.7 ± 10.9 years). These patients had histologically diagnosed high/intermediate- (N=8, 42%) or low-grade (N=11, 58%) NHL with at least one lymphoma mass lesion of three or more centimetres in diameter either in the abdominal area (N=16) or in the clavicular and axillary lymph node area (N=3). Exclusion criteria were a history of other neoplasms, central nervous disease; congestive heart failure NYHA stages III–IV, serious psychiatric disease, human immunodeficiency virus infection and pregnancy.

Patients were treated with chemotherapy alone or in combination with a humanised antibody, rituximab. Chemotherapy regimens were selected according to patients' clinical status. No exceptions were made to standard treatment procedures; chemotherapy was administered in three-week cycles, and 4 to 9 courses were given according to clinical response. The treatment regimens and the number of courses are explained in detail in (Study I).

4.2.2 Mild traumatic brain injury

Patients with mild traumatic brain injury (MTBI) having a GCS score of 13-15 on arrival to the hospital emergency room were recruited for the project. For this study, forty-two patients (17 males, 25 females; mean age ± SD, 38.8 ± 13.6 years) were included. All patients met the criteria of MTBI according to the WHO Collaborating Centre for Neurotrauma Task Force on Mild Traumatic Brain Injury (Carroll et al., 2004). Their CT and MRI scan findings were normal based on qualitative visual evaluation. Exclusion criteria were age under 18 or over

65, presence of severe traumatic brain injury, previous brain trauma, other major cognitive disorder, and history of major alcohol or drug abuse. The reference group consisted of ten healthy age- and gender-matched controls (4 males, 6 females; mean age ± SD, 39.8 ± 12.9 years; range 28 to 61 years).

4.2.3 Multiple sclerosis

In this study, thirty-eight consecutive multiple sclerosis patients with a definite diagnosis based on revised McDonald criteria (McDonald et al., 2001; Polman et al., 2005) were included (15 males, 23 females; mean age ± SD, 42 ± 12 years). They were participating in a study project of neuroinflammatory disease patients in which biomarkers and new imaging techniques were evaluated. The only exclusion criterion was cortisone treatment within the eight weeks prior to the MRI examination.

4.2.4 Trabecular bone

Ninety-one adult female athletes competing actively at the national or international level and twenty non-athletic referents participated in this cross-sectional study. The exercise-loading types represented by the athletes were grouped into five categories according to a recent protocol (Nikander et al., 2009): 1) the high-impact (H-I) exercise-loading group comprised of triple-jumpers (N=9) and high-jumpers (N=10) (mean age ± SD, 22.3 ± 4.1 years); 2) the odd-impact (O-I) exercise-loading group comprised of soccer (N=10) and squash (N=10) players (25.3 ± 6.7 years); 3) the high-magnitude (H-M) exercise-loading group comprised of power-lifters (N=17) (27.5 ± 6.3 years); 4) the repetitive, low-impact (L-I) exercise-loading group comprised of endurance runners (N=18) (28.9 ± 5.6 years); and 5) the repetitive, non-impact (N-I) exercise-loading group comprised of swimmers (N=18) (19.7 ± 2.4 years). The non-athletic reference group (N=20) mean age was 23.7 years and SD 3.8 years.

4.3 Magnetic resonance image acquisition

The MR imaging for all four studies was performed with 1.5 T scanners. The imaging in the non-Hodgkin lymphoma study was performed with a GE Signa HD scanner (GE Healthcare, Milwaukee, Wisconsin, USA), and the three other studies were imaged with a Magnetom Avanto scanner (Siemens Medical Solutions, Erlangen, Germany). These MRI scanners are maintained under the Tampere University Hospital quality control program. The quality of image sets used in analyses were evaluated by an experienced radiologist and certified as uniform and of good quality.

4.3.1 Non-Hodgkin lymphoma

Three timepoints were included in the TA: The first MR imaging was carried out at the diagnostic stage, before any treatment was administered (examination 1). The following MR examinations were performed after the first chemotherapy cycle (examination 2) and after the fourth chemotherapy cycle (examination 3).

The analysis of lymphoma mass volumes was performed for the first and second examinations. The analysed sequence was an axial T2-weighted fast spin echo (FSE) fat saturation (FAT SAT) sequence (TR 620 ms, TE 10 ms, slice thickness 5 mm-12 mm, matrix 256 x 256, pixel size 1.33 mm x 1.33 mm to 1.80 mm x 1.80 mm) acquired with intravenous contrast agent gadolinium chelate (gadobenate dimeglumine).

Texture analysis was performed on both T1-weighted and T2-weighted axial image sequences from the three imaging timepoints of every patient. The T1-weighted series contained T1-weighted spin echo (SE) and T1-weighted SE FAT SAT sequences (TR 320-700 ms, TE 10 ms, slice thickness 5 mm-12 mm, pixel size 1.33 mm x 1.33 mm to 1.80 mm x 1.80 mm), and the T2-weighted sequences were FSE FAT SAT (TR 3 320–10 909 ms, TE 96 ms, slice thickness 5 mm-12 mm, pixel size 1.33 mm x 1.33 mm to 1.80 mm x 1.80 mm). Imaging sequence parameters, such as TR and slice thickness, varied between and within patients according to their clinical status.

4.3.2 Mild traumatic brain injury

MRI was performed within three weeks from the day of patient admission to the hospital. The fixed imaging sequences included in the texture analysis were 1) an axial T2-weighted FLAIR (TR 9000 ms, TE 109 ms, TI 2500 ms, slice thickness

5.0 mm, pixel size 0.90 mm x 0.90 mm) and 2) a sagittal T1-weighted 3D magnetization prepared gradient echo (T1w MPR) (TR 1910 ms, TE 3.1 ms, TI 1100 ms, slice thickness 1.0 mm, pixel size 0.98 mm x 0.98 mm, flip angle 15°).

4.3.3 Multiple sclerosis

The fixed MRI protocol for texture analysis included 1) an axial T1-weighted 3D magnetization prepared gradient echo sequence (T1w MPR) (TR 1160 ms, TE 4.24 ms, TI 600 ms, slice thickness 0.9 mm, pixel size 0.45 mm x 0.45 mm, echo train length 1, flip angle 15°); 2) the same T1-weighted gradient echo sequence acquired with the intra-venous contrast agent gadoterate meglumine; and 3) an axial T2-weighted FLAIR (named as TIRM in Study III) sequence (TR 8500 ms, TE 100 ms, TI 2500 ms, slice thickness 5 mm, pixel size 0.45 mm x 0.45 mm, echo train length 17, flip angle 150°).

4.3.4 Trabecular bone

MRI of the proximal femurs of participants' dominant legs was performed with careful imaging plane orientation setting; the plane was set perpendicular to the femoral neck axis according to information from the localisation series. The sequences for analyses were 1) an axial 3D T1-weighted FLASH (Fast Low Angle SHot) sequence with interpolation in slice selection direction (TR 15.3 ms, TE 3.32 ms, slice thickness 1.00 mm, pixel size 0.91 mm x 0.91 mm, flip angle 10°) and 2) an axial 3D heavily T2*-weighted spoiled gradient echo sequence called MEDIC (TR 40 ms, TE 17 ms, slice thickness 1.00 mm, pixel size 0.91 mm x 0.91 mm, flip angle 10°). Image slice samples from both sequences with magnified images of the region of interest are shown in Figure 2.

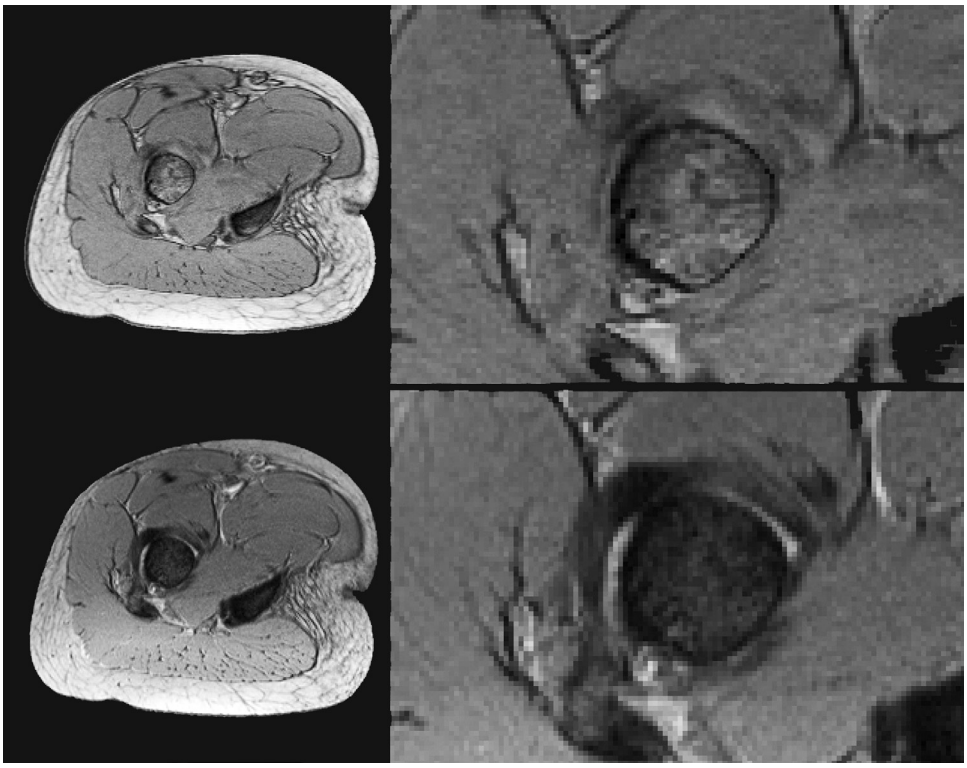

FIGURE 2. *MRI images of a femoral neck. The imaging plane has been set perpendicular to the axis of the femoral neck. A FLASH image is shown in the first row on the left, with a magnified image of the region of interest shown at right. A MEDIC image is shown in a similar way below.*

4.4 Texture analysis

Analysis of the DICOM format images was conducted in a Microsoft Windows XP environment. The stand-alone DICOM viewer Osiris (Windows version 4.19, The Digital Imaging Unit of the Service for Medical Computing of the University Hospitals of Geneva, Switzerland) was used to select slices from each image series for analysis.

The MaZda software package (MaZda version 3.20 for studies I, III, IV; and version 4.5 for Study II) was used for the texture analysis. MaZda calculates almost 300 texture parameters divided into the following feature sets: histogram, gradient, run-length matrix, co-occurrence matrix, autoregressive model and wavelet-derived parameters. The texture parameters are discussed in Chapter 2.3, and mathematical equations are presented in Appendix. Run-length matrix parameters were calculated in four directions: horizontal (0^o), vertical (90^o), 45^o and 135^o, and co-occurrence matrix parameters were calculated at five distances (1, 2, 3, 4 and 5 pixels), four times for each distance (at $\theta = 0^o, 45^o, 90^o$ and 135^o). Regions of interest (ROI) were set manually by freehand drawing or by placing pre-defined fixed-size ROI-boxes on the image. Grey level intensities were normalised in the range $[\mu-3\sigma, \mu+3\sigma]$, where μ is the mean grey level value and σ is the standard deviation.

4.4.1 Non-Hodgkin lymphoma

This portion of the study focused on the detection of subtle non-visible textural changes in lymphoma masses during treatment. The homogeneous parts of the lymphoma lesions were set as ROIs by freehand drawing method on selected image slices originating from the three evaluation stages. Membranous marginals and non-homogenous parts of the masses were excluded. Texture parameters based on histogram, gradient, run-length matrix, co-occurrence matrix, autoregressive model and wavelet methods were calculated. Automated Fisher and POE+ACC methods provided by MaZda were used to establish the best discriminating texture features to highlight changes in lymphoma tissue texture during treatment. The identified parameters were then used as feature sets in further analyses. T1- and T2-weighted images were analysed separately. Figures 3 and 4 show images from a single patient with ROIs.

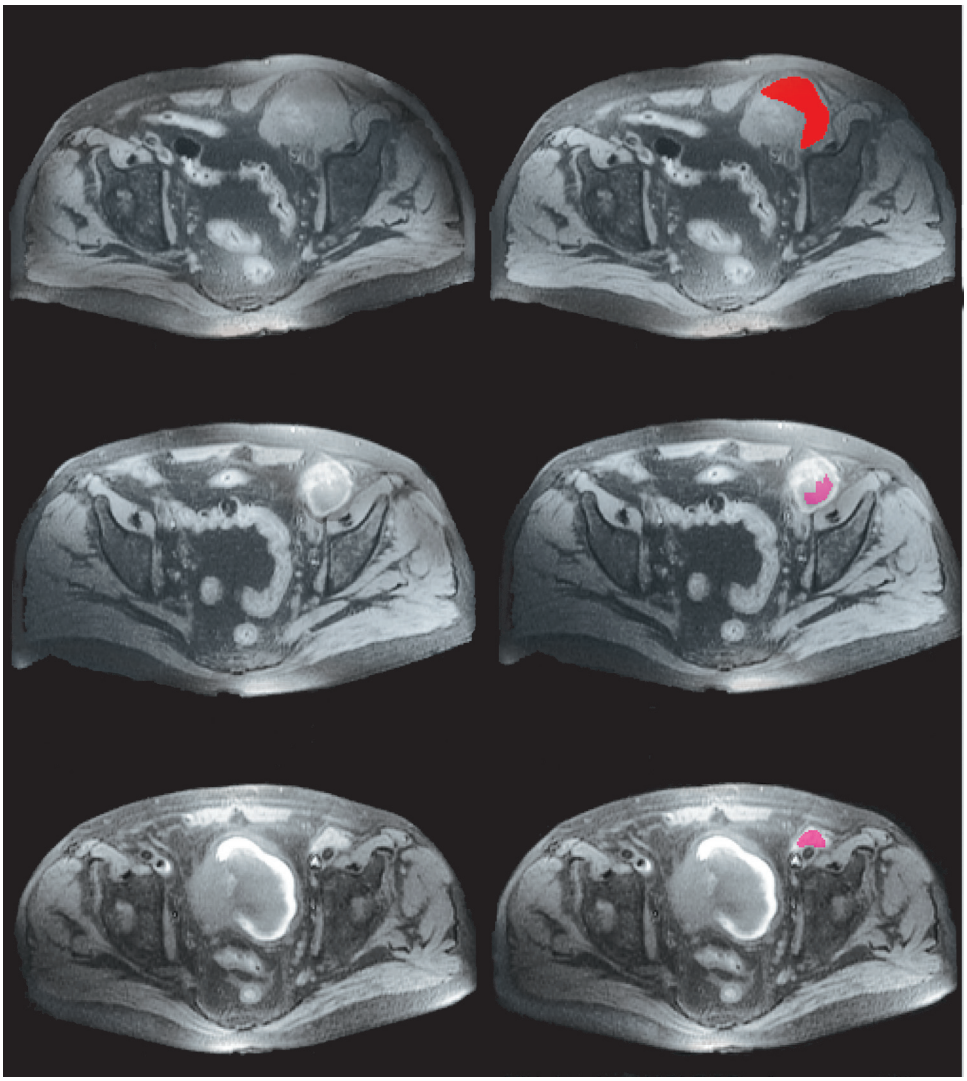

FIGURE 3. *Axial T1-weighted SE fat saturation image slices of a typical subject (left), and ROIs drawn on a lymphoma mass (right). Images in the first row are from the diagnostic phase (examination 1), images in the second row are from examination 2, and images in the last row are from examination 3.*

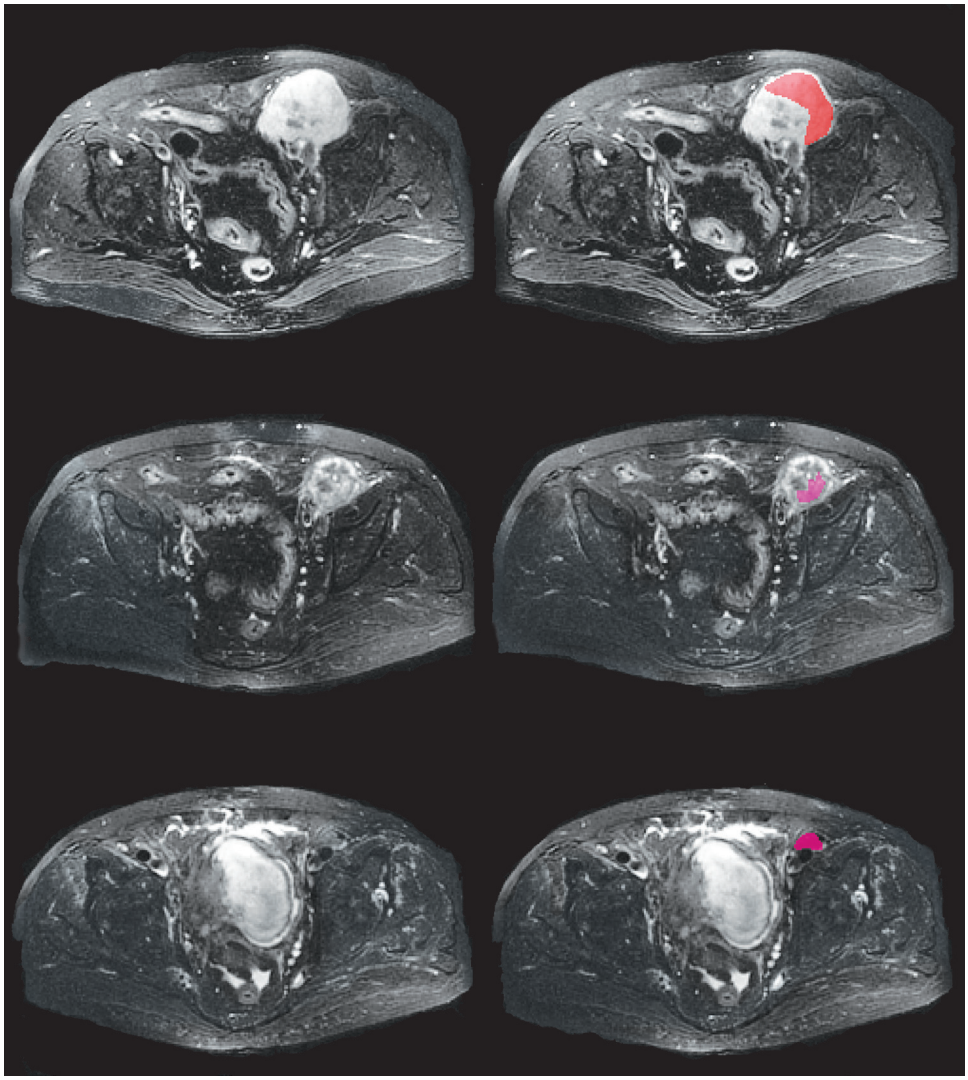

FIGURE 4. *Axial T2-weighted FSE fat saturation image slices of a typical subject (left), and ROIs drawn on the lymphoma mass (right). Images in the first row are from the diagnostic phase (examination 1), images in the second row are from examination 2, and images in the last row are from examination 3.*

4.4.2 Mild traumatic brain injury

Texture analysis was focused on identifying non-visible traumatic changes in brain tissue on certain anatomical locations of interest. Another aim of this study was to evaluate the effect of ROI placement on tissue texture appearance. The locations were named as levels in image sets. One image slice from image set was selected to represent each level. Levels 1–3 were derived from the axial FLAIR sequence, with level 1 containing the mesencephalon, level 2 containing the corona radiata and level 3 containing the centrum semiovale. Level 4 was a corpus callosum image obtained from a sagittal T1w MPR sequence.

For each image ROIs were manually placed symmetrically on the left and right hemispheres on each level of interest. A detailed description of ROIs is presented in Table 3. Two freehand-drawn ROIs covered the mesencephalon cross section, and the size of these ROIs varied depending on the size of the individual mesencephalon. The white matter and corpus callosum ROIs (rostrum, body and splenium) were predefined circles. Their size was defined based on the common size of the corpus callosum and when considering white matter, such that other structures and possibly observed microhaemorrhages, macroscopic hemosiderin deposits or hyperintensities could be carefully avoided to overlap. However, all patient scans were normal without evidence of contusion. The anatomical locations investigated with ROIs marked are presented in Figures 5 and 6.

TABLE 3. *Description of ROIs used in the MTBI study. "Levels" refers to anatomical levels in the axial view: 1) mesencephalon; 2) corona radiata; 3) centrum semiovale; or in the sagittal view 4) midline. The ROI sizes are given in pixels.*

Level	ROI	ROI type	ROI size
1	Mesencephalon (left, right)	Freehand	~1200
1, 2	White matter, temporal lobe, (left, right)	Circular	177
3	White matter, anterior (left, right)	Circular	177
3	White matter, medial (left, right)	Circular	177
3	White matter, posterior (left, right)	Circular	177
4	Corpus Callosum, splenium	Circular	68
4	Corpus Callosum, body	Circular	68
4	Corpus Callosum, rostrum	Circular	68

Image histogram, co-occurrence matrix, run-length matrix, absolute gradient, autoregressive model and wavelet-based textural features were calculated from each ROI. Texture feature subsets were selected automatically by the Fisher coefficient method.

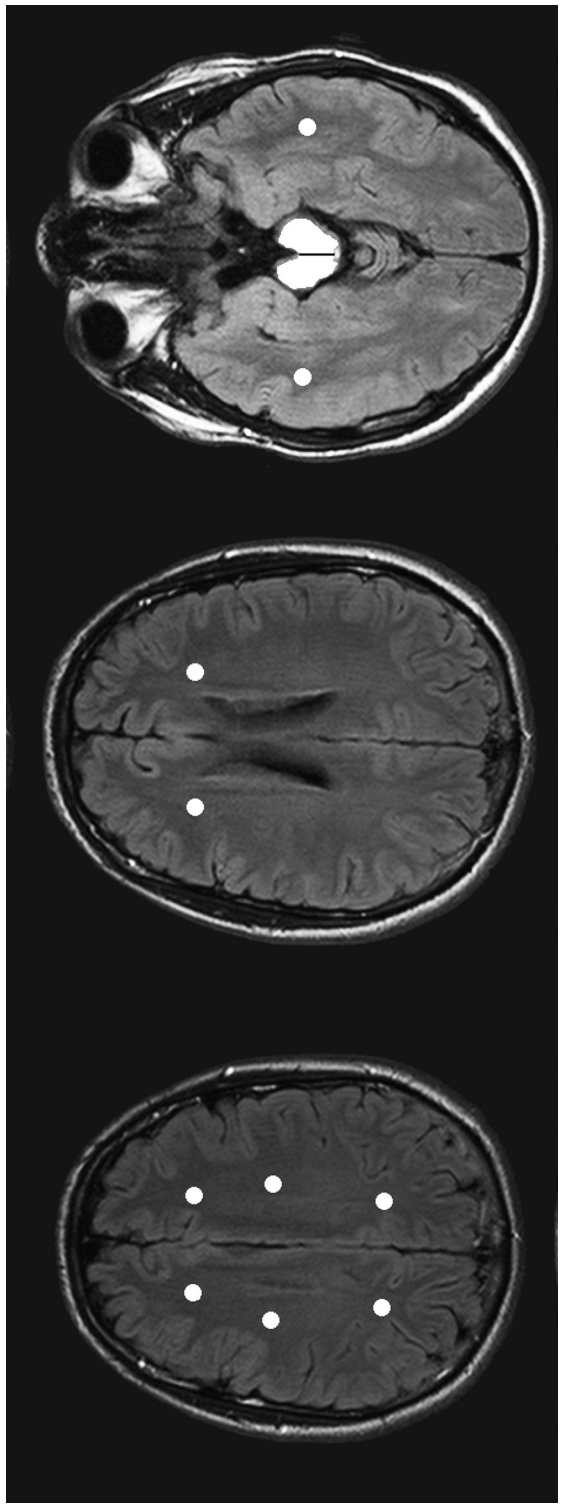

FIGURE 5. *Axial FLAIR image slices on selected anatomical levels from left to right: centrum semiovale, corona radiata and mesencephalon. ROIs have been drawn in the images.*

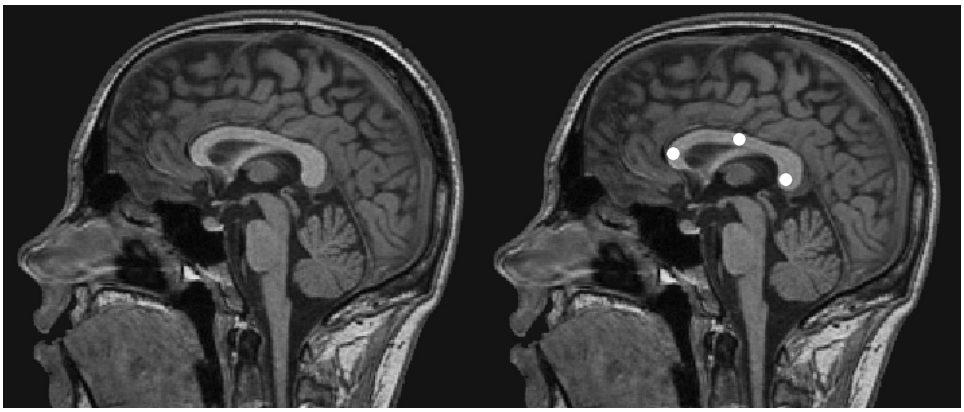

FIGURE 6. *Sagittal T1w MPR showing the corpus callosum included in the analysis on the left side. ROIs are drawn in the image at right. The anterior ROI was placed at the rostrum, the middle ROI was placed at the body and the posterior ROI was placed at the splenium of the corpus callosum.*

4.4.3 Multiple sclerosis

This analysis concentrated on detecting textural differences in normal and disease-burden tissue samples and on the robustness of the analysis protocol. Variation in intra-tissue textural appearance between three sequential image slices and image slices originating from two anatomical levels was investigated. The texture classification power of three MRI sequences was evaluated. Two types of ROIs were used, fixed size ROI-boxes and freehand drawn ROIs on focal MS lesions. Figure 7 shows examples of ROI setting with both methods. The two anatomical levels taken into analysis based on anatomical landmarks were the 1) corona radiata/centrum semiovale and 2) basal ganglia. The ROIs of different structures defined from images are presented in Table 4. The criteria for the selection of an ROI representing an MS focal lesion was a T2-weighted plaque in the cerebral hemisphere, while the NAWM ROIs were defined as the white matter surrounding the focal MS lesion. Figures 8 and 9 present the anatomical levels analysed with image slices and ROIs drawn on them.

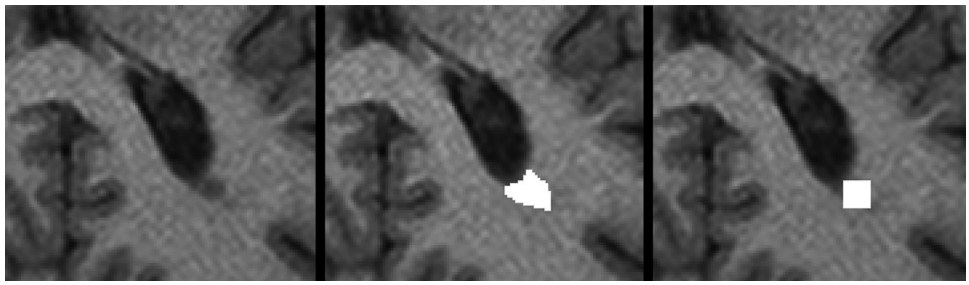

FIGURE 7. *Detail from a brain image at the level of the basal ganglia showing an MS-plaque near the posterior horn of the lateral ventricle. The centre and right images show examples of freehand and fixed-size ROI setting, respectively.*

TABLE 4. *Description of ROIs used in the MS study. The level numbers indicate the anatomical levels: 1) corona radiata/centrum semiovale, 2) basal ganglia. The ROI sizes are given in pixels.*

Level	ROI	ROI type	ROI size
1, 2	White matter (WM)	square	100
1, 2	Normal-appearing white matter (NAWM)	square	100
1, 2	Cerebrospinal fluid	square	100
1, 2	Normal-appearing grey matter apart lesion	square	36
1, 2	Normal-appearing grey matter near lesion	square	36
2	Nucleus caudatus	square	100
2	Nucleus lentiformis	square	100
1, 2	MS plaque, freehand ROI	freehand	varying
1, 2	MS plaque, fixed-size ROI	square	100

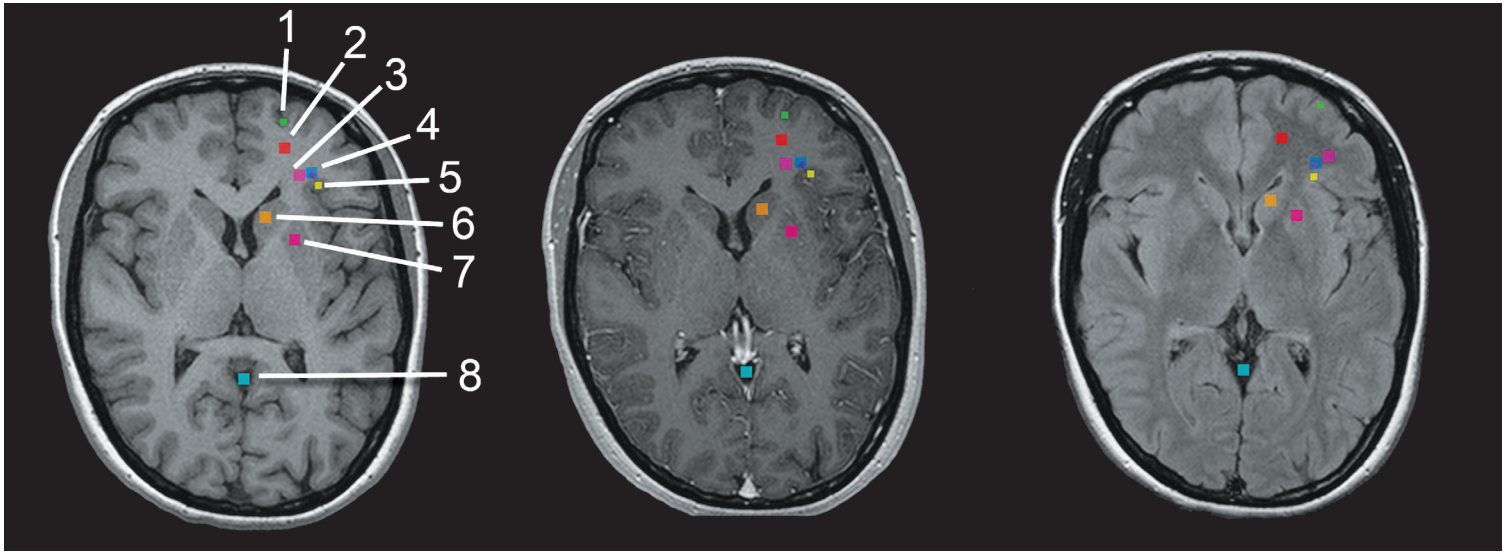

FIGURE 8. *Brain images from the basal ganglia, with ROIs indicated on the images. Left, T1w MPR image; centre, T1w MPR acquired with contrast agent; right, FLAIR image. Different ROIs are indicated by numbers and colours: 1) green, cortex apart from lesions (grey matter); 2) red, white matter; 3) pink, normal-appearing white matter; 4) blue, MS plaque (10x10 ROI) and violet, hand-drawn MS plaque; 5) yellow, cortex near lesion (normal-appearing grey matter); 6) orange, nucleus caudatus; 7) darker pink, nucleus lentiformis and 8) aquamarine, cerebrospinal fluid.*

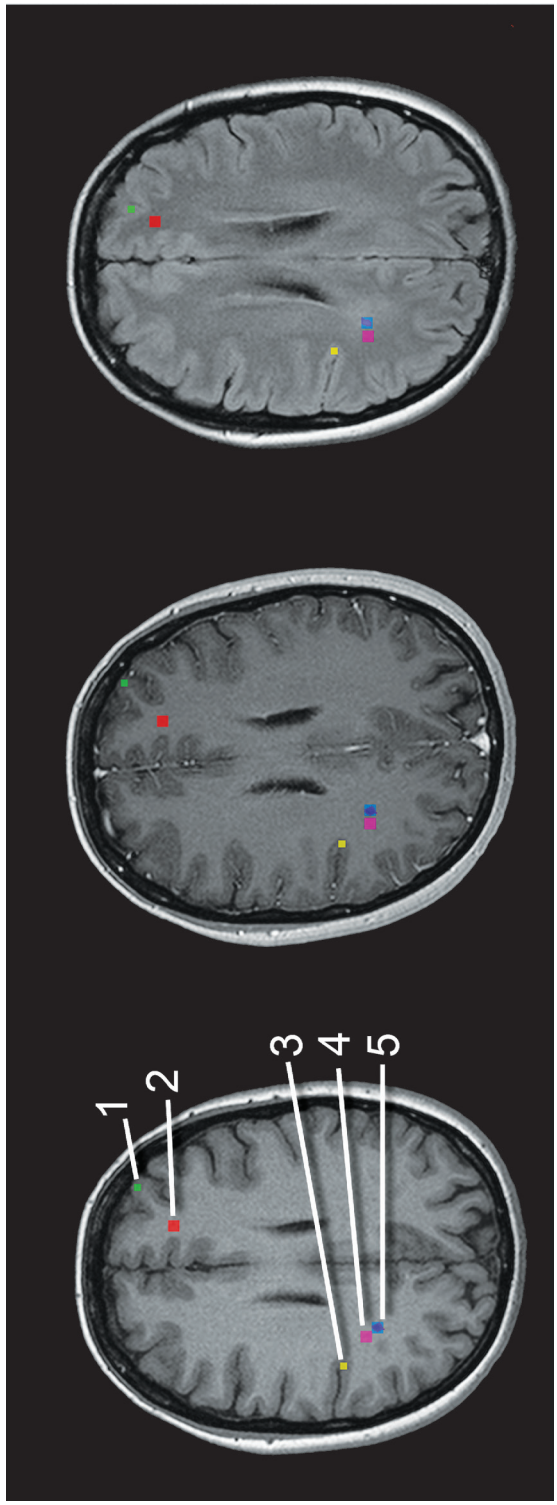

FIGURE 9. *Brain images from the corona radiata, with ROIs indicated on the images. Left, T1w MPR image; centre, T1w MPR acquired with contrast agent; right, FLAIR image. Different ROIs are represented by numbers and colours: 1) green, cortex apart from lesions (grey matter); 2) red, white matter; 3) yellow, cortex near lesion (normal-appearing grey matter) 4) pink, normal-appearing white matter and 5) blue, MS plaque (10x10 ROI) and violet, hand-drawn MS plaque.*

Texture features based on image histogram, co-occurrence matrix, run-length matrix, absolute gradient, autoregressive model and wavelets were calculated for each ROI. Two automated methods, Fisher and POE+ACC, were used to identify the 10 texture features that gave the best discrimination between tissue pairs. In addition, 25 texture features that were reported to be efficient in a recent multiple sclerosis study (Zhang et al., 2008) were used (Table 5). These three textural feature sets were then used for further analyses.

TABLE 5. *A list of the texture parameters used in manual feature selection. For co-occurrence matrix parameters, the distance between analysed pixels is 1, and parameters are calculated in four directions. Run-length parameters are calculated in four angles.*

Parameters used in manual feature selection	
Parameter group	**Parameter**
Co-occurrence matrix	Contrast
Co-occurrence matrix	Difference variance
Co-occurrence matrix	Sum of squares
Co-occurrence matrix	Sum variance
Run-length matrix	Grey level nonuniformity
Gradient	Mean absolute gradient
Gradient	Variance of absolute gradient
AR model	Standard deviation
Wavelet	Energy, subband 1, HL
Wavelet	Energy, subband 2, HL

4.4.4 Trabecular bone

This analysis was focused on the cross-section of the femoral neck at the insertion of the articulation capsule to find co-occurrence matrix-based texture differences due to exercise loading. Image slices representing the anatomical region of interest were selected manually from both sequences and were included in the analysis. Inferior (I), anterior (A), superior (S) and posterior (P) quadrants of the trabecular bone were set as ROIs (Figure 10). Three co-occurrence matrix texture parameters that had previously shown significant correlation with trabecular structural indices (Tameem et al., 2007) were calculated for further analyses. These parameters were 1) angular second moment, 2) entropy and 3) sum entropy. Each parameter was calculated for four distances between pixels and in four directions for each distance for each ROI, producing a total of 48 textural features for each ROI. Variation in intra-tissue textural appearance between two adjacent image slices

was analysed to test the reproducibility of these measurements. In addition, the usability of two sequences was evaluated.

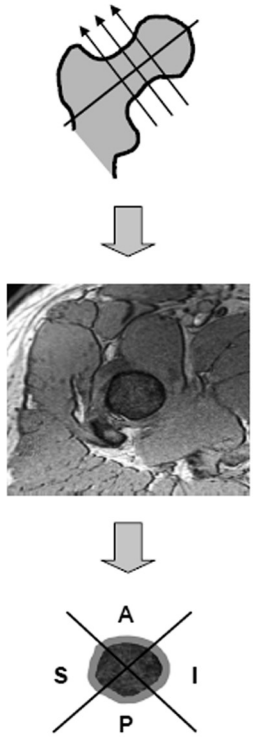

Image plane was set perpendicular to femoral neck axis with help of localization series.
Two sequences including 120 image slices with thickness of 1.00mm were obtained for TA purposes.

The image stacks were scrolled trough to find image slices with anatomical landmarks: articulation capsule insertion to femoral neck. These images were stored in DICOM format.

Selected image slices were opened in MaZda texture analysis software. Trabecular bone was divided manually into four ROIs representing the anatomical quadrants (anterior, inferior, posterior and superior).

FIGURE 10. *Trabecular bone texture analysis: Phases of the analysis process before texture parameter calculation.*

4.5 Statistics and classification

4.5.1 Non-Hodgkin lymphoma

Analyses were run between all combinations of three imaging stages separately for T1- and T2-weighted images. Default neural network parameters in the B11 application (version 3.4, MaZda software package) were used for texture data analyses: the first hidden layer = 1; the second hidden layer = 2; backprop eta = 0.15; backprop iter. limit = 150 000 and optimisation iter. limit = 50. Nearest-neighbour (1-NN) classification was performed for the raw data, the most expressive features resulting from PCA and the most discriminating features resulting from LDA. Nonlinear discriminant analysis carried out the classification of features with ANN.

Two statistical analyses, the Gage R&R test (Statistica/W, version 5.1, 98 edition. Statsoft Inc, Tulsa, OK, USA) and Wilcoxon Signed Ranks test (SPSS for Windows, version 14.0.2. SPSS Inc., Illinois, USA), were run for the selected feature groups. A p-value < 0.05 was considered statistically significant. A summary of the Gage R&R terminology in this application is given in Table 6.

TABLE 6. *Summary of Standard Gage R&R terminology and its application in Study I.*

Standard Gage R&R terminology	Study I application of R&R terminology
Operators	Timepoints of MRI examinations (diagnostic stage, two response evaluation stages).
Parts	Patients
Trials	Repeated measurements (ROIs from adjacent image slices) at fixed timepoints.
Repeatability	Difference across measurements (texture parameter value variation between two adjacent image slices originating from a single patient and from the same sequence at a fixed timepoint). Repeatability was expected to be zero.
Reproducibility	Difference across timepoints (texture parameter value variation between image slices originating from the same sequence type at different timepoints). Reproducibility was expected to be quite large and significant according to research topic.
Variability	Difference across patients (there is no exact expected value for patient-to-patient variation).

4.5.2 Mild traumatic brain injury

The texture features selected by the Fisher criterion were subjected to statistical analyses. Textural differences between tissue samples in different hemispheres were analysed by Wilcoxon signed ranks test. The Friedman test was used to compare tissue samples originating from different anatomical levels of the same hemisphere and samples from the corpus callosum (rostrum, body and splenium). These tests were run separately for patients and healthy referents. Statistically significant difference was defined as a p-value under 0.05. Analyses were run in SPSS (SPSS for Windows, version 14.0.2, SPSS Inc., Illinois, USA).

4.5.3 Multiple sclerosis

Intra-tissue textural variation between anatomical levels was analysed by calculating Wilcoxon signed ranks test values for all 280 texture parameters for all ROIs and evaluating the number of statistically significant differences ($p < 0.05$). These tests were run separately for each MR sequence. Intra-tissue textural variation between sequential image slices were run for T1-weighted images of randomly sampled sub-population (N=23) by the Friedman test with the same method used for the test between anatomical levels.

Texture classification for tissue pairs was run using the 10 best texture features selected with both automated methods as well as for the 25 manually selected features in B11. Principal component analysis was followed by 1-NN classification with the leave-one-out-method for the most expressive features identified by PCA. NDA was run with ANN classification included. In addition, the 10 features that best performed the classification of white matter and MS in different sequences were examined with Wilcoxon signed ranks test to detect statistical differences between tissue pairs (WM vs. MS freehand ROI, WM vs. MS fixed-size ROI, NAWM vs. MS freehand ROI, and NAWM vs. MS fixed-size ROI) for both imaging levels and all three sequences. A level of $p < 0.05$ was considered statistically significant.

Wilcoxon signed ranks tests and Friedman tests were performed using SPSS for Windows (Version 16.0.2. SPSS Inc., Illinois, USA).

4.5.4 Trabecular bone

A Kruskal-Wallis test was conducted to evaluate overall differences among the five groups of athletes and their referent group. A p-value < 0.0033 was considered

significant. *Post hoc* analysis based on the Mann-Whitney test was performed between each exercise-loading group and the referent group, and a significance criterion of $p < 0.01$ was used. These tests were performed for the three selected texture parameters angular second moment, entropy and sum entropy, with each parameter determined for four distances between pixels and four directions for each distance. Reproducibility testing between two sequential image slices was conducted for both sequences for the three texture parameters, with inter-pixel distance showing the most consistent discrimination between the groups. The measure of reproducibility, or R-value, was calculated by dividing the variance of differences between the texture parameter values of two adjacent slices by the variance of a given parameter in the population.

Tests were run in SPSS for Windows, version 16.0.2. SPSS Inc. Illinois, USA.

5. RESULTS

5.1 Characterisation of visible lesions on normal-appearing tissue

In Study III, the classification of multiple sclerosis plaques from white matter and normal-appearing white matter close to the focal lesions was evaluated. Four tissue pairs 1) WM fixed size ROI vs. MS freehand ROI; 2) WM fixed size ROI vs. MS fixed size ROI; 3) NAWM fixed size ROI vs. MS freehand ROI; and 4) WM fixed size ROI vs. MS fixed size ROI were defined from two anatomical levels on fixed axial imaging sequences, FLAIR, and T1-weighted magnetization prepared gradient echo with and without contrast agent. Classification procedures, run separately for each image series, showed highly accurate classification. There were slight differences in classification results between the methods used for feature selection, ROI type (fixed-size and freehand drawn) and imaging sequence. The best classification was achieved by the POE+ACC automated feature selection method, but the other methods achieved almost the same level of accuracy. The Wilcoxon signed ranks test showed highly significant statistical differences between all tested tissue pairs, anatomical level and sequence combinations. T1-weighted magnetization-prepared gradient echo sequence acquired with intravenous contrast agent performed slightly better than the other two series. A summary of classification results obtained with NDA and ANN is presented in Table 7.

TABLE 7. *Correct classification of focal MS lesions from white matter (WM) and normal-appearing white matter (NAWM) based on three imaging sequences: T1-weighted magnetization prepared gradient echo (T1w MPR), previous with contrast agent (T1w MPR+C) and FLAIR. The percentage of correct classifications is presented for four tissue pairs of interest and for three feature selection methods: Fisher (F), POE+ACC (P) and manual (M). Imaging level 1 refers to corona radiata/centrum semiovale, and level 2 refers to basal ganglia.*

Imaging sequence	Imaging level	Feature selection	WM vs. MS freehand ROI	WM vs. MS fixed ROI	NAWM vs. MS freehand ROI	NAWM vs. MS fixed ROI
T1w MPR	**1**	**F**	100 %	100 %	100 %	98 %
		P	100 %	100 %	100 %	98 %
		M	100 %	98 %	100 %	98 %
	2	**F**	98 %	97 %	100 %	100 %
		P	100 %	100 %	100 %	100 %
		M	98 %	98 %	100 %	97 %
T1w MPR+C	**1**	**F**	100 %	100 %	96 %	100 %
		P	100 %	100 %	100 %	100 %
		M	100 %	96 %	100 %	96 %
	2	**F**	100 %	100 %	98 %	100 %
		P	100 %	100 %	97 %	100 %
		M	98 %	98 %	98 %	98 %
FLAIR	**1**	**F**	100 %	97 %	100 %	96 %
		P	100 %	98 %	100 %	96 %
		M	100 %	96 %	100 %	98 %
	2	**F**	100 %	97 %	100 %	97 %
		P	100 %	100 %	100 %	98 %
		M	100 %	98 %	100 %	98 %

5.2 Detection of non-visible changes in tissues

Non-Hodgkin lymphoma treatment evaluation by MRI in Study I showed that as lymphoma masses decreased in size between diagnosis and treatment, the texture of the masses also changed. The classification of lymphoma tissue changes between different timepoints in the treatment process was challenging; the overall accuracy of classification performed with 1-NN on the basis of RDA, PCA, and LDA, and ANN on the basis of features of NDA, achieved only moderate success. ANN run on the most expressive features of NDA reached a classification accuracy of up to 96% in T2-weighted series within diagnostic stage and second treatment evaluation and 95% within T1-weighted images. In analyses based on RDA, PCA and LDA in this timepoint combination, classification accuracy reached 82–87% in T1-weighted images and 79–86% in T2-weighted images. Discrimination between other combinations of timepoints produced marked misclassification. NDA-based analyses of combinations of diagnostic stage vs. first response evaluation and first vs. second evaluations maintained a classification accuracy of 75–88%, while other analyses were less effective. The combination of all three imaging timepoints was the worst, with classification accuracies of 53–70%. Classification accuracy by ANN run with NDA in MaZda is summarised in Table 8.

TABLE 8. *Correct classification of imaging stages in non-Hodgkin lymphoma treatment response evaluation. ANN classification included non-linear discriminant analysis (NDA) in the MaZda software package. T1w refers to T1-weighted images, and T2w refers to T2-weighted images. The classification results for imaging timepoints are given in rows. E1, examination 1; E2, examination 2; E3, examination 3.*

Examinations	T1w	T2w
E1, E2, E3	69%	70%
E1, E2	84%	65%
E1, E3	95%	96%
E2, E3	87%	88%

Statistical tests were calculated from images of 18 patients. One patient who had been included in the primary MaZda texture parameter calculation was excluded due to a smaller amount of image data than other patients, leading to reduced textural data. Wilcoxon test results were in line with the classification results, i.e., the most statistically significant differences were found between diagnostic stage and second response evaluation, particularly in T2-weighted images. In other comparisons, the statistically significant differences for separability of timepoints are quite heterogeneous among texture parameters ranked as good

for discrimination by MaZda. The variation in texture parameter values between image slices originating from a single patient and the same sequence at a fixed timepoint were measured by Gage R&R test repeatability. This test showed some differences, indicating that visually homogenous parts of a lymphoma mass have some textural differences between image slices. The reproducibility parameter showed clear changes between timepoints, exceeding the changes detected between image slices and therefore representing significant difference in texture between evaluation timepoints.

Mild traumatic brain injury patients with visually normal MRI scans and their healthy referents were investigated in Study II using texture analysis to detect non-visible changes due to trauma. Wilcoxon and Friedman tests were used to evaluate the number of texture parameter value differences between tissue samples as a sign of traumatic changes. Patients clearly demonstrated more differences between the left and right mesencephalon than did controls (39% and 13%, respectively). Analyses of differences in white matter between hemispheres showed quantitatively fewer statistically significant changes; however, MTBI patients distinctly had more statistically significant hemisphere differences, especially in the level of corona radiata (23% vs. 5%). In addition, differences in white matter texture at different anatomical locations within the same hemisphere were detected. The white matter textural appearance at the level of the mesencephalon was somewhat different from that at locations in the superior brain. Furthermore, in the antero-posterior view at the level of the centrum semiovale, posterior white matter samples were different from frontal and central samples in both hemispheres. The body of the corpus callosum had a different texture in patients compared to the controls, and in addition, the rostrum and splenium were distinct from the body. A brief summary of interhemispheric and midline structure differences is given in Table 9. The results are presented in full detail in Study II.

TABLE 9. *Interhemispheric and midline structure differences in MTBI patients and healthy referents. Percentages represent texture parameters with statistically significant differences ($p < 0.05$) in interhemispheric and midline comparisons. The Wilcoxon test was used for WM and mesencephalon, and the three ROIs representing the corpus callosum were analysed with the Friedman test. A total of 277 parameters were analysed. Level 1, mesencephalon; level 2, corona radiata; level 3, centrum semiovale.*

Interhemispheric and midline structure differences	patients	referents
Mesencephalon, patients	39 %	13 %
WM, level 1	10 %	4 %
WM, level 2	23 %	5 %
WM, level 3	7 %	4 %
Corpus callosum, rostrum	2 %	2 %
Corpus callosum, body	18 %	1 %
Corpus callosum, splenium	2 %	1 %

In addition to Study II, cerebral tissue was examined also in Study III. Normal-appearing white matter near the focal lesion was compared to white matter sample further from the lesion. These tissue samples could not be distinguished visually, but texture-based classification was 85% accurate, indicating that there are textural differences between these tissue samples. In the studied MRI images, the texture of the nucleus caudatus and nucleus lentiformis were visually indistinguishable. The quantitative methods used also failed to classify these structures.

In Study IV, textural differences in trabecular bone due to exercise loading were evaluated in a large cohort of top-level athletes and healthy referents. Kruskal-Wallis test for the superior part of the femoral neck showed a clear overall separability of all groups on FLASH sequence data. In contrast, the MEDIC data did not show any statistically significant difference between groups when evaluated with strict criteria for significance ($p < 0.0033$). Post-hoc analysis based on Mann-Whitney tests of paired comparisons between athlete groups and referents showed statistically significant differences in odd-impact and high-magnitude exercise loading groups compared to controls. The post-hoc tests showed differences primarily at the superior region of the femoral neck.

5.3 Comparison of the ROI setting and imaging sequences for texture analysis protocol

5.3.1 Regions of Interest (ROI)

In Study III, ROI setting with fixed-size vs. freehand ROIs were compared in one type of tissue sample, the MS plaque. The freehand-drawn ROIs lead to slightly better differentiation between MS focal lesions and WM than the manually placed fixed-size ROIs. These results are presented in Table 6. When anatomical levels and slice-to-slice variation was investigated, the textural appearance of freehand-drawn ROIs differed in more parameters than did fixed-size ROIs (Figure 11).

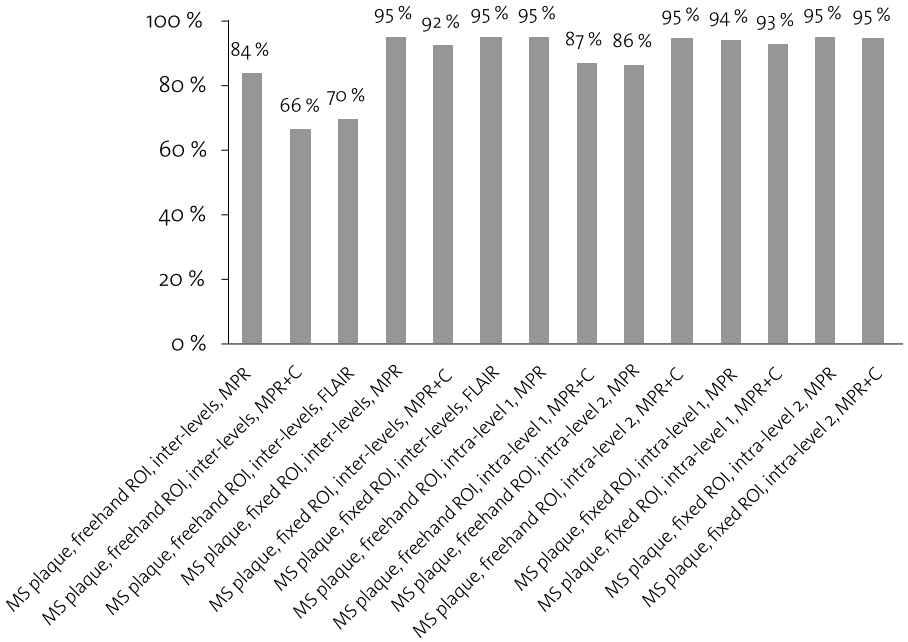

FIGURE 11. *Reproducibility of texture parameter values calculated from fixed-size and freehand-drawn ROIs of MS plaques. The results for T1w MPR, T1w MPR+contrast agent and FLAIR MRI sequences are presented. "Inter-levels" refers to comparisons of ROIs drawn on two image slices originating from different anatomical locations of single image sequences. Intra-level analysis of three sequential slices is given for both anatomical levels considered, and information about the level in question is given in the figure. The evaluation of intra-tissue differences is given as the percentage of texture parameters with no statistically significant difference among a total of 280 parameters.*

5.3.2 Selection of images for analyses

In Studies II and III, several anatomical locations for ROIs were considered. In Study II, textural differences in brain tissues between hemispheres and different anatomical locations were investigated in mild traumatic brain injury patients and their healthy referents. More statistically significantly different parameters between analysed locations were observed in MTBI patients than in controls, indicating that the presence of differences is possibly related to tissue damage. Therefore, only the results of controls (N=10) were used to evaluate the influence of ROI placement at different anatomical locations. A total of 277 texture parameters were calculated from each ROI. In the area of mesencephalon, the left and right sides of the cross section of the structure were investigated, and statistically significant differences were found in 13% of all parameters. Distinct anatomical parts of the corpus callosum differed from each other in 1–2% of parameters. In comparisons of white matter between hemispheres, 4–5% of parameters exhibited significant differences (Figure 12).

In Study III, the textural appearance of a large set of brain tissues was evaluated in two anatomical locations and in three sequential image slices with the same method as the images in Study II. A total of 280 parameters were evaluated. Estimation of anatomical level effect on tissue sample texture showed changes in white matter in 3% of parameters in T1w MPR, 6% in T1w MPR+C and 12% in FLAIR sequence. Fixed-size ROIs encompassing normal-appearing white matter, cerebrospinal fluid, normal-appearing grey matter, nucleus caudatus, nucleus lentiformis and MS plaques showed statistically significant differences in 1–9% of 280 parameters. A marked difference in textural appearance was detected between freehand-drawn ROIs of MS in different levels (16-30%). T1-weighted images with and without contrast enhancement were used in an analysis of intra-tissue textural changes between sequential image slices. Test was applied for the anatomical levels and tissues used in the inter-level testing. In the T1-weighted native series white matter samples had 5% of parameters statistically significantly different at the anatomical level of the corona radiata and centrum semiovale; and 7% at the level of the basal ganglia. In contrast series, these percentages were 4% and 5%, respectively. Other samples of fixed-size ROIs lead to differences in 1–13% of all parameters. Freehand-drawn ROIs on MS showed differences in 5–13% of parameters. The full details of those results are presented in Study III (Figure 12).

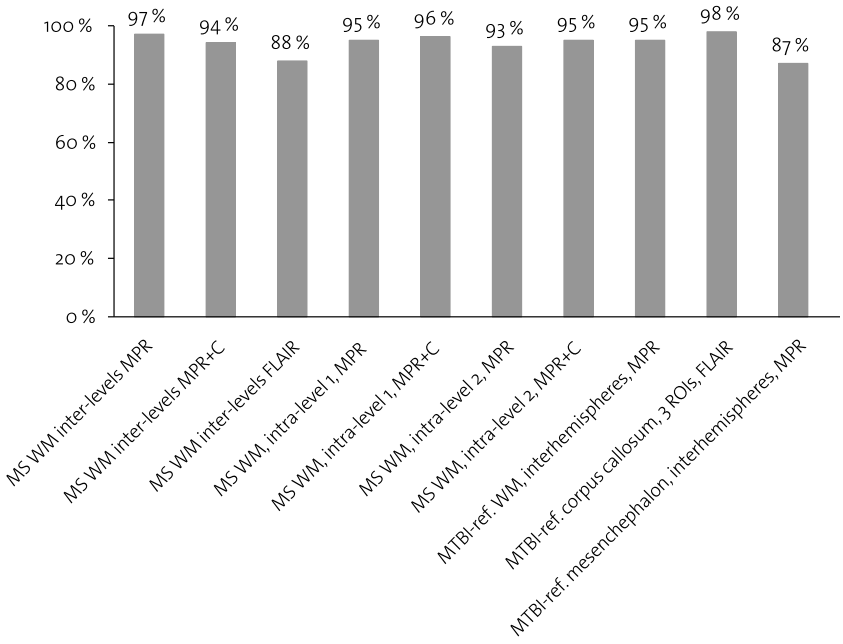

FIGURE 12. *Reproducibility of texture parameter values calculated from ROIs representing single tissues in different anatomical locations of a single image slice, sequential slices and slices originating from a single MRI sequence but at different locations. Intra-tissue differences are given as the percentage of texture parameters with no statistically significant differences (280 total parameters in MS, 277 total parameters in MTBI). Here, white matter (WM) differences among MS study (III) participants are presented for comparison of different anatomical levels and for sequential image slices of two levels. Healthy MTBI study referents (II) were used to investigate interhemispheric changes in white matter and mesencephalon and sagittal changes in the corpus callosum (3 ROIs). Three MRI sequences (T1w MPR, T1w MPR+contrast agent and FLAIR) are presented.*

5.3.3 Selection of sequences for analyses

In Study I, the data were comprised of T1- and T2-weighed sequences with variable acquisition parameters. The classification of pre-treatment and under-treatment lymphoma masses was challenging. Differences between timepoints were quite small when evaluated by classification results provided by B11 analyses. However, when concentrating on Wilcoxon test results, textural data originating from T2-weighted images showed several statistically significant differences, particularly in comparisons of the first and third imaging stages.

In Study III, texture information calculated from three different sequences produced similar classification results, while the T1-weighted contrast-enhanced

series showed slightly better performance than FLAIR or the T1-weighted magnetization prepared gradient echo sequence without contrast enhancement.

Study IV compared axial FLASH and axial MEDIC sequences. The textural data calculated from the FLASH sequence enabled clear discrimination between referents and two groups of athletes, but the MEDIC sequence could not capture between-group differences with strict criteria for significance. Data not presented in Study IV showed that texture data from MEDIC images have the same trend as the FLASH data but with weaker *p*-values for significance.

Table 10 shows a ranking of the sequences used in different materials.

TABLE 10. *Ranking of MRI sequences used in analyses and recommendations for their usage in clinical protocols based on their performance in the present studies. In Study II, the sequences used are marked with ● but could not be compared because the different sequences were used to visualise different anatomical locations.*

MRI sequences used in analyses	Study I NHL	Study II MTBI	Study III MS	Study IV Bone
T1w SE, FAT SAT	2nd choice			
T2w FSE, FAT SAT	1st choice			
T1w MPR		●	2nd choice	
T2w FLAIR		●	2nd choice	
T1w MPR+contrast agent			1st choice	
FLASH				1st choice
MEDIC				-

5.4 The applicability of MRI-based texture analysis in clinical imaging settings

The four studies presented here analyse images of different areas and structures within the body. They are related to different types of medical (studies I–III) and physiological (Study IV) conditions. Table 1 summarises the features of the data. Table 11 addresses the specific study questions and the overall performance from a clinical perspective.

TABLE 11. *Specific study questions and overall performance of the texture analysis applications in studies I–IV.*

Study questions and overall performance	**Study I NHL**	**Study II MTBI**	**Study III MS**	**Study IV Bone**
Detection of visible lesions			●	
Detection of non-visible changes	●	●	●	●
Analysis of freehand and fixed-size ROIs			●	
Analysis of ROI placement		●	●	
Analysis of image sequences for TA	●		●	●
Overall performance of TA in addressing the clinical question	**poor**	**moderate**	**good**	**good**

6. DISCUSSION

6.1 Effectiveness of texture analysis for the characterisation of visible lesions on normal-appearing tissue

In the literature, texture analyses for the differentiation of normal tissue from pathological focal lesions have achieved very good classification results. In Study III, imaging was performed according to the hospital's clinical protocol for neuroinflammatory disease imaging, thus providing a strong clinical basis for the texture analysis. The results demonstrated the accurate classification of MS plaques from white matter and lesion-adjacent normal-appearing white matter by TA on data from three sequences. This strengthens the results recently obtained in the field of MRI TA on MS (Zhang et al., 2008). The results show that TA based on statistical, auto-regressive-model and wavelet-derived parameters achieve excellent discrimination between different tissues of interest. Because these lesions have different micro-texture appearances relative to normal tissues, quantitative discrimination using TA is effective.

6.2 Effectiveness of texture analysis for the detection of non-visible changes in tissues

Lymphoma response to chemotherapy treatment was evaluated in Study I. The lymphoma mass response to the treatment was controlled by early lesion volume calculations from images at the diagnostic stage compared to their volumes after the first treatment. The volume evaluation showed lymphoma mass reductions in all patients, indicating good early treatment response. The texture analysis did not show similarly clear changes in tissue microstructure within the same time interval, but in a comparison between the diagnostic stage and the second treatment evaluation stage, the power of texture parameters to classify changes was increased. The classification accuracy might have been better if fixed acquisition protocols

had been used for imaging. However, for clinical use, treatment-related textural changes in lymphoma masses should be detected as early as possible, ideally at the first response evaluation, to give clinicians the most timely information about treatment effectiveness. Other limitations of this study include its small sample size and the lack of healthy control tissue. The usage of healthy referents' lymph nodes as reference tissue for lymphoma masses was withdrawn in the initial phase of setting up the TA study protocol because the estimated size of healthy lymph nodes would not have been sufficient for accurate manual segmentation (i.e., ROI drawing) or for texture calculation. However, these MR images on treatment response evaluation represent the true clinical imaging practice at the time of data collection (2002-2005) in Tampere University Hospital, and the extracted textural properties of the lymphoma masses demonstrated relevant changes. This can be seen as an encouraging start for further studies on larger cohort sizes using present-day imaging processes to assess the impact of TA as an adjuvant tool in therapy response evaluation and therapeutic decision making.

Imaging symptomatic mild traumatic brain injury patients may reveal only normal findings in CT and MRI, despite the presence of small injuries in the brain that result in neuropsychological findings. Study II focused on texture analysis of the visually normal MRI scans of MTBI patients and their healthy referents. Inter-hemisphere differences in texture appearance in the mesencephalon and intra- and inter-hemisphere differences in white matter were detected in MTBI patients. Also anatomical parts of the corpus callosum differed from each other. This likely reflects that the anatomical parts of the corpus callosum have different physiological functions. In addition, the density of the white matter tracts differs in the different parts of the corpus callosum. As a first approach to detect mild traumatic changes in cerebral tissue by means of texture analysis, there were certain challenges. In this study, no clinical information about patient symptoms was provided to correlate with image analysis or to suggest specific brain locations that should be searched for traumatic changes. However, texture analysis based on normal clinical imaging procedures was able to detect changes associated with traumatic injury in cerebral tissue. Future research projects should be dedicated to understanding injury-related changes in TA of different parts of the corpus callosum and white matter locations, as well as investigating their correlation with neuropsychological findings. In the initial stages of MTBI, TA could be used as an additional tool to analyse cases with normal-appearing conventional MRI.

In Study III, the differentiation between NAWM and WM was evaluated. Depending on the threshold value, correct classification of 85% in FLAIR images can be categorized as moderate performance, indicating that WM near MS focal lesions has a somewhat different textural appearance from WM apart from the lesions. This result is congruent with the recent results published by Zhang et

al. (2008). It should be considered whether the classification accuracy could be enhanced by the use of new imaging sequences, specific texture analysis or classification methods. The lack of a control group is a limitation of this study, particularly when focusing on non-visible changes. A healthy control group would have been useful in strengthening the results in classification of normal and normal-appearing white matter and also could have increased the sample size for intra-tissue comparisons, which will be discussed in 6.3.2.

Very little is known about the exercise load-related textural changes that occur in trabecular bone. Study IV was performed using a clinical scanner with two commonly used sequences, and co-occurrence matrix-based texture features were calculated from a large study population of different types of athletes and their referents. Texture analysis successfully identified differences between two groups of top-level female athletes (odd-impact and high-magnitude) and the normally exercising referents. These findings represent subtle changes emerging from the size of single trabeculae in the bone. Limited spatial resolution is a known disadvantage of this clinical imaging method, but in the light of these results and those of a recent study (Tameem et al., 2007), even normal clinical resolution images may capture textural features that reflect trabecular architecture and thus provide a non-ionising method for assessing bone structure. However, additional studies should be carried out to validate this method.

6.3 Comparison of ROI setting and imaging sequences for texture analysis protocols

6.3.1 Regions of Interest (ROI)

Quantitative analyses may be performed with manual, semi-automated or automated applications. The manual or semi-automated phase of data collection mainly concerns ROI drawing. Depending on the study questions and materials as well as the algorithm, automated methods can sometimes perform this task accurately and successfully. Despite the substantial advances in automated methods, there is still a need for the radiologist's learned professional skill in visually evaluating normal and abnormal findings, and manual or semi-automated applications may outperform automated processes. It should be taken into consideration that applications based on the manual definition of areas are dependent on the expertise of the performer, as well as the clinical complexity of the materials may vary. The current literature contains many examples of fixed-size ROIs as well as freehand-drawn ROIs; however comparisons of

the manual methods of ROI placement in MRI TA have not been examined. The topic of ROI drawing is relevant from both a scientific and clinical point of view. Study III showed that freehand-drawn ROIs of MS lesions produce somewhat better differentiation from WM than do fixed-size ROIs. However, when between anatomical levels and slice-to-slice variation was investigated, the textural appearance of freehand-drawn ROIs differed in more parameters than did fixed-size ROIs. Thus, standard size ROI boxes are more reproducible than manually defined freehand ROIs. On the other hand, the benefit of manually defined freehand ROI is that it avoids pixels representing surrounding tissues. Standard size ROI box may overlap with neighbouring tissue, thus incorporating partial volume pixels or even whole pixels from adjacent tissues in the calculated parameter values. Focal lesions can often be visually detected based on grey level contrast and appearance of the lesion and normal tissues. Therefore, the placement of ROIs for analyses with visual inspection-based manual methods is quite straightforward for users with clinical experience, and the usage of automated segmentation methods can be considered as well. However, for certain clinical applications, it may be faster and easier to place pre-defined fixed size ROI boxes on appropriate structures than to trace tumour or lesion borders, particularly in cases of diffuse changes caused by disease or lesions with indistinct transitions to normal-appearing tissues.

6.3.2 Selection of images for analyses

In Studies II and III, several anatomical locations for ROIs were considered. Study III tested a protocol that included two anatomical levels based on anatomical landmarks and clinical knowledge of common sites for MS plaque appearance. Texture information calculated from two anatomical levels from each sequence lead to similar classification results for white matter/MS plaque tissue pairs. When anatomical levels and three sequential image slices from each level were compared with intra-tissue calculations, fixed-size ROIs of different tissues lead to uniform results, and a few parameters exhibited differences between anatomical levels. The mean percentages of a total of 280 parameters with no statistically significant variation between image slices were at least 90%.

The image selection analysis in Study II focused on healthy controls, and 277 texture parameters were investigated. When interhemispheric differences in white matter were investigated, 95% of parameters were not significantly different between hemispheres. Three anatomical parts of the corpus callosum (sagittal view) were precisely equal, with only 1-2% parameters differing, but parameters calculated from the mesencephalon showed a moderate difference between the left

and right sides. These results indicate that the intracranial tissues and structures investigated with fixed size ROIs are consistent with respect to anatomical level changes. This provides the clinical operator some freedom for slice and ROI selection. However, careful attention should be paid to location selection, and the microstructure underlying homogenous-appearing tissue in image should be considered. However, if the study protocol leaves some freedom for selecting ROI locations, it is preferable for ROIs to be drawn with a uniform method to avoid unnecessary variation.

6.3.3 Selection of sequences for analyses

In Study I, textural changes in lymphoma masses were detected better with T2-weighted image data in the most prominent comparison: pre-treatment stage vs. second treatment evaluation. It should be noted that there were certain differences in acquisition parameters between patients that may have masked some subtle similarity in images within groups, although TA studies on variable acquisition properties have reported successful (Juntu et al., 2010; Herlidou-Meme et al., 2003). No contrast enhancement media was included in the sequences used for TA, so it remains to be investigated if contrast enhancement may provide any additional information on lymphoma texture.

In Study III, texture information calculated from three different sequences lead to similar classification results. However, between the two T1-weighted series collected, the contrast-enhanced series performed slightly better than the series without and also performed better than the T2-weighted FLAIR.

Study IV compared the performance of axial FLASH and MEDIC series. The textural data calculated from FLASH images discriminated between referents and two groups of athletes with high accuracy, while textural data based on MEDIC failed to do so with strict criteria for significance.

In general, in the light of the recent studies described in the literature review (2.4) and those included in this thesis, a wide variety of imaging sequences have been used for texture analysis with promising results. The selection of imaging sequence is always driven by the clinical imaging question; however, as seen in these studies, some sequences are more suitable than others for detecting textural changes.

6.4 Applicability of MRI-based texture analysis in clinical imaging settings

Texture analysis is based on pixels or voxels, the smallest elements in an image. Visual inspection is not well capable of detecting and differentiating between all of the complex textural features that can be formed by these small elements. The current literature, including the results of this study, has proven that MRI data of different tissues, organs and pathologies contain texture features that can be detected with several mathematical methods. These features provide clinical radiologists with a potential quantitative means increasing the specificity and sensitivity of primary diagnostics and in disease follow-up. The investigations presented in this study are based on routine clinical imaging protocols with commonly available 1.5 T scanners. The trend in clinically routine imaging can also be seen in recent publications, where studies performed at 3.0 T are increasingly performed in addition to the most common field strength of 1.5 T.

In Study I, there were variations in acquisition parameters due to the clinical status of the patients. Despite this, moderately successful overall classification could still be achieved. Furthermore, two recent studies on soft tissue masses were performed with some variations in acquisition parameters with promising results (Mayerhoefer et al., 2008; Juntu et al., 2010). A multicentre study on intracranial tumours by Herlidou et al. (Herlidou-Meme et al., 2003) also showed that image sets with acquisition variation could be suitable for texture analysis. Mayerhoefer et al. discovered variations in acquisition parameters and stated that as long as spatial resolution is sufficiently high, clinically feasible variations in acquisition parameters have little effect on classification results (Mayerhoefer et al., 2009b). These results indicate that images acquired with different parameters or in different centres are not inappropriate for texture analysis.

In imaging certain diseases and organs, many imaging centres have fixed MRI protocols that may also be used for quantitative image analyses, as was the case for the studies II–III presented here.

Study II demonstrated the potential of combining several texture parameters to detect subtle, diffuse changes possibly related to mild traumatic brain injury. The detection and assignment of the traumatic changes is clinically important, and this initial approach should be further verified to determine the clinical relevance of different magnitudes of textural changes. MRI texture analysis for detecting non-visible traumatic changes could be used in combination with clinical tests or other advanced imaging methods, such as DTI, to estimate the injury load in MTBI, especially in the patient group for which conventional scans remain negative. However, more specific studies and application development must be

conducted before this kind of computer-aided diagnosis application can be used in a clinical environment. The other neuroradiological study, III, concentrated on multiple sclerosis, with clear success. In the future, it would be interesting to apply texture calculation over ROIs covering all normal-appearing white matter in a 2D image slice or all white matter volume in a 3D analysis and to investigate how sensitive this method is in detecting subtle changes in a larger ROI. In this study, analyses were run in a 2D environment because the software used in the three studies was implemented in 2D analyses. Furthermore, radiologists generally conduct visual inspection of MRI image data by scrolling through a series of 2D images, so this approach is familiar to clinicians. The present version of MaZda software is implemented in both 2D and 3D analyses. There are also several 3D applications that have been reported to perform texture-based classification and tissue characterisation with equal or superior results to 2D methods (Mahmoud-Ghoneim et al., 2003; Georgiadis et al., 2009).

Study IV used skeletal MRI and focused on small anatomical details in the structure of trabecular bone. With a large cohort size, it was possible to show physiological load-related changes in the femoral necks of two athlete groups. This particular study was part of a wider project (Nikander et al., 2009) on detecting sports-related positive changes in bone strength and offers new insight on MRI as a non-ionising imaging method for population screening. The ability to conduct quantitative image analysis further increases the applicability of this method.

Evaluating the performance of the present studies is somewhat challenging because to best of my knowledge, this is the first data on lymphoma treatment evaluation based on MRI texture analysis; the MTBI and trabecular bone study settings are also experimental and do not have precedents in the literature. Only the MS data may be compared to reference studies on the same study question.

In summary, in this study, texture analysis has been performed in order to obtain clinically important information on diffuse changes that are difficult to detect by qualitative visual inspection and to determine the tissue characterisation power of texture parameters in visually separable focal structures. A large collection of texture parameters based on histogram, autoregressive model, wavelet, and gradient-, run-length- and co-occurrence matrices were calculated from 1.5 T image data. The combined results of these studies provide promising evidence of the applicability of texture analysis for clinical imaging as well as a guide to the next steps of developing a clinical analysis protocol. The capability of TA to detect and characterise pathological and physiological changes in tissues has been shown in this study, as well as in other recent studies. However, it is also important to focus on other imaging and clinical findings, including histopathological findings of the patients and normal control populations whenever possible, to define normal threshold values for texture parameters.

7. CONCLUSIONS

1) The effectiveness of texture analysis for the characterisation of focal, visible lesions on normal-appearing tissue was investigated in multiple sclerosis patients in Study III. Texture analysis based on statistical, autoregressive model and wavelet texture parameters derived from MRI data were able to discriminate focal MS lesions from white matter and normal-appearing white matter with excellent accuracy and high statistical significance. As performed, this texture analysis method is suitable for similar tasks.

2) The effectiveness of texture analysis for the detection of non-visible changes in tissues was investigated in Studies I, II, III and IV. The performance varied somewhat between the studies. However, non-visible diffuse changes were detected in all studies, and as Studies I, II and IV represent experimental studies in their fields, the texture analysis method shows clear potential for detecting subtle non-visible changes. The challenge for future research remains to validate these results in larger and prospective clinical trials.

3) A comparison of freehand-drawn and fixed-size ROIs in Study III (MS lesions) revealed that freehand-drawn ROIs were better able to differentiate between tissues. Meanwhile, fixed-size ROIs provided better reproducibility. In Studies II and III, analyses of ROI placement in different image slices originating from different anatomical locations of the brain showed no significant differences in the cerebral structures and tissues investigated.

   According to the present study, the performance of data originating from different imaging sequences on texture analysis varied to some extent. T2-weighted series performed best in the NHL treatment response evaluation (I); T1-weighted MPR with contrast enhancement produced the best classification in the MS Study (III); and FLASH images highlighted the load-specific changes of femoral neck trabecular bone (IV).

4) The overall applicability of MRI-based texture analysis in common clinical imaging settings and the selected study materials was acceptable. In light of this study, routine clinical images are suitable for this kind of quantitative analysis. However, as Studies I, II, and IV are experimental and there are no earlier studies

on the same questions performed by other groups, information on the level of expected differences between tissues and lesions investigated is lacking, and there may be under- or over-detection of the changes. Further validation is needed to verify the utility and normal threshold values of these approaches.

ACKNOWLEDGEMENTS

The work presented in this thesis was carried out at the Department of Radiology, Medical Imaging Centre, Tampere University Hospital, Pirkanmaa Hospital District; University of Tampere Medical School, and the Department of Biomedical Engineering, Tampere University of Technology during the years 2005–2011.

I want to express my deepest gratitude to my supervisors, Professor Seppo Soimakallio and Docent Prasun Dastidar for providing excellent research facilities and invaluable guidance and support at all stages of this study.

I am also very grateful to Professor Hannu Eskola for continuous encouragement and supervision.

I wish to thank Docents Harri Sievänen and Pertti Ryymin and my supervisory board members, Professors Juha Öhman, Irina Elovaara, Pirkko-Liisa Kellokumpu-Lehtinen and Docent Ritva Järvenpää, for their patient guidance and friendly help with my study.

I likewise want to express my gratitude to PhD Riku Nikander, all co-authors of the original articles cited in this thesis and present and past members of the TIC-research team for their professional help.

I thank the official reviewers, Professors Ritva Vanninen and Andrzej Materka, for their excellent commentary on this thesis.

I wish to give very special thanks to my great friends and colleagues, MSc Kirsi Holli, MSc Maija Rossi and MSc Minna Sikiö for all the time at the Komentokeskus and after science as well – without your friendship this work would have been so much less fun.

I thank MSc Tiina Luukkaala and MSc Mika Helminen for their help with statistical work.

Warm thanks are due to Ms Marjut Keskivinkka and the personnel of the Department of Radiology, Medical Imaging Centre and all participating departments for their assistance with the data collection and radiological imaging.

I greatly appreciate the willingness of all the voluntary participants in these studies.

I wish to thank Professors Leena Lindgren and Arvi Yli-Hankala, and all my colleagues and the entire personnel in the Department of Anaesthesiology at Tampere University Hospital and District Hospital of Valkeakoski for their support and encouraging interest in my study.

I would like to thank all my friends for fun and relaxing times; being there in all weather and situations during the years that have passed while working on this thesis – it is impossible to thank all of you by name, but to mention a few families and groups, I would like to thank The Cape Horn Sailing Crew of TS Helena, the sailing crews of SY Vahine and SY Anna Nimue, Kulttuurikerho, the Hakamäki family, the Mittilä family, the Koskelainen family and the Mättö&Haajanen family. To those who are not mentioned, that does not mean that I have forgotten you!

Finally, I owe the deepest gratitude to my family for their understanding and support. I would like to thank my mother, Kaija, for providing a loving home; and I thank my mother, my brother Martin and his wife Katri for their encouragement throughout these years. I am especially grateful to my dear daughters Ronja and Sorje for all of their patience and love.

This study was supported by the Medical Research Fund of the Pirkanmaa Hospital District and the Finnish Medical Society Duodecim.

Tampere, August 2011

Lara Harrison

REFERENCES

Adams, JE. (2009): Quantitative computed tomography. European Journal of Radiology 71: 415–424.

Aikuisiän aivovammat. Current Care guideline. (2008): Working group set up by the Finnish Medical Society Duodecim and the Finnish Societies of Neurology, Neurosurgery, Neuropsychology, Insurance medicine, and Physical medicine and rehabilitation. Helsinki: Finnish Medical Society Duodecim. Available online at: www.kaypahoito.fi Accessed 7/2011.

Allen RL and Mills DW. (2004): Signal analysis: Time, frequency, scale, and structure [E-book]. John Wiley & Sons, pp. 500.

Ansell SM and Armitage J. (2005): Non-Hodgkin lymphoma: Diagnosis and treatment. Mayo Clinic Proceedings 80: 1087–1097.

Antel SB, Collins DL, Bernasconi N, Andermann F, Shinghal R, Kearney RE, Arnold DL, and Bernasconi A. (2003): Automated detection of focal cortical dysplasia lesions using computational models of their MRI characteristics and texture analysis. Neuroimage 19: 1748–1759.

Bernasconi A, Antel SB, Collins DL, Bernasconi N, Olivier A, Dubeau F, Pike GB, Andermann F, and Arnold DL. (2001): Texture analysis and morphological processing of magnetic resonance imaging assist detection of focal cortical dysplasia in extra-temporal partial epilepsy. Annals of Neurology 49: 770–775.

Blake GM and Fogelman I. (2010): An Update on Dual-Energy X-Ray Absorptiometry. Seminars in Nuclear Medicine 40:62–73.

Bloch F. (1952): The principle of nuclear induction. http://nobelprize.org/nobel_prizes/physics/laureates/1952/bloch-lecture.pdf Nobel Lecture, Physics, December 11, 1952. Accessed 3/2011.

Bonilha L, Kobayashi E, Castellano G, Coelho G, Tinois E, Cendes F, and Li LM. (2003): Texture analysis of hippocampal sclerosis. Epilepsia 44: 1546–1550.

Brown R, Zlatescu M, Sijben A, Roldan G, Easaw J, Forsyth P, Parney I, Sevick R, Yan E, Demetrick D, Schiff D, Cairncross G, and Mitchell R. (2008): The use of magnetic resonance imaging to noninvasively detect genetic signatures in oligodendroglioma. Clinical Cancer Research 14: 2357–2362.

Bydder GM and Chung CB. (2009): Magnetic resonance imaging of short T2 relaxation components in the musculoskeletal system. Skeletal Radiology 38: 201–205.

Carroll LJ, Cassidy JD, Holm L, Kraus J, and Coronado VG. (2004): Methodological issues and research recommendations for mild traumatic brain injury: The WHO collaborating centre task force on mild traumatic brain injury. Journal of Rehabilitation Medicine Suppl: 113–125.

Castellano G, Bonilha L, Li LM, and Cendes F. (2004): Texture analysis of medical images. Clinical Radiology 59: 1061–1069.

Chien YP and Fu K. (1974): Recognition of X-ray picture patterns. Systems, Man and Cybernetics, IEEE Transactions on SMC 4: 145–156.

Collewet G, Strzelecki M, and Mariette F. (2004): Influence of MRI acquisition protocols and image intensity normalization methods on texture classification. Magnetic Resonance Imaging 22: 81–91.

COST B11. (2001): COST B11 Quantitation of magnetic resonance image texture. http://phase.pki.uib.no Accessed 3/2011.

COST B21. (2008): COST B21 physiological modelling of MR image formation. http://www.die.upm.es/costb21/ Accessed 3/2011.

De Nunzio G, Pastore G, Donativi M, Castellano A, and Falini A. (2011): A CAD system for cerebral glioma based on texture features in DT-MR images. Nuclear Instruments and Methods in Physics Research Section A: Accelerators, Spectrometers, Detectors and Associated Equipment 648: Suppl. 1: S100–S102.

Eisenhauer EA, Therasse P, Bogaerts J, Schwartz LH, Sargent D, Ford R, Dancey J, Arbuck S, Gwyther S, Mooney M, Rubinstein L, Shankar L, Dodd L, Kaplan R, Lacombe D, Verweij J. (2008): New response evaluation criteria in solid tumours: Revised RECIST guideline (version 1.1). European Journal of Cancer 45 : 228–247.

Freeborough PA and Fox NC. (1998): MR image texture analysis applied to the diagnosis and tracking of Alzheimer's disease. IEEE Transactions on Medical Imaging 17: 475–479.

Galea I, Freedman MS, Thompson EJ. (2011): Cerebrospinal fluid analysis in the 2010 revised McDonald's multiple sclerosis diagnostic criteria. Annals of Neurology 70: 183.

Galloway MM. (1975): Texture analysis using run lengths. Computer Graphics and Image Processing 4: 172–179.

Georgiadis P, Cavouras D, Kalatzis I, Glotsos D, Athanasiadis E, Kostopoulos S, Sifaki K, Malamas M, Nikiforidis G, and Solomou E. (2009): Enhancing the discrimination accuracy between metastases, gliomas and meningiomas on brain MRI by volumetric textural features and ensemble pattern recognition methods. Magnetic Resonance Imaging 27: 120–130.

Gibbs P and Turnbull LW. (2003): Textural analysis of contrast-enhanced MR images of the breast. Magnetic Resonance in Medicine 50: 92–98.

Goutsias J, Vincent L, and Bloomberg DS. (2000): Mathematical morphology and its applications to image and signal processing. Kluwer Academic Publishers, pp. 456.

Hájek M, Dezortová M, Materka A, and Lerski R. (2006): Texture analysis for magnetic resonance imaging. Prague, Czech Republic: Med4publishing s.r.o.; 234 p.

Hampson FA and Shaw AS. (2008): Response assessment in lymphoma. Clinical Radiology 63: 125–135.

Haralick RM. (1979): Statistical and structural approaches to texture. Proceedings of the IEEE 67: 786–804.

Haralick RM, Shanmugam K, and Dinstein I. (1973): Textural features for image classification. Systems, Man and Cybernetics, IEEE Transactions on SMC 3: 610–621.

Herlidou S, Grebe R, Grados F, Leuyer N, Fardellone P, and Meyer M. (2004): Influence of age and osteoporosis on calcaneus trabecular bone structure: A preliminary in vivo MRI study by quantitative texture analysis. Magnetic Resonance Imaging 22: 237–243.

Herlidou-Même S, Constans JM, Carsin B, Olivie D, Eliat PA, Nadal-Desbarats L, Gondry C, Le Rumeur E, Idy-Peretti I, and de Certaines JD. (2003): MRI texture analysis on texture test objects, normal brain and intracranial tumors. Magnetic Resonance Imaging 21: 989–993.

Holli K, Lääperi A-, Harrison L, Luukkaala T, Toivonen T, Ryymin P, Dastidar P, Soimakallio S, and Eskola H. (2010): Characterization of breast cancer types by texture analysis of magnetic resonance images. Academic Radiology 17: 135–141.

Jafari-Khouzani K, Elisevich K, Patel S, Smith B, and Soltanian-Zadeh H. (2010): FLAIR signal and texture analysis for lateralizing mesial temporal lobe epilepsy. Neuroimage 49: 1559–1571.

Jain AK. (1989): Fundamentals of digital image processing. Englewood Cliffs (NJ): Prentice-Hall, USA, pp. 569.

Jirák D, Dezortová M, Taimr P, and Hájek M. (2002): Texture analysis of human liver. Journal of Magnetic Resonance Imaging 15: 68–74.

Julesz B, Gilbert EN, Shepp LA, and Frisch HL. (1973): Inability of humans to discriminate between visual textures that agree in second order statistics: Revisited. Perception 2: 391–405.

Juntu J, Sijbers J, De Backer S, Rajan J, and Van Dyck D. (2010): Machine learning study of several classifiers trained with texture analysis features to differentiate benign from malignant soft-tissue tumors in T1-MRI images. Journal of Magnetic Resonance Imaging 31: 680–689.

Kaizer H. (1955): A quantification of textures on aerial photographs. Technical Note 121, AD 69484, Boston University Research Laboratory.

Kassner A, Liu F, Thornhill RE, Tomlinson G, and Mikulis DJ. (2009): Prediction of hemorrhagic transformation in acute ischemic stroke using texture analysis of postcontrast T1-weighted MR images. Journal of Magnetic Resonance Imaging 30: 933–941.

Kassner A and Thornhill RE. (2010): Texture analysis: A review of neurologic MR imaging applications. American Journal of Neuroradiology 31: 809–816.

Kato H, Kanematsu M, Zhang X, Saio M, Kondo H, Goshima S, and Fujita H. (2007): Computer-aided diagnosis of hepatic fibrosis: Preliminary evaluation of MRI texture analysis using the finite difference method and an artificial neural network. American Journal of Roentgenology 189: 117–122.

Kilsdonk ID, Barkhof F, and Wattjes MP. (2011): 2010 revisions to McDonald criteria for diagnosis of multiple sclerosis: Impact of 3-tesla magnetic resonance imaging. Annals of Neurology 70: 182–183.

Kwee TC, Kwee RM, and Nievelstein RA (2008): Imaging in staging of malignant lymphoma: a systematic review. Blood 111:504–516.

Lahtinen M. (2009): Description of texture analysis algorithms for medical images. Tampere University of Technology, MSc Thesis.

Lauterbur PC. (2003): All science is interdisciplinary – from magnetic moments to molecules to men. Nobel lecture, Medicine, December 8, 2003. http://nobelprize.org/nobel_prizes/medicine/laureates/2003/lauterbur-lecture.pdf Accessed 3/2011.

Lee FK-h, King AD, Ma BB-Y, and Yeung DK-w. (2011): Dynamic contrast enhancement magnetic resonance imaging (DCE MRI) for differential diagnosis in head and neck cancers. European Journal of Radiology. Article in press. doi:10.1016/j.ejrad.2011.01.089

Mahmoud-Ghoneim D, Toussaint G, Constans J, and de Certaines JD. (2003): Three dimensional texture analysis in MRI: A preliminary evaluation in gliomas. Magnetic Resonance Imaging 21: 983–987.

Mandelbrot BB. (1977): Fractals: Form, chance and dimension. Freeman, San Francisco, CA, USA, pp. 365.

Mansfield P. (2003): Snap-shot MRI. Nobel lecture, Medicine, December 8, 2003. http://nobelprize.org/nobel_prizes/medicine/laureates/2003/mansfield-lecture.pdf Accessed 3/2011.

Manske SL, Macdonald HM, Nishiyama KK, Boyd SK, and McKay HA. (2010): Clinical tools to evaluate bone strength. Clinical Reviews in Bone and Mineral Metabolism 8: 112–134.

Materka A and Strzelecki M. (1998): Texture analysis methods—a review. Technical University of Lodz, Poland: COST B11 Report.

Materka A, Strzelecki M, and Szczypiński P. (2006): MaZda manual 2006. http://www.eletel.p.lodz.pl/mazda/download/mazda_manual.pdf Accessed 3/2011.

Mathias JM, Tofts PS, and Losseff NA. (1999): Texture analysis of spinal cord pathology in multiple sclerosis. Magnetic Resonance in Medicine 42: 929–935.

Mayerhoefer ME, Breitenseher M, Amann G, and Dominkus M. (2008): Are signal intensity and homogeneity useful parameters for distinguishing between benign and malignant soft tissue masses on MR images?: Objective evaluation by means of texture analysis. Magnetic Resonance Imaging 26: 1316–1322.

Mayerhoefer ME, Schima W, Trattnig S, Pinker K, Berger-Kulemann V, and Ba-Ssalamah A. (2010): Texture-based classification of focal liver lesions on MRI at 3.0 Tesla: A feasibility study in cysts and hemangiomas. Journal of Magnetic Resonance Imaging 32: 352–359.

Mayerhoefer ME, Szomolanyi P, Jirak D, Berg A, Materka A, Dirisamer A, and Trattnig S. (2009a): Effects of magnetic resonance image interpolation on the results of texture-based pattern classification a phantom study. Investigative Radiology 44: 405–411.

Mayerhoefer ME, Szomolanyi P, Jirak D, Materka A, and Trattnig S. (2009b): Effects of MRI acquisition parameter variations and protocol heterogeneity on the results of texture analysis and pattern discrimination: An application-oriented study. Medical Physics 36: 1236–1243.

MaZda. MaZda program. http://www.eletel.p.lodz.pl/programy/cost/progr_mazda_eng.html Accessed 3/2011.

McDonald WI, Compston A, Edan G, Goodkin D, Hartung HP, Lublin FD, McFarland HF, Paty DW, Polman CH, Reingold SC, Sandberg-Wollheim M, Sibley W, Thompson A, van den Noort S, Weinshenker BY, and Wolinsky JS. (2001): Recommended diagnostic criteria for multiple sclerosis: Guidelines from the international panel on the diagnosis of multiple sclerosis. Annals of Neurology 50: 121–127.

Nie K, Chen J, Yu HJ, Chu Y, Nalcioglu O, and Su M. (2008): Quantitative analysis of lesion morphology and texture features for diagnostic prediction in breast MRI. Academic Radiology 15: 1513–1525.

Nikander R, Kannus P, Dastidar P, Hannula M, Harrison L, Cervinka T, Narra NG, Aktour R, Arola T, Eskola H, Soimakallio S, Heinonen A, Hyttinen J, and Sievänen H. (2009): Targeted exercises against hip fragility. Osteoporosis International 20: 1321–1328.

Pentland AP. (1984): Fractal-based description of natural scenes. Pattern Analysis and Machine Intelligence, IEEE Transactions on 6: 661–674.

Perrone A, Guerrisi P, Izzo L, D'Angeli I, Sassi S, Mele LL, Marini M, Mazza D, Marini M. (2011): Diffusion-weighted MRI in cervical lymph nodes: differentiation between benign and malignant lesions. European Journal of. Radiology 77: 281–286.

Polman CH, Reingold SC, Banwell B, Clanet M, Cohen JA, Filippi M, Fujihara K, Havrdova E, Hutchinson M, Kappos L, Lublin FD, Montalban X, O'Connor P, Sandberg-Wollheim M, Thompson AJ, Waubant E, Weinshenker B, and Wolinsky JS. (2011): Diagnostic criteria for multiple sclerosis: 2010 revisions to the McDonald criteria. Annals of Neurology 69:292–302.

Polman CH, Reingold SC, Edan G, Filippi M, Hartung H-, Kappos L, Lublin FD, Metz LM, McFarland HF, O'Connnor PW, Sandberg-Wollheim M, Thompson AJ, Weinshenker BG, and Wolinsky JS. (2005): Diagnostic criteria for multiple sclerosis: 2005 revisions to the "McDonald criteria". Annals of Neurology 58: 840–846.

Purcell EM. (1952): Research in nuclear magnetism. Nobel lecture, Physics, December 11, 1952. http://nobelprize.org/nobel_prizes/physics/laureates/1952/purcell-lecture.pdf Accessed 3/2011.

Qian S and Chen D. (1993): Discrete Gabor transform. Signal Processing, IEEE Transactions on 41: 2429–2438.

Russ JC. (2002): The image processing handbook 4th Ed. CRC Press LLC, pp. 732.

Rutgers DR, Toulgoat F, Cazejust J, Fillard P, Lasjaunias P, and Ducreux D. (2008): White matter abnormalities in mild traumatic brain injury: A diffusion tensor imaging study. American Journal of Neuroradiology 29: 514–519.

Sankar T, Bernasconi N, Kim H, and Bernasconi A. (2008): Temporal lobe epilepsy: Differential pattern of damage in temporopolar cortex and white matter. Human Brain Mapping 8: 931–944.

Stockwell RG, Mansinha L, and Lowe RP. (1996): Localization of the complex spectrum: The S transform. Signal Processing, IEEE Transactions on 44: 998–1001.

Szczypiński PM, Strzelecki M, Materka A, and Klepaczko A. (2009): MaZda-A software package for image texture analysis. Computer Methods and Programs in Biomedicine 94: 66–76.

Tameem HZ, Selva LE, and Sinha US. (2007): Texture measure from low resolution MR images to determine trabecular bone integrity in osteoporosis. Engineering in Medicine and Biology Society, 2007 EMBS 2007 29th Annual International Conference of the IEEE: 2027–2030.

Theocharakis P, Glotsos D, Kalatzis I, Kostopoulos S, Georgiadis P, Sifaki K, Tsakouridou K, Malamas M, Delibasis G, Cavouras D, and Nikiforidis G. (2009): Pattern recognition system for the discrimination of multiple sclerosis from cerebral microangiopathy lesions based on texture analysis of magnetic resonance images. Magnetic Resonance Imaging 27: 417–422.

Therasse P, Arbuck SG, Eisenhauer EA, Wanders J, Kaplan RS, Rubinstein L, Verweij J, Van Glabbeke M, Van Oosterom AT, Christian MC, and Gwyther SG. (2000): New guidelines to evaluate the response to treatment in solid tumors. Journal of National Cancer Institute 92: 205–216.

Therasse P, Eisenhauer EA, and Verweij J. (2006): RECIST revisited: A review of validation studies on tumour assessment. European Journal of Cancer 42: 1031–1039.

Torabi M. (2006): Discrimination between Alzheimer's disease and control group in MR-images based on texture analysis using artificial neural network. Biomedical and Pharmaceutical Engineering, 2006 ICBPE 2006 International Conference on: 79–83.

Tuceryan M. and Jain AK. (1998): Texture Analysis. In: The Handbook of Pattern Recognition and Computer Vision, World Scientific Publishing Co, USA, pp. 207–248.

WHO handbook for reporting results of cancer treatment (1979). Geneva, Switzerland: World Health Organization Offset Publication No. 48.

Yu O, Mauss Y, Namer IJ, and Chambron J. (2001): Existence of contralateral abnormalities revealed by texture analysis in unilateral intractable hippocampal epilepsy. Magnetic Resonance Imaging 19: 1305–1310.

Zacharaki EI, Wang S, Chawla S, Yoo DS, Wolf R, Melhem ER, and Davatzikos C. (2009): Classification of brain tumor type and grade using MRI texture and shape in a machine learning scheme. Magnetic Resonance in Medicine 62: 1609–1618.

Zhang J, Tong L, Wang L, and Li N. (2008): Texture analysis of multiple sclerosis: A comparative study. Magnetic Resonance Imaging 26: 1160–1166.

Zhang Y, Zhu H, Mitchell JR, Costello F, and Metz LM. (2009): T2 MRI texture analysis is a sensitive measure of tissue injury and recovery resulting from acute inflammatory lesions in multiple sclerosis. Neuroimage 47: 107–111.

APPENDIX

Histogram-based features

Normalized histogram vector $p(i),\ i = 1, 2, .., N,$

N number of intensity levels

Mean:

$$\mu = \sum_{i=1}^{N} ip(i)$$

Variance:

$$\sigma^2 = \sum_{i=1}^{N} (i - \mu)^2 p(i)$$

Skewness:

$$\mu_3 = \sigma^{-3} \sum_{i=1}^{N} (i - \mu)^3 p(i)$$

Kurtosis:

$$\mu_4 = \sigma^{-4} \sum_{i=1}^{N} (i - \mu)^4 p(i) - 3$$

Wavelet parameters

Discrete wavelet transformation is computed with a filter a cascade.

Only subband energy is calculated on different scales.

Energy of the scale subband:

$$E_{subband,scale} = \sum_{x,y \in ROI} \left(i_{x,y}^{subband} \right)^2 / n$$

Gradient-based features

Region of interest is *ROI*

Neighborhood of image pixel $x(i, j)$:

$$\begin{matrix} A & B & C & D & E \\ F & G & H & I & J \\ K & L & x(i,j) & N & O \\ P & Q & R & S & T \\ U & V & W & Y & Z \end{matrix}$$

The absolute gradient value ($ABSV(i,j)$) for each pixel calculated for a 5x5 pixel neighborhood is

$$ABSV(i,j) = \sqrt{(W-C)^2 + (O-K)^2}$$

Mean absolute gradient:

$$g_1 = \frac{1}{x(i,j)} \sum_{i,j \in ROI} ABSV(i,j)$$

Variance of absolute gradient:

$$g_2 = \frac{1}{x(i,j)} \sum_{i,j \in ROI} (ABSV(i,j) - g_1)^2$$

Skewness of absolute gradient:

$$g_3 = \frac{1}{(\sqrt{g_2})^3} \frac{1}{x(i,j)} \sum_{i,j \in ROI} (ABSV(i,j) - g_1)^3$$

Kurtosis of absolute gradient:

$$g_4 = \frac{1}{(\sqrt{g_2})^4} \frac{1}{x(i,j)} \sum_{i,j \in ROI} (ABSV(i,j) - g_1)^4 - 3$$

Run-length matrix-based features

Number of grey levels: N_g

Number of runs: N_r

Number of times there is a run of length j having grey level i : $p(i, j)$

Short run emphasis inverse moments:

$$r_1 = \left(\sum_{i=1}^{N_g}\sum_{j=1}^{N_r}\frac{p(i,j)}{j^2}\right) / \sum_{i=1}^{N_g}\sum_{j=1}^{N_r} p(i,j)$$

Long run emphasis moments:

$$r_2 = \left(\sum_{i=1}^{N_g}\sum_{j=1}^{N_r} j^2 p(i,j)\right) / \sum_{i=1}^{N_g}\sum_{j=1}^{N_r} p(i,j)$$

Grey level nonuniformity:

$$r_3 = \left(\sum_{i=1}^{N_g}\left(\sum_{j=1}^{N_r} p(i,j)\right)^2\right) / \sum_{i=1}^{N_g}\sum_{j=1}^{N_r} p(i,j)$$

Run length nonuniformity:

$$r_4 = \left(\sum_{j=1}^{N_r}\left(\sum_{i=1}^{N_g} p(i,j)\right)^2\right) / \sum_{i=1}^{N_g}\sum_{j=1}^{N_r} p(i,j)$$

Fraction of image in runs:

$$r_5 = \sum_{i=1}^{N_g}\sum_{j=1}^{N_r} p(i,j) / \sum_{i=1}^{N_g}\sum_{j=1}^{N_r} jp(i,j))$$

Co-occurrence matrix-derived parameters

'The given image $f(x, y)$ with N_g discrete intensity levels.

The second order histogram is defined as the co-occurrence matrix $P_{d\theta}(i, j)$, where d is distance (d = 1, 2, 3, 4, 5) and θ angle ($\theta = 0, 45^{o}, 90^{o}, 135^{o}$) between two pixels, and where its (i, j)th entry is equal to the number of times that $f(x_1, y_1) = i$ and $f(x_2, y_2) = j$;

$(x_2, y_2) = (x_1, y_1) + (d \cos\theta, d \sin\theta)$.

Total number of neighboring pixels in ROI $R(d, \theta)$.

The (i,j)th entry in a normalized co-occurrence matrix $p(i, j) = P(i, j) / R$.

Marginal-probability matrices

$$p_x(i) = \sum_{j=1}^{N_g} P(i, j),$$

$$p_y(j) = \sum_{i=1}^{N_g} P(i, j).$$

Means of the p_x, p_y are μ_x, μ_y, and standard deviations are σ_x, σ_y.

$$p_{x+y}(k) = \sum_{\substack{i=1 \\ i+j=k}}^{N_g} \sum_{j=1}^{N_g} p(i, j), \quad k = 2, 3, ..., 2N_g$$

$$p_{x-y}(k) = \sum_{\substack{i=1 \\ |i-j|=k}}^{N_g} \sum_{j=1}^{N_g} p(i, j), \quad k = 0, 1, ..., N_g - 1$$

Means of the p_{x+y}, p_{x-y} are μ_{x+y}, μ_{x-y},

and standard deviations are $\sigma_{x+y}, \sigma_{x-y}$.

Angular second moment:

$$f_1 = \sum_{i=1}^{N_g} \sum_{j=1}^{N_g} p(i,j)^2$$

Contrast:

$$f_2 = \sum_{n=0}^{N_g - 1} n^2 \sum_{\substack{i=1 \\ |i-j|=n}}^{N_g} \sum_{j=1}^{N_g} p(i,j)$$

Correlation:

$$f_3 = \left(\sum_{i=1}^{N_g} \sum_{j=1}^{N_g} ijp(i,j) - \mu_x \mu_y \right) / \sigma_x \sigma_y$$

Sum of squares:

$$f_4 = \sum_{i=1}^{N_g} \sum_{j=1}^{N_g} (i - \mu_x)^2 \, p(i,j)$$

Inverse difference moment:

$$f_5 = \sum_{i=1}^{N_g} \sum_{j=1}^{N_g} \frac{1}{1 + (i-j)^2} p(i,j)$$

Sum average:

$$f_6 = \sum_{i=1}^{2N_g} i p_{x+y}(i)$$

Sum variance:

$$f_7 = \sum_{i=1}^{2N_g} (i - f_6)^2 \, p_{x+y}(i)$$

Sum entropy:

$$f_8 = -\sum_{i=1}^{2N_g} p_{x+y}(i) \log(p_{x+y}(i))$$

Entropy:

$$f_9 = -\sum_{i=1}^{N_g} \sum_{j=1}^{N_g} p(i,j) \log(p(i,j))$$

Difference variance:

$$f_{10} = \sum_{i=0}^{N_g - 1} (i - \mu_{x-y})^2 \, p_{x-y}(i)$$

Difference entropy:

$$f_{11} = -\sum_{i=1}^{N_g - 1} p_{x+y}(i) \log(p_{x+y}(i))$$

Autoregressive model (AR) parameters

The given image f is a NxN zero-mean random field,

where f_S is the image intensity at site s.

e_S is independent and identically distributed noise.

σ is the standard deviation of the driving noise e_S. N_S is the neighbourhood of s.

$\theta = [\theta_1, \theta_2, \theta_3, \theta_4]$ is a vector of model parameters.

$\mathbf{w_S} = \text{col}[f_i, i \in N_S]$.

Local neighbourhood of image element f_s

$$\begin{array}{ccccc} O & O & O & O & O \\ O & O^{\theta_2} & O^{\theta_3} & O^{\theta_4} & O \\ O & O^{\theta_1} & O^{s} & O & O \\ O & O & O & O & O \end{array}$$

An AR causal model for f is defined as:

$$f_s = \sum_{r \in N_s} \theta_r f_r + e_s$$

Sum of squared error:

$$\sum_{\mathrm{s}} \mathrm{e}_{\mathrm{s}}^2 = \sum \left(f_s - \hat{\theta} \mathbf{w_s} \right)^2$$

Parameters can be estimated by minimizing the sum of squared error through the following equations:

$$\hat{\theta} = \left(\sum_s \mathbf{w_s} \mathbf{w_s}^T \right)^{-1} \left(\sum_s \mathbf{w_s} f_s \right)$$

$$\sigma^2 = N^{-2} \sum \left(f_s - \hat{\theta} \mathbf{w_s} \right)^2$$

ORIGINAL PUBLICATIONS

Journal of Experimental & Clinical Cancer Research

BioMed Central

Research

Open Access

Non-Hodgkin lymphoma response evaluation with MRI texture classification

Lara CV Harrison*[1,2], Tiina Luukkaala[3,4], Hannu Pertovaara[5], Tuomas O Saarinen[1], Tomi T Heinonen[2,6], Ritva Järvenpää[6], Seppo Soimakallio[1,6], Pirkko-Liisa I Kellokumpu-Lehtinen[1,5], Hannu J Eskola[2,6] and Prasun Dastidar[1,2,6]

Address: [1]Tampere University Medical School, Tampere, Finland, [2]Department of Biomedical Engineering, Tampere University of Technology, Tampere, Finland, [3]Science Center, Pirkanmaa Hospital District, Tampere, Finland, [4]Tampere School of Public Health, University of Tampere, Tampere, Finland, [5]Department of Oncology, Tampere University Hospital, Tampere, Finland and [6]Department of Radiology, Regional Imaging Centre, Pirkanmaa Hospital District, Tampere, Finland

Email: Lara CV Harrison* - lara.harrison@tut.fi; Tiina Luukkaala - tiina.luukkaala@uta.fi; Hannu Pertovaara - hannu.pertovaara@pshp.fi; Tuomas O Saarinen - tuomas.saarinen@uta.fi; Tomi T Heinonen - tomi.heinonen@tut.fi; Ritva Järvenpää - ritva.jarvenpaa@pshp.fi; Seppo Soimakallio - seppo.soimakallio@pshp.fi; Pirkko-Liisa I Kellokumpu-Lehtinen - Pirkko-Liisa.Kellokumpu-Lehtinen@pshp.fi; Hannu J Eskola - hannu.eskola@tut.fi; Prasun Dastidar - prasun.dastidar@pshp.fi

* Corresponding author

Published: 22 June 2009

Journal of Experimental & Clinical Cancer Research 2009, **28**:87 doi:10.1186/1756-9966-28-87

Received: 11 March 2009
Accepted: 22 June 2009

This article is available from: http://www.jeccr.com/content/28/1/87

Abstract

Background: To show magnetic resonance imaging (MRI) texture appearance change in non-Hodgkin lymphoma (NHL) during treatment with response controlled by quantitative volume analysis.

Methods: A total of 19 patients having NHL with an evaluable lymphoma lesion were scanned at three imaging timepoints with 1.5T device during clinical treatment evaluation. Texture characteristics of images were analyzed and classified with MaZda application and statistical tests.

Results: NHL tissue MRI texture imaged before treatment and under chemotherapy was classified within several subgroups, showing best discrimination with 96% correct classification in non-linear discriminant analysis of T2-weighted images.

Texture parameters of MRI data were successfully tested with statistical tests to assess the impact of the separability of the parameters in evaluating chemotherapy response in lymphoma tissue.

Conclusion: Texture characteristics of MRI data were classified successfully; this proved texture analysis to be potential quantitative means of representing lymphoma tissue changes during chemotherapy response monitoring.

Background

Quantitative image analysis may provide new clinically relevant information on the target of interest, constituting a major advantage in clinical work as well as in research. The most significant objectives in quantitative image analysis are to find tissue-characterizing features with biologi-

cal significance and which correlate with pathophysiology detected by other methods, i.e. clinical examination, other imaging modalities and pathological-anatomical diagnosis, and secondly to provide this new information on the properties of tissues to be used alone or in combination with other clinical information allowing more reliable detection of disease and sophisticated tissue classification as a clinical diagnostic and follow-up tool.

Precise and earlier diagnostics and monitoring treatment response are significant both for the individual patient's prognosis and on a larger scale in developing treatment procedures, especially in malignant diseases. Within the research on solid tumors extensive and widely used Response Evaluation Criteria in Solid Tumors (RECIST) Guidelines may be followed to obtain intra- and inter center comparable results. RECIST defines measurability of tumor lesions and specifies methods of measurements with different techniques [1]. According to the RECIST criteria measure of tumor response from radiological images is done by measuring lesions one-dimensionally, furthermore the World Health Organization (WHO) criteria use two dimensional analysis and several research groups volumetric three-dimensional analysis [2].

Staging of non-Hodgkin's lymphomas (NHL) is the key element of treatment planning for this heterogeneous group of malignancies. A variety of diagnostic tools, including biopsies, computed tomography (CT), magnetic resonance imaging (MRI), ^{18}F-fluorodeoxyglucose positron emission tomography (FDG-PET) or molecular markers are used in pre-treatment staging [3]. Enhancement with contrast media could also help the evaluation in using different imaging modalities. The same tools are applied to evaluate the response to different types of treatment. Novel techniques such as hybrid positron emission tomography – computed tomography (PET-CT) imaging and new PET tracers like ^{18}F-fluoro-thymidine (^{18}F-FLT) may increase the sensitivity of response assessment [4]. Reports aiming international standardization of clinical response criteria for NHL have been published [5,6], and these criteria are in wide clinical use. A combination of cyclophosphamide, doxorubicin, vincristine and prednisone (CHOP) remains the mainstay of therapy. The addition of a chimeric-anti-CD20 immunoglobulin G1 monoclonal antibody, rituximab (Mabthera®), has resulted in a dramatic improvement in the outcome of the most common NHL, diffuse large B-cell lymphoma, but has also been shown to effective in other type of B-cell lymphomas [7-9].

Several quantitative MRI studies have indicated that texture analysis (TA) has the ability to detect differences between tissues and subtle changes between disease burden and normal tissue. Successful applications of TA have been reported from studying neurological diseases [10-15], brain tumors [16,17], amygdale activation [18], muscles [19,20], trabecular bone [21-23], liver [24-26], breast cancer [27-31] and lymphomas [32].

In this paper we report the ability of TA to detect changes in NHL solid tissue masses during chemotherapy. The change in texture appearance is controlled by quantitative volumetric analysis. We classify statistical, autoregressive (AR-) model and wavelet texture parameters representing pre-treatment and two under chemotherapy stages of tumors with four analyses: raw data analysis (RDA), principal component analysis (PCA), linear (LDA) and nonlinear discriminant analysis (NDA). The final objective is to show that these texture parameters of MRI data can be successfully tested with Wilcoxon paired test and Repeatability and Reproducibility (R&R) test for assess the impact of the parameters usability in evaluating chemotherapy response in lymphoma tissue.

Methods

Tumor Response Evaluation (TRE) is a wide prospective clinical project ongoing at our university hospital on cancer patients, where tumor response to treatment is evaluated and followed up using simultaneously CT, MRI and PET imaging methods. Clinical responses for these lymphoma patients were assessed according to the guidelines of the international working group response criteria. In this texture analysis study, as a part of extensive project, the focus was on quantitative imaging methods and only the response in predefined solid NHL masses was evaluated. The ethics committee of the hospital approved the study and participants provided written informed consent. Primary inclusion criteria were NHL patients with at least one bulky lesion (over 3 centimeters) coming for curative aimed treatment. Exclusion criteria were central nervous disease, congestive heart failure New York Heart Association Classification (NYHA) III-IV, serious psychiatric disease, HIV infection and pregnancy.

Patients

MRI images of nineteen NHL patients participating in the TRE project were selected for the first part of this study. One of these patients was excluded due to the smaller amount of image data from the second part analyses. There were 14 male and 5 female patients aged 34–75. These patients had untreated or relapsed histologically diagnosed high/intermediate (N = 8, 42%) or low-grade (N = 11, 58%) NHL with an evaluable lymphoma lesion either in the abdominal area (N = 16) or in the clavicular and axillary lymph node area (N = 3). The treatment given was chemotherapy alone or combined with humanized antibody, rituximab (Mabthera®). Therapy regimens were CHOP (N = 5), R-CHOP (rituximab and CHOP) (N = 8), and CVP (cyclophosphamide, vincristine and pred-

nisone) (N = 1), CHOP-like CNOP (cyclophosphamide, mitoxantrone, vincristine and prednisone) (N = 1), ChlP (chlorambucil and prednisone) (N = 1), starting with CHOP and changing to R-CHOP (N = 2), starting with R-CHOP and changing to R-CVP (N = 1). Chemotherapy regimens were selected according to patients' clinical status. Chemotherapy courses were repeated every three weeks, and 4 to 9 courses were given according to clinical response. Two patients received 4 cycles, four patients 6 cycles, one patient 7 cycles, and 11 received 8 cycles, and one 9 cycles.

MR imaging schedule

MR imaging in clinical practice as well as in this study was carried out at staging phase before any treatment (examination 1, E1), after the first chemotherapy cycle (examination 2, E2), and after the fourth chemotherapy cycle (examination 3, E3). In addition patients were followed up by using MRI six months and 6–61 months after the completion of therapy. The time frame of the study is presented in Figure 1.

MR image acquisition

Imaging was performed on a 1.5 T MRI device (GE Signa, Wisconsin, USA).

One contrast enhanced sequence acquired from the first and second imaging timepoint were included for volume analysis of lymphoma masses. The sequence used was axial T2-weighted fast spin echo (FSE) fat saturation (FAT SAT) sequence (TR 620 ms, TE 10 ms), with intravenous contrast agent gadolinium chelate (gadobenate dimeglumine, 0.2 mg/ml, 10 ml), slice thickness ranged from 5 mm to 12 mm.

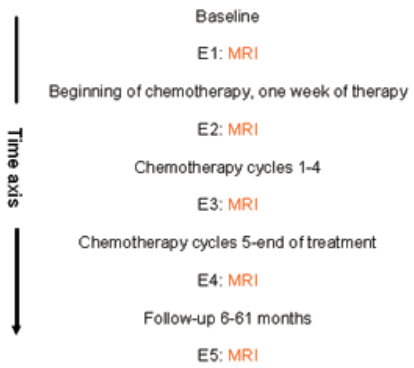

Figure 1
Time frame of the study. E1-E5 refers to the MRI examination timepoints 1–5, respectively.

One or two T1- and T2-weighted axial image serquences from the first three imaging timepoints of every patient were taken for texture analysis. The T1-weighted series comprised T1-weighted spin echo (SE) and T1-weighted SE FAT SAT sequences (TR 320–700 ms, TE 10 ms), the T2-weighted sequences were FSE FAT SAT (TR 3 320–10 909 ms, TE 96 ms). Repetition time TR varied between and within patients. Slice thickness varied between patients according to clinical status from 5 mm to 12 mm; most patients had two different slice thickness series, the general combination was 5 mm and 8 mm series. Pixel size varied from 1.33 mm*1.33 mm to 1.80 mm*1.80 mm, and a 256*256 matrix was used.

Texture analysis with MaZda

Texture parameter calculation was the first stage of the texture analyses. Stand-alone DICOM viewer application was used to select three to five slices from every image series for analysis. Region of interest (ROI) setting and texture analysis were carried out with MaZda software (MaZda 3.20, The Technical University of Lodz, Institute of Electronics) [33,34]. The lymphoma masses were manually selected and set as ROIs (Figure 2). Texture features calculated were based on histogram, gradient, run-length matrix, co-occurrence matrix, autoregressive model and wavelet-derived parameters [34]. Image grey level intensity normalization computation separately for each ROI was performed with method limiting image intensities in the range $[\mu-3\sigma, \mu+3\sigma]$, where μ is the mean grey level value and σ the standard deviation. This method has been shown to enhance differences between two classes when comparing image intensity normalization methods in texture classification [35].

Fisher coefficient (Fisher) and classification error probability (POE) combined with average correlation coefficients (ACC) provided by MaZda were used to identify the

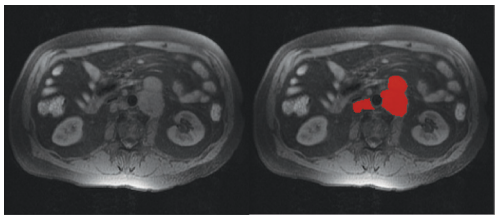

Figure 2
Axial T1-weighted fat saturation image slice of the abdomen of a typical subject (left), and ROI drawn on lymphoma mass (right).

most significant texture features to discriminate and classify the three evaluation stages of lymphoma tissue. Ten texture features were chosen by both methods (Fisher, POE+ACC). This feature selection was performed separately for the T1- and T2-weighted image sets. In these subgroups feature selection was run for the following imaging stages: combination of all imaging timepoints (E1, E2, and E3), and all combinations of the two aforementioned. Slice thickness was not taken into account.

Volumetric analysis

The volumetry of the solid lymphoma masses was evaluated between diagnostic stage (E1) and after the first treatment (E2). The masses were selected for evaluation before chemotherapy. The same masses were followed after the first treatment. Volumetric analysis based on MRI images was performed with semiautomatic segmentation software Anatomatic™ [36] with region growing method. [37].

Clinical parameters analyses

The patients' subjective views on their clinical symptoms was observed between two stages: at the diagnosis and after the first treatment. The subjective views were set in two groups: symptoms unchanged or relieved.

Grade of malignity was classed into two groups: 1) low; 2) high/intermediate.

Tissue classification

B11 application (version 3.4) of MaZda software package was used for texture data analysis and classification. Analyses were run between all combinations of imaging stages separately for T1- and T2-weighted images. Analyses were performed for combination of parameters selected automatically with Fisher and POE+ACC methods for 1) the specific imaging timepoint pair in question and 2) for all imaging stages in particular image type (T1-, T2-weighted). Feature standardization was used in B11, the mean value being subtracted from each feature and the result divided by the standard deviation. Raw data analysis (RDA), principal component analysis (PCA), and linear (LDA) and nonlinear discriminant analysis (NDA) were run for each subset of images and chosen texture feature groups. B11 default neural network parameters were used. Nearest-neighbor (1-NN) classification was performed for the raw data, the most expressive features resulting from PCA and the most discriminating features resulting from LDA. Nonlinear discriminant analysis carried out the classification of the features by artificial neural network (ANN). These classification procedures were run by B11 automatically.

Statistical analyses

Statistical analyses were run for the texture features MaZda's automatic methods (Fisher and POE+ACC) had shown to give best discrimination between imaging timepoints. The T1- and T2-weighted image texture parameters were tested separately. Texture parameters for 18 patients were included in the test, one patient participating in MaZda texture parameter calculation was excluded because of smaller amount of image data than other patients leading to reduced textural data.

In analyzing and seeking the best parameters for classification, it is vital to ensure low overall variation in the treatment process and to ascertain how this variation can be focused onto different components in the whole process. In the present study the repeatability and reproducibility (R&R) method was applied. The design of the study was experimental, the aim being to estimate different sources of variation in the lymphoma texture at the three different timepoints (examinations 1, 2, and 3) and repeating the same measurements three times. Because the distributions were skewed, the range method was used.

According to the standard Gage R&R terminology timepoints stand for operators, patients for parts and repeated measurements for trials. In statistical terms the following variance components were estimated: repeatability (difference across measurements), reproducibility (difference across timepoints) and variability (difference across patients). Repeatability describes intrapatient variation, i.e., how a given measurer repeats the same planning process. Reproducibility describes interpatient variation, i.e., how different measurements at the timepoints follow the same planning process and variability describes interpatient variation, i.e. how well the same physician can repeat the planning process for different kinds of patients. The total error – also known as the combined R&R effect – includes repeatability and reproducibility, and only patient-to-patient variation is excluded. In industrial applications the combined R&R should not exceed 10% of the total variation, but in certain situations a total error up to 30% may be acceptable. The present statistical analyses were performed by Statistica/W (Version 5.1, 98 edition, Statsoft. Inc, Tulsa, OK, USA).

Textural data from T1- and T2-weighted fat saturation image series were analysed separately and both groups divided into two subgroups according to slice thickness: 5–7 mm and 8–12 mm. Differences between imaging timepoints were analysed by Wilcoxon Signed Ranks.

Mann-Whitney test was used to test rank parameters grouped by grade of malignity and subjective change of

symptoms. These analyses were performed by SPSS for Windows, version 14.0.2.

Results

Volumetric analysis

The median volume of the lymphoma masses before treatment (E1) was 429 cm^3, ranging from 72 cm^3 to 2144 cm^3. The median volume of the masses calculated from the second imaging timepoint (E2) was 190 cm3, ranging from 30 cm^3 to1622 cm^3. After the first treatment cycle, the lymphoma mass volume had decreased in all patients. The median decline in volume was 32%, ranging from 3% to 76%. The results of this volumetric analysis have been published earlier in more detail [37]. The volumetry results of the first and second imaging are given in cm^3, and the volume change is calculated in percentages in Table 1.

Clinical parameters analyses

According to the patient's subjective estimates clinical symptoms between first and second imaging timepoint were unchanged in eight patients and relieved in 11 patients. Grades of malignancy and subjective view on symptoms are presented in Table 1 with volumetry results.

Texture data: MaZda and B11 analyses

We included in the analyses 108 T1-weighted and 113 T2-weighted images from E1; 103 T1-weighted and 105 T2-weighted images from E2; and 97 T1-weighted images and 99 T2-weighted images from E3.

Texture features were selected with Fisher and POE+ACC methods in MaZda from 300 original parameters calculated for each of the four subgroups in both image data classes T1- and T2-weighted.

We found that the most significant features varied clearly between imaging stages. The whole of 74 TA features ranked first to tenth significant feature in tested subgroups. There were three histogram parameters, 55 co-occurrence parameters, nine run-length parameters, four absolute gradient parameters and three autoregressive model parameters. No wavelet parameters were placed in the top group.

Data analyses RDA, PCA, LDA and NDA show texture changes between imaging points. The analyses did not perform well the task of discriminating all three imaging timepoints (E1, E2, E3) at same time. Slightly better classification was achieved between the first and second examinations, and between the second and third examinations. The method was successful in classifying the textural data achieved from the pre-treatment and third imaging timepoints, the best discrimination was obtained within T2-weighted leading to NDA classification error of 4%, and within T1-weighted NDA 5% error. Classification of different examination stages lead to same level results

Table 1: Grade of malignancy (1 = low, 2 = high/intermediate), subjective view of change in symptoms between pretreatment stage (E1) and after first chemotherapy cycle (E2) (0 = unchanged, 1 = relieved).

Patient	Grade of malignity	Symptoms	Volume		
	1 = low 2 = high/intermediate	0 = unchanged 1 = relieved	E1 (cm3)	E2 (cm3)	Change%
1	2	1	429	105	-76%
2	2	1	183	64	-65%
3	1	1	173	66	-62%
4	1	1	529	459	-13%
5	1	0	570	419	-26%
6	1	1	800	595	-26%
7	2	1	146	118	-19%
8	2	0	118	80	-32%
9	1	1	367	246	-33%
10	1	0	850	769	-10%
11	2	1	2144	1622	-24%
12	2	1	72	30	-58%
13	2	0	140	52	-63%
14	2	1	274	93	-66%
15	1	1	795	190	-76%
16	1	0	824	797	-3%
17	1	0	750	579	-23%
18	1	0	273	66	-76%
19	1	0	771	522	-32%

Results of the volumetric analysis of first (E1) and second imaging stages (E2). Volumes are given in cm^3, and the volume change calculated in percentages.

in T1- and T2-weighted images. The overall classification results are presented in Table 2 and Table 3.

Texture data: Statistical analyses

The values of 73 features obtained with MaZda feature selection methods were tested with Wilcoxon paired test for groups obtained from imaging timepoints a) E1 and E2, b) E2 and E3, c) E1 and E3. T1- and T2-weighted fat saturation image series data were set as their own groups and further into two subgroups according to slice thickness: 5–7 mm and 8–12 mm.

R&R test parameter repeatability was used to describe the variation in texture features between image slices within imaging sequence, and parameter reproducibility to describe the variation between examination stages. This test was performed separately for T1- and T2-weighted images in all three combinations of two imaging points. Differences in slice thickness were not taken into account. Reproducibility values were expected to be quite large because the aim was that the treatment given between imaging stages would take effect and be shown in image texture. In contrast, repeatability values (i.e. differences between images taken at the same timepoint) were expected to be zero. There is no exact expected ratio for reproducibility and patient-to-patient variation in such studies and thus no exact value for percentage of reproducibility, so that the difference between different imaging stages was significant.

The texture parameters giving the best discrimination within T1-weighted image groups in two imaging stage comparison are given in Table 4, Table 5 and Table 6; and respectively for T2-weighted image groups in Table 7, Table 8 and Table 9. Reproducibility percentage and Repeatability percentage of the total are given for all parameters. Wilcoxon paired test p-values are given for all parameters for separate groups regarding slice thickness (groups 5–7 mm and 8–12 mm).

R&R inverted ratio and the small difference between values are associated with poor results in Wilcoxon test with certain exceptions. Comparisons between first and third imaging points achieved significant Wilcoxon test p-values most consistently: within T2-weighted images in both slice thickness groups, and within T1-weighted images in the group of thinner slices. Features ranked in T1-weighted image data were tested in T2-weighted image data and vice versa. These tests with ranked features transposed with T1- and T2-weighted image groups lead to statistically relevant p-values in thinner T1-weighted images and all images in T2-weighted group. In the analyses of first and second imaging timepoints thin slices in general achieved poorer separation than thick slices. Between the second and third imaging sessions Wilcoxon test gave an unsatisfactory result in T1-weighted group. This trend can be seen in the B11 classification results in the framework of T1-weighted images, while the T2-weighted image analyses in B11 show better classification between second and third than first and second imaging points. The best overall discrimination between imaging timepoints in T1-weighted images was given by the run-length matrix parameters describing grey level non-uniformity, run-length non-uniformity, short-run emphasis and fraction of image in runs in one or more directions calculated (horizontal, vertical, 45 degrees and 135 degrees). In the framework of T2-weighted image analyses best the performers were absolute gradient mean and grey level non-uniformity There were some scattering in well acquitted parameters between sub analyses.

Table 2: MaZda classification results – results obtained within T1-weighted images.

T1-weighted images classification Examinations		**RDA** mis%	**PCA** mis%	**LDA** mis%	**NDA** mis%
E1, E2, E3	Combination E1, E2, E3	36%	34%	46%	31%
E1, E2	Combination E1, E2, E3	36%	34%	46%	31%
	Combination E1, E2	24%	26%	34%	16%
E1, E3	Combination E1, E2, E3	18%	18%	13%	6%
	Combination E1, E3	17%	17%	15%	5%
E2, E3	Combination E1, E2, E3	26%	26%	34%	18%
	Combination E2, E3	25%	27%	30%	13%

Imaging timepoint (E1, E2, E3) combinations for classification analyses. Feature selection methods given in rows. Misclassification percentage (mis%) given for raw data analysis (RDA), principal component analysis (PCA), linear discriminant analysis (LDA) and non-linear discriminant analysis (NDA) in columns. "Combination E1, E2, E3" in feature selection methods refers to features, which have proved to give best discrimination in all imaging timepoints analyses with Fisher and POE+ACC methods, combination of two imaging timepoints refers respectively to features from the analyses in question.

Table 3: MaZda classification results – results in groups of T2-weighted images.

T2-weighted images classification		RDA	PCA	LDA	NDA
Examinations	**Feature selection method**	mis%	mis%	mis%	mis%
E1, E2, E3	Combination E1, E2, E3	34%	35%	47%	30%
E1, E2	Combination E1, E2, E3	29%	29%	39%	19%
	Combination E1, E2	37%	35%	40%	35%
E1, E3	Combination E1, E2, E3	15%	14%	19%	4%
	Combination E1, E3	16%	17%	21%	4%
E2, E3	Combination E1, E2, E3	25%	24%	25%	14%
	Combination E2, E3	24%	23%	30%	12%

Imaging timepoint (E1, E2, E3) combinations for classification analyses. Feature selection methods given in rows. Misclassification percentage (mis%) given for raw data analysis (RDA), principal component analysis (PCA), linear discriminant analysis (LDA) and non-linear discriminant analysis (NDA) in columns. "Combination E1, E2, E3" in feature selection methods refers to features, which have proved to give best discrimination in all imaging timepoints analyses with Fisher and POE+ACC methods, combination of two imaging timepoints refers respectively to features from the analyses in question.

Table 4: Summary table of texture parameters ranked 1-10 with Fisher and POE+ACC methods according to test subgroup T1-weighted images and imaging timepoints E1 and E2.

T1-WEIGHTED IMAGES	R&R	R&R	Wilcoxon	Wilcoxon
E1-E2 analyses	Repeatability % of total	Reproducibility % of total	Slice thickness <8 mm *p*	Slice thickness >= 8 mm *p*
HISTOGRAM PARAMETERS				
Percentile, 1%	15.349	0.069	0.286	0.672
CO-OCCURENCE MATRIX PARAMETERS				
Difference entropy S(1,0)	6.874	25.411	0.074	0.018
Difference entropy S(0,1)	7.725	26.783	0.074	0.028
Difference entropy S(1,1)	6.970	24.413	0.139	0.018
Difference entropy S(2,0)	8.409	28.186	0.114	0.018
Sum average S(0,2)	52.143	4.597	0.285	0.499
Difference entropy S(2,2)	11.265	22.824	0.093	0.018
Difference entropy S(3,0)	15.434	11.836	0.241	0.018
Angular second moment S(5,-5)	18.976	7.234	0.093	0.612
Sum of squares S(5,-5)	58.267	1.780	0.721	0.310
Sum average S(5,-5)	15.420	16.235	0.445	1.000
RUN-LENGTH MATRIX PARAMETERS				
Grey level nonuniformity, 0°	6.015	43.441	0.051	0.128
Grey level nonuniformity, 90°	8.822	35.055	0.028	0.091
Grey level nonuniformity, 45°	4.635	13.324	0.028	0.176
Grey level nonuniformity, 135°	4.734	39.630	0.037	0.249
ABSOLUTE GRADIENT PARAMETERS				
Variance	28.133	22.699	0.445	0.018
AUTOREGRESSIVE MODEL PARAMETERS				
Teta 2	65.193	2.741	0.575	0.237
Teta 4	66.319	2.285	0.575	0.398

Texture parameters are given in rows. In the columns R&R repeatability and reproducibility of total, and Wilcoxon test for fat saturation series grouped with image slice thickness less than 8 mm, and 8 mm or thicker.

Table 5: Summary table of texture parameters ranked 1-10 with Fisher and POE+ACC methods according to test subgroup T1-weighted images and imaging timepoints E2 and E3.

T1-WEIGHTED IMAGES	R&R	R&R	Wilcoxon	Wilcoxon
E2-E3 analyses	Repeatability % of total	Reproducibility % of total	Slice thickness <8 mm *p*	Slice thickness >= 8 mm *p*
HISTOGRAM PARAMETERS				
Variance	11.452	22.145	0.953	0.465
CO-OCCURENCE MATRIX PARAMETERS				
Contrast S(2,0)	31.815	28.807	0.139	0.465
Contrast S(3,0)	27.957	40.317	0.051	0.144
Difference variance S(3,0)	26.169	35.250	0.139	0.273
Contrast S(4,0)	29.032	37.330	0.051	0.144
Correlat S(4,0)	25.661	36.025	0.086	0.144
Correlat S(0,4)	21.528	38.249	0.139	0.068
Correlat S(5,0)	23.130	39.697	0.038	0.068
Sum average S(5,0)	55.837	4.961	0.214	0.144
Sum average S(0,5)	44.169	6.142	0.859	0.715
Inverse difference moment S(5,5)	53.397	24.684	0.678	0.465
Difference variance S(5,-5)	50.986	14.473	0.515	0.715
RUN-LENGTH MATRIX PARAMETERS				
Grey level nonuniformity, 0°	6.015	43.441	0.066	0.273
Run length nonuniformity, 45°	7.013	31.416	0.139	0.068
Grey level nonuniformity, 45°	4.635	13.324	0.066	0.465
Short run emphasis, 135°	13.062	21.630	0.021	0.144
ABSOLUTE GRADIENT PARAMETERS				
Mean	24.582	28.201	0.038	0.144
Kurtosis	60.387	1.194	0.767	1.000
AUTOREGRESSIVE MODEL PARAMETERS				
Teta 3	58.511	0.000	0.028	0.465

Texture parameters are given in rows. In the columns R&R repeatability and reproducibility of total, and Wilcoxon test for fat saturation series grouped with image slice thickness less than 8 mm, and 8 mm or thicker.

Mann-Whitney test was performed for all texture features ranked 1–5 in any classification sub-analysis separately in T1- and T2-weighted images and further subgroups according to slice thickness to analyze differences between stage of malignity (low vs. high/intermediate) and between subjective change of symptoms (unchanged vs. relieved). These analyses did not yield any relevant and consequential additional information on the relation of texture features to grouping parameters.

Discussion

The goals of this study were show that a) MRI texture analysis can be used in NHL chemotherapy response evaluation b) statistical tests Wilcoxon paired test and R&R can be used to evaluate the separability of texture parameters used to describe textural changes in NHL.

Limitations of our study may be the non-standardized MRI sequence protocols within intra and inter patient images and the use of different slice thickness due to imaging in clinical practice, where patient's clinical stage and the size of the tumor were taken into account when

Table 6: Summary table of texture parameters ranked 1-10 with Fisher and POE+ACC methods according to test subgroup T1-weighted images and imaging timepoints E1 and E3.

T1-WEIGHTED IMAGES	R&R	R&R	Wilcoxon	Wilcoxon
E1-E3 analyses	Repeatability % of total	Reproducibility % of total	Slice thickness <8 mm *p*	Slice thickness >= 8 mm *p*
HISTOGRAM PARAMETERS				
MinNorm	24.793	2.445	0.504	0.465
Percentile, 1%	15.349	0.069	0.964	0.715
CO-OCCURENCE MATRIX PARAMETERS				
Inverse difference moment S(2,0)	20.950	29.298	0.008	0.068
Contrast S(3,0)	27.957	40.317	0.008	0.068
Correlation S(3,0)	24.569	38.395	0.021	0.068
Difference variance S(3,0)	26.169	35.250	0.021	0.068
Contrast S(4,0)	29.032	37.330	0.010	0.068
Correlation S(4,0)	25.661	36.025	0.021	0.068
Inverse difference moment S(4,0)	19.088	34.553	0.004	0.068
Correlation S(4,4)	17.730	40.414	0.021	0.068
Sum of squares S(4,-4)	52.253	2.218	0.859	1.000
Correlation S(5,0)	23.130	39.697	0.016	0.068
Inverse difference moment S(5,0)	23.111	37.188	0.013	0.068
Sum of squares S(0,5)	66.827	1.190	0.041	0.715
Sum of squares S(5,5)	64.191	3.647	0.477	0.715
RUN-LENGTH MATRIX PARAMETERS				
Grey level nonuniformity, 45°	4.635	13.324	0.003	0.068
Grey level nonuniformity, 135°	4.734	39.630	0.003	0.068
Fraction of image in runs, 135°	13.014	23.544	0.003	0.068

Texture parameters are given in rows. In the columns R&R repeatability and reproducibility of total, and Wilcoxon test for fat saturation series grouped with image slice thickness less than 8 mm, and 8 mm or thicker.

setting imaging parameters. However, multicenter studies on MRI TA have shown transferability of TA parameters achieved from MRI images obtained at different MRI centers with own acquisition parameters [16,38].

To achieve new clinical relevant information by means of texture analysis, the texture changes should come out at the same or earlier timepoint as other quantitative measures of tumor response, for example decrease in tumor volume. The RECIST and WHO criteria for evaluating tumor response in one- or two-dimensional (diameter and product) tumor size is equivalent to a 65% decrease in tumor volume [1]. In this study we calculated tumor size decrease in a short time period: before and after the first cycle of chemotherapy. There are no commonly used criteria for early response assessment using volumetric analysis for use as early in the therapy course as our volumetric evaluation was performed. Considering this, we

Table 7: Summary table of texture parameters ranked 1-10 with Fisher and POE+ACC methods according to test subgroup T2-weighted images and imaging timepoints E1 and E2.

T2-WEIGHTED IMAGES	R&R	R&R	Wilcoxon	Wilcoxon
E1-E2 analyses	Repeatability % of total	Reproducibility % of total	Slice thickness <8 mm *p*	Slice thickness >= 8 mm *p*
HISTOGRAM PARAMETERS				
MinNorm	14.090	24.380	0.861	0.636
CO-OCCURENCE MATRIX PARAMETERS				
Difference variance S(1,-1)	24.802	17.121	0.249	0.266
Sum average S(2,2)	38.483	23.527	0.552	0.163
Contrast S(3,0)	22.618	45.195	0.087	0.025
Contrast S(3,3)	23.282	48.345	0.152	0.102
Contrast S(4,0)	26.599	44.458	0.221	0.013
Contrast S(4,4)	31.083	41.015	0.116	0.049
Difference variance S(4,4)	35.305	32.674	0.196	0.019
Contrast S(4,-4)	40.897	22.850	0.013	0.266
Sum average S(4,-4)	10.802	1.906	0.345	0.210
Contrast S(5,0)	30.110	41.229	0.422	0.007
Sum of squares S(5,0)	64.138	7.335	0.807	0.076
Difference variance S(5,0)	34.811	32.369	0.917	0.009
Contrast S(0,5)	41.519	29.671	0.055	0.210
Contrast S(5,5)	39.461	38.040	0.133	0.102
Sum of squares S(5,5)	80.906	0.000	0.972	0.906
RUN-LENGTH MATRIX PARAMETERS				
Short run emphasis, 90°	10.659	12.516	0.087	0.149
Fraction of image in runs, 90°	11.662	12.685	0.101	0.124
ABSOLUTE GRADIENT PARAMETERS				
Mean	18.036	44.271	0.046	0.287
Skewness	63.599	15.598	0.382	0.492

Texture parameters are given in rows. In the columns R&R repeatability and reproducibility of total, and Wilcoxon test for fat saturation series grouped with image slice thickness less than 8 mm, and 8 mm or thicker.

can use the volumetric results as indicative of early imaging based evaluation of response, not to meet response, and also accept tumor volume decrease percentages smaller than 65% as consequential decrease in tumor size. However, in lymphomas, final clinical response evaluation should include other clinical tests according to [5,6].

Wilcoxon test showed encouraging values in the analyses of E1 and E3, including transferability of feature sets between T1- and T2-weighted images. This confirms our recent results with smaller patient data MaZda texture analysis of combination of T1- and T2-weighted images in single analysis [32].

Our study show that the statistical and autoregressive model texture parameters of MRI data can be successfully tested one by one with Wilcoxon paired test and Gage Repeatability and Reproducibility test to assess the impact of parameter separability in evaluating chemotherapy response in lymphoma tissue. Our results strengthen the applicability of Fisher and POE+ACC methods used in MaZda for automatic feature selection, and also confirm the suitability of the raw parameters in statistical tests. This indicates that raw parameters may be used in analyses other than LDA, NDA and PCA tests to acquire classification.

Table 8: Summary table of texture parameters ranked 1-10 with Fisher and POE+ACC methods according to test subgroup T2-weighted images and imaging timepoints E2 and E3.

T2-WEIGHTED IMAGES	R&R	R&R	Wilcoxon	Wilcoxon
E2-E3 analyses	Repeatability % of total	Reproducibility % of total	Slice thickness <8 mm *p*	Slice thickness >= 8 mm *p*
HISTOGRAM PARAMETERS				
MinNorm	14.090	24.380	0.002	0.124
Variance	1.655	16.743	0.028	0.149
CO-OCCURENCE MATRIX PARAMETERS				
Contrast S(2,0)	19.563	41.264	0.055	0.001
Contrast S(2,2)	23.139	43.325	0.033	<0,001
Contrast S(3,0)	22.618	45.195	0.023	0.002
Correlation S(3,0)	21.555	40.965	0.009	0.001
Contrast S(0,3)	30.424	34.725	0.116	<0,001
Contrast S(3,3)	23.282	48.345	0.023	0.004
Correlation S(3,3)	22.095	44.779	0.016	0.010
Contrast S(4,0)	26.599	44.458	0.006	0.011
Correlation S(4,0)	23.479	41.166	0.003	0.009
Sum of squares S(4,0)	71.978	3.535	0.807	0.868
Correlation S(4,4)	23.823	42.301	0.016	0.055
Difference entropy S(4,-4)	10.347	7.011	0.039	0.210
Sum average S(0,5)	35.828	0.000	0.972	0.011
Angular second moment S(5,-5)	8.994	12.106	0.064	0.015
Inverse difference moment S(5,-5)	46.459	0.000	0.917	0.795
RUN-LENGTH MATRIX PARAMETERS				
Grey level nonuniformity, 135°	6.265	33.780	0.003	0.004
ABSOLUTE GRADIENT PARAMETERS				
Mean	18.036	44.271	0.039	<0,001
Skewness	63.599	15.598	0.221	0.044

Texture parameters are given in rows. In the columns R&R repeatability and reproducibility of total, and Wilcoxon test for fat saturation series grouped with image slice thickness less than 8 mm, and 8 mm or thicker.

We have shown that texture parameters change during tumor response to chemotherapy. Comparing initial imaging to the second imaging timepoint, just after the first chemotherapy cycle, there were not such clear changes as at the third imaging timepoint, after four cycles of chemotherapy. The difference in texture appearance between staging and the third imaging timepoint was distinct and emerged from the results of other combinations in both T1-weighted and T2-weighted image types. There might have been better separation in texture features between diagnostic and first evaluation stage if standardized imaging sequence had been used. Our non-standardized MRI sequence may lead too heterogeneous TA features to exactly describe subtle changes in lymphoma tissue in extremely early stages of therapy response evaluation. We still cannot state the importance of subtle textural changes in early response assessment in comparison to volumetric changes in the same time intervals. Further, as controls for examined NHL masses no normal lymph nodes neither NHL masses after treatment were analyzed, since their small size leading to not exact differentiation from surrounding soft tissue structures in MR images.

The response evaluation of lymphomas under treatment using radiological imaging methods is connected strongly with tumor dimensions, instead when using positron emission tomography, tumor lesion activity of tracer uptake is measured. Both methods have certain advantages and disadvantages; major disadvantages related to sensitivity to differentiate residual masses and inflammatory processes from active disease. Functional responses for nocicepti stimuli and antivascular therapy have been detected in recent MRI TA studies [18,31]. In this context changes in textural appearance in MRI during the treat-

Table 9: Summary table of texture parameters ranked 1-10 with Fisher and POE+ACC methods according to test subgroup T2-weighted images and imaging timepoints E1 and E3.

T2-WEIGHTED IMAGES	R&R	R&R	Wilcoxon	Wilcoxon
E1-E3 analyses	Repeatability % of total	Reproducibility % of total	Slice thickness <8 mm *p*	Slice thickness >= 8 mm *p*
HISTOGRAM PARAMETERS				
MinNorm	14.090	24.380	0.003	0.130
CO-OCCURENCE MATRIX PARAMETERS				
Contrast S(2,0)	19.563	41.264	0.011	0.001
Contrast S(2,2)	23.139	43.325	0.006	<0,001
Contrast S(3,0)	22.618	45.195	0.009	0.001
Correlation S(3,0)	21.555	40.965	0.007	0.001
Sum average S(3,0)	28.935	19.345	0.033	0.035
Contrast S(3,3)	23.282	48.345	0.006	<0,001
Correlation S(3,3)	22.095	44.779	0.007	<0,001
Sum average S(3,-3)	20.384	0.353	0.087	0.017
Contrast S(4,0)	26.599	44.458	0.007	0.001
Contrast S(4,4)	31.083	41.015	0.009	<0,001
Correlation S(4,4)	23.823	42.301	0.007	<0,001
Sum of squares S(4,4)	82.108	0.686	0.345	0.687
Correlation S(5,-5)	39.239	25.122	0.023	0.035
RUN-LENGTH MATRIX PARAMETERS				
Short run emphasis, 90°	10.659	12.516	0.001	<0,001
Grey level nonuniformity, 45°	15.649	11.529	0.001	<0,001
ABSOLUTE GRADIENT PARAMETERS				
Mean	18.036	44.271	0.002	0.001
Skewness	63.599	15.598	0.046	0.007

Texture parameters are given in rows. In the columns R&R repeatability and reproducibility of total, and Wilcoxon test for fat saturation series grouped with image slice thickness less than 8 mm, and 8 mm or thicker.

ment process probably reflect chemotherapy induced changes in cellular proliferation.

In treatment with a curative orientation it is essential to get early an estimate of response to determine further treatment. MRI texture analysis may provide new insight to be used alone or in combination with other tools in diagnostics and response monitoring of non-Hodgkin lymphomas.

Conclusion

In conclusion NHL tissue MRI texture imaged before treatment and during chemotherapy can be correctly classified. Our results show promise for texture analysis as a possible new quantitative means for evaluating NHL response. Statistical and autoregressive model texture parameters of MRI data can be successfully tested with Wilcoxon paired test and Gage Repeatability and Reproducibility test to assess the impact of the parameters separability in evaluating chemotherapy response in lymphoma tissue.

Competing interests

The authors declare that they have no competing interests.

Authors' contributions

HP, RJ, PLIKL, HJE and PD designed and coordinated the TRE-project. LCVH designed this study, PLIKL, HJE, PD and SS participated in its coordination. LCVH performed the texture data collection and classification, and drafted the manuscript. TL performed statistical analyses. TOS performed the volumetric analysis. TTH designed and made the application for volumetric analysis. All authors participated in manuscript modification, read and approved the final manuscript.

Acknowledgements

The authors thank Research Nurse Tuula Nuuttila and Maija Rossi, MSc for their assistance with graphical layout and cooperation.

References

1. Therasse P, Arbuck SG, Eisenhauer EA, Wanders J, Kaplan RS, Rubinstein L, Verweij J, Van Glabbeke M, Van Oosterom AT, Christian MC, Gwyther SG: **New guidelines to evaluate the response to treatment in solid tumors. European Organization for Research and Treatment of Cancer, National Cancer Institute of the United States, National Cancer Institute of Canada.** *J Natl Cancer Inst* 2000, **92(3):**205-216.
2. Therasse P, Eisenhauer EA, Verweij J: **RECIST revisited: A review of validation studies on tumour assessment.** *Eur J Cancer* 2006, **42(8):**1031-1039.
3. Ansell SM, Armitage J: **Non-Hodgkin lymphoma: diagnosis and treatment.** *Mayo Clinic proceedings* 2005, **80(8):**1087-1097.
4. Hampson FA, Shaw AS: **Response assessment in lymphoma.** *Clin Radiol* 2008, **63(2):**125-135.
5. Cheson BD, Pfistner B, Juweid ME, Gascoyne RD, Specht L, Horning SJ, Coiffier B, Fisher RI, Hagenbeek A, Zucca E, Rosen ST, Stroobants S, Lister TA, Hoppe RT, Dreyling M, Tobinai K, Vose JM, Connors JM, Federico M, Diehl V, The International Harmonization Project on Lymphoma: **Revised response criteria for malignant lymphoma.** *J Clin Oncol* 2007, **25(5):**579-586.
6. Cheson BD, Horning SJ, Coiffier B, Shipp MA, Fisher RI, Connors JM, Lister TA, Vose J, Grillo-López A, Hagenbeek A, Cabanillas F, Klippensten D, Hiddemann W, Castellino R, Harris NL, Armitage JO, Carter W, Hoppe R, Canellos GP: **Report of an international workshop to standardize response criteria for non-Hodgkin's lymphomas. NCI Sponsored International Working Group.** *J Clin Oncol* 1999, **17(4):**1244.
7. Sehn LH, Donaldson J, Chhanabhai M, Fitzgerald C, Gill K, Klasa R, MacPherson N, O'Reilly S, Spinelli JJ, Sutherland J, Wilson KS, Gascoyne RD, Connors JM: **Introduction of combined CHOP plus rituximab therapy dramatically improved outcome of diffuse large B-cell lymphoma in British Columbia.** *J Clin Oncol* 2005, **23(22):**5027-33.
8. Weingart O, Rehan FA, Schulz H, Naumann F, Knauel I, Bohlius CB, Engert A: **Sixth biannual report of the Cochrane Haematological Malignancies Group--focus on non-Hodgkin lymphoma.** *J Natl Cancer Inst* 2007, **99(17):**E1.
9. Anderson VR, Perry CM: **Fludarabine: a review of its use in non-Hodgkin's lymphoma.** *Drugs.* 2007, **67(11):**1633-1655.
10. Freeborough PA, Fox NC: **MR image texture analysis applied to the diagnosis and tracking of Alzheimer's disease.** *IEEE transactions on medical imaging* 1998, **17(3):**475-479.
11. Mathias JM, Tofts PS, Losseff NA: **Texture analysis of spinal cord pathology in multiple sclerosis.** *Magn Reson Med* 1999, **42(5):**929-935.
12. Bonilha L, Kobayashi E, Castellano G, Coelho G, Tinois E, Cendes F, Li LM: **Texture Analysis of Hippocampal Sclerosis.** *Epilepsia* 2003, **44(11):**1546-1550.
13. Antel SB, Collins DL, Bernasconi N, Andermann F, Shinghal R, Kearney RE, Arnold DL, Bernasconi A: **Automated detection of focal cortical dysplasia lesions using computational models of their MRI characteristics and texture analysis.** *NeuroImage* 2003, **19(4):**1748-1759.
14. Sankar T, Bernasconi N, Kim H, Bernasconi A: **Temporal lobe epilepsy: Differential pattern of damage in temporopolar cortex and white matter.** *Hum Brain Mapp* 2008, **29(8):**931-44.
15. Jafari-Khouzani K: **Hippocampus Volume and Texture Analysis for Temporal Lobe Epilepsy.** *Electro/information Technology, 2006 IEEE International Conference on* 2006:394-397.
16. Herlidou-Meme S, Constans JM, Carsin B, Olivie D, Eliat PA, Nadal-Desbarats L, Gondry C, Le Rumeur E, Idy-Peretti I, de Certaines JD: **MRI texture analysis on texture test objects, normal brain and intracranial tumors.** *Magn Reson Imaging* 2003, **21(9):**989-993.
17. Mahmoud-Ghoneim D, Toussaint G, Constans J, de Certaines JD: **Three dimensional texture analysis in MRI: a preliminary evaluation in gliomas.** *Magn Reson Imaging* 2003, **21(9):**983-987.
18. Yu O, Parizel N, Pain L, Guignard B, Eclancher B, Mauss Y, Grucker D: **Texture analysis of brain MRI evidences the amygdala activation by nociceptive stimuli under deep anesthesia in the propofol-formalin rat model.** *Magn Reson Imaging* 2007, **25(1):**144-146.
19. Herlidou S, Rolland Y, Bansard JY, Le Rumeur E, de Certaines JD: **Comparison of automated and visual texture analysis in MRI: Characterization of normal and diseased skeletal muscle.** *Magn Reson Imaging* 1999, **17(9):**1393-1397.
20. Skoch A, Jirák D, Vyhnanovská P, Dezortová M, Fendrych P, Rolencov E, Hájek M: **Classification of calf muscle MR images by texture analysis.** *Magma* 2004, **16(6):**259-67.
21. Herlidou S, Grebe R, Grados F, Leuyer N, Fardellone P, Meyer M: **Influence of age and osteoporosis on calcaneus trabecular bone structure: a preliminary in vivo MRI study by quantitative texture analysis.** *Magn Reson Imaging* 2004, **22(2):**237-243.
22. Krug R, Carballido-Gamio J, Burghardt AJ, Haase S, Sedat JW, Moss WC, Majumdar S: **Wavelet-based characterization of vertebral trabecular bone structure from magnetic resonance images at 3 T compared with micro-computed tomographic measurements.** *Magn Reson Imaging* 2007, **25(3):**392-398.
23. Harrison LCV, Nikander R, Sievänen H, Eskola H, Dastidar P, Soimakallio S: **Physical load-associated differences in femoral neck MRI texture [abstract].** *European Radiology Supplements, ECR 2008 Book of Abstracts* 2008, **18:**247.
24. Jirák D, Dezortová M, Taimr P, Hájek M: **Texture analysis of human liver.** *J Magn Reson Imaging* 2002, **15(1):**68-74.
25. Zhang X, Fujita H, Kanematsu M, Zhou X, Hara T, Kato H, Yokoyama R, Hoshi H: **Improving the Classification of Cirrhotic Liver by using Texture Features.** *Conf Proc IEEE Eng Med Biol Soc* 2005, **1:**867-870.
26. Kato H, Kanematsu M, Zhang X, Saio M, Kondo H, Goshima S, Fujita H: **Computer-aided diagnosis of hepatic fibrosis: preliminary evaluation of MRI texture analysis using the finite difference method and an artificial neural network.** *AJR Am J Roentgenol* 2007, **189(1):**117-122.
27. Sinha S, Lucas-Quesada FA, Debruhl ND, Sayre J, Farria D, Gorczyca DP, Bassett LW: **Multifeature analysis of Gd-enhanced MR images of breast lesions.** *J Magn Reson Imaging* 1997, **7(6):**1016-1026.
28. Chen W, Giger ML, Li H, Bick U, Newstead GM: **Volumetric texture analysis of breast lesions on contrast-enhanced magnetic resonance images.** *Magn Reson Med* 2007, **58(3):**562-571.
29. Gibbs P, Turnbull LW: **Textural analysis of contrast-enhanced MR images of the breast.** *Magn Reson Med* 2003, **50(1):**92-98.
30. Woods BJ, Clymer BD, Kurc T, Heverhagen JT, Stevens R, Orsdemir A, Bulan O, Knopp MV: **Malignant-lesion segmentation using 4D co-occurrence texture analysis applied to dynamic contrast-enhanced magnetic resonance breast image data.** *J Magn Reson Imaging* 2007, **25(3):**495-501.
31. Chen G, Jespersen S, Pedersen M, Pang Q, Horsman MR, StØdkilde JØrgensen H: **Evaluation of anti-vascular therapy with texture analysis.** *Anticancer Res* 2005, **25(5):**3399-3405.
32. Harrison L, Dastidar P, Eskola H, Järvenpää R, Pertovaara H, Luukkaala T, Kellokumpu-Lehtinen P, Soimakallio S: **Texture analysis on MRI images of non-Hodgkin lymphoma.** *Comput Biol Med* 2008, **38(4):**519-524.
33. Szczypinski PM, Strzelecki M, Materka A: **Mazda – a software for texture analysis.** *Information Technology Convergence, ISITC* 2007:245-249.
34. Szczypiński PM, Strzelecki M, Materka A, Klepaczko A: **MaZda – A software package for image texture analysis.** *Comput Methods Programs Biomed* 2009, **94(1):**66-76.
35. Collewet G, Strzelecki M, Mariette F: **Influence of MRI acquisition protocols and image intensity normalization methods on texture classification.** *Magn Reson Imaging* 2004, **22(1):**81-91.
36. Heinonen T, Dastidar P, Kauppinen P, Malmivuo J, Eskola H: **Semi-automatic tool for segmentation and volumetric analysis of medical images.** *Med Biol Eng Comput* 1998, **36(3):**291-296.
37. Saarinen T, Dastidar P, Peltola R, Järvenpää R, Pertovaara H, Arola T, Heinonen T, Hyttinen J, Kellokumpu-Lehtinen P, Soimakallio S: **Evaluation of the treatment outcome of lymphoma patients after the first treatment using magnetic resonance imaging based volumetry [abstract].** *Proceedings of the 3rd European Medical & Biological Engineering Conference, EMBEC'05. IFMBE Proceedings* 2005.
38. Mayerhoefer ME, Breitenseher MJ, Kramer J, Aigner N, Hofmann S, Materka A: **Texture analysis for tissue discrimination on T1-weighted MR images of the knee joint in a multicenter study: Transferability of texture features and comparison of feature selection methods and classifiers.** *J Magn Reson Imaging* 2005, **22(5):**674-680.

Holli *et al. BMC Medical Imaging* 2010, **10**:8
http://www.biomedcentral.com/1471-2342/10/8

BMC Medical Imaging

RESEARCH ARTICLE Open Access

Texture analysis of MR images of patients with Mild Traumatic Brain Injury

Kirsi K Holli*[1,2], Lara Harrison[1,2,3], Prasun Dastidar[1,3], Minna Wäljas[5], Suvi Liimatainen[4,8], Tiina Luukkaala[6,7], Juha Öhman[4,5], Seppo Soimakallio[1,3] and Hannu Eskola[1,2]

Abstract

Background: Our objective was to study the effect of trauma on texture features in cerebral tissue in mild traumatic brain injury (MTBI). Our hypothesis was that a mild trauma may cause microstructural changes, which are not necessarily perceptible by visual inspection but could be detected with texture analysis (TA).

Methods: We imaged 42 MTBI patients by using 1.5 T MRI within three weeks of onset of trauma. TA was performed on the area of mesencephalon, cerebral white matter at the levels of mesencephalon, corona radiata and centrum semiovale and in different segments of corpus callosum (CC) which have been found to be sensitive to damage. The same procedure was carried out on a control group of ten healthy volunteers. Patients' TA data was compared with the TA results of the control group comparing the amount of statistically significantly differing TA parameters between the left and right sides of the cerebral tissue and comparing the most discriminative parameters.

Results: There were statistically significant differences especially in several co-occurrence and run-length matrix based parameters between left and right side in the area of mesencephalon, in cerebral white matter at the level of corona radiata and in the segments of CC in patients. Considerably less difference was observed in the healthy controls.

Conclusions: TA revealed significant changes in texture parameters of cerebral tissue between hemispheres and CC segments in TBI patients. TA may serve as a novel additional tool for detecting the conventionally invisible changes in cerebral tissue in MTBI and help the clinicians to make an early diagnosis.

Background

Mild traumatic brain injury (MTBI) accounts for 70 - 90% of all treated brain injuries [1]. MTBI is usually caused by a relatively mild blow to the brain that causes just enough physical injury to possibly compromise the normal brain functions of memory, attention, mental organization, and logical thinking may be compromised. Damage to the brain is often found in the corpus callosum, brain stem, and in subcortical white matter (WM) regions at the site of impact or on the contralateral side after MTBI [2].

One of the biggest challenges in addressing neuropsychological functioning and recovery from MTBI is the diagnosing itself. A variety of neuroimaging modalities can be used to assist in making the diagnosis of MTBI [3], but currently CT scan and MRI are the modalities of choice as a diagnostic tool for acute MTBI. The vast majority of MTBI patients have normal CT scans, and although MRI has been found to be more sensitive to traumatic lesions than CT, most symptomatic patients also have normal MRI scans.

MR images of tissues contain a lot of microscopic information that may not be assessed visually and texture analysis (TA) technique provides the means for obtaining this information [4]. Texture is the visual cue due to the repetition of image patterns that can be described for example, as smooth or rough, regular or irregular, coarse or fine. Some textures display complex patterns but may appear visually regular and are therefore relatively easy to extract even by visual inspection. However, for textures that exhibit random appearance patterns where textural primitives are randomly placed it becomes much more difficult to recognize and interpreter these textures. These kind of random patterns rather than regular textures are more often encountered in medical images. Basically texture is an image feature which corresponds

* Correspondence: kirsi.holli@tut.fi
[1] Medical Imaging Center, Tampere University Hospital, Tampere, Finland
Full list of author information is available at the end of the article

to both brightness value and pixel locations from which TA allows one to calculate mathematical patterns, texture features that can be used to discriminate and characterize the properties of tissues.

TA of MR images is a quantitative method that can be used to quantify and detect structural abnormalities in different tissues. TA can be divided into categories such as structural, model-based, statistical and transform, according to the means employed to evaluate the interrelationships of the pixels [5]. Statistical methods are the most widely used in medical images. The statistical approaches analyze the spatial distribution of grey values, computing local features at each point in the image, and deriving a set of statistics from the distributions of the local features. Local features are defined by the combination of intensities at specific position relative to each point in image. Statistics are classified as a first-, second- or higher-order statistics according to the number of points which define the local feature. In first- order statistics image properties depend solely on individual pixel values, whereas second-order statistics are properties of pixel pairs [4]. First order statistics include mean grey scale, standard deviation of the mean, skewness (deviation of the pixel distribution) and the kurtosis (stepness of the pixel distribution) which can usually be detected visually. Second order statistically methods utilizes grey-level run-length measures and grey-level co-occurrence matrix. Methods based on second-order statistics tend to obtain higher discrimination indexes and can not be visually detected. Therefore the interest in medical image TA mainly lays in the random textures of second- or higher order. The most popular texture method for MR images seems to be the grey-level co-occurrence matrix first proposed by Haralick [6].

Many promising studies have been reported with TA in the classification of pathological tissues from normal tissues for example from the liver, breast, tumours with variable locations such as lymphomas and muscles [7-13]. With regard to TA of brain, texture parameters based on the histogram, co-occurrence matrix, gradient and run-length matrix have been shown to be good for the characterization of healthy and pathological human cerebral tissues [14-18]. Co-occurrence matrix-based TA has also been found to be sensitive in differentiating Alzheimer's disease patients from normal controls [19] and histologically proven hippocampal sclerosis (HS) from normal hippocampal cerebral tissue [20]. Mahmoud-Ghoneim et al. [21] have proposed a three-dimensional (3D) approach using co-occurrence matrix analysis to increase the sensitivity and specificity of brain tumor characterization and treatment follow-up with promising results. Ganeshan [22] and associates 3D selective- and relative-scale texture analysis to quantify the presence of grey-matter and white-matter textural abnormalities associated with schizophrenia concluding that 3D TA of brain MR enables detection of subtle distributed morphological features associated with schizophrenia. Kovalev and associates [23] also tested 3D co-occurrence matrix TA in analyzing cerebral tissue and glioma in T1-weighted MR-images. TA has also been used in analyzing age-related changes [24] and gender-related differences [25] with promising results.

In this study we concentrated on evaluating the ability of two-dimensional (2D) MRI-based TA to characterize the changes caused by MTBI in cerebral tissue by applying TA methods. To the best of our knowledge, there are no published studies on the application of quantitative MRI TA in studying MTBI.

Methods

Patients with MTBI (GCS score 13-15) were recruited from the emergency room of Tampere University Hospital during the period 2006-2007. For the TA study 42 consecutive patients (17 male, 25 female; mean age ± SD, 38.8 ± 13.6 years; range 18 to 60 years) were included. Clinical examination on admission and CT examination on the day of the accident and MRI within three weeks from the day of admission were conducted on all patients. All patients met the criteria of MTBI according to the World Health Organization Collaborating Centre for Neurotrauma Task Force on Mild Traumatic Brain Injury [26]. Exclusion criteria for this study were age under 18 or over 65, severe traumatic brain injury, previous brain trauma, other major cognitive disorder, history of major alcohol or drug abuse. Ten healthy age and gender matched controls (4 males, 6 females; mean age ± SD, 39.8 ± 12.9 years; range 28 to 61 years) were also recruited to form a control group. All patients and healthy controls gave their written consent and the study was approved by the Ethics Committee of Tampere University Hospital. All 42 patients were evaluated to have a normal CT and MRI scan by a specialized radiologist. The patient's degree of consciousness was assessed to determine the severity of brain injury using the Glasgow Coma Scale (GCS) [27]. Possible loss of consciousness (LOC) was recorded (length in minutes or hours) as well as post-traumatic amnesia (PTA) (length in minutes or hours). A number of neurocognitive tests were also performed within 6 weeks of the injury.

MRI examinations

All 42 patients were studied on a 1.5 Tesla MRI machine (Magnetom Avanto, Siemens Medical Solutions, Erlangen, Germany). The MRI machine is under quality control program, which includes daily, monthly, and quarterly measurements. Main magnetic field homogeneity and RF -amplifier properties are measured and controlled four times a year. A prescan normalisation filter

was used for the correction of intensity inhomogeneity in images. The data used for homogenisation were acquired through a preliminary low-resolution measurement. An elliptical filter was used within the slice planes to improve the signal-to-noise ratio. The sequences included in the MRI protocol are presented in Table 1.

Texture analysis

For texture analysis an axial FLAIR (T2w FLAIR) and sagittal T1w 3D magnetization prepared gradient echo (T1w MPR) image series were selected from the whole MRI study. Three image slices from imaging sequences T2w FLAIR on three selected levels of interest and one slice from sequence T1w MPR were chosen for further analysis. Level 1 was level of mesencephalon, level 2 corona radiata and level 3 centrum semiovale. Level 4 was corpus callosum from sagittal view in caudo-cranial direction from the T1w MPR sequence. Image selection was performed with a DICOM viewer Osiris (Windows version 4.19, The Digital Imaging Unit (UIN) of the Service for Medical Computing (SIM) of the Radiology Department of the University Hospital of Geneva, Switzerland).

TA was performed with the software package MaZda (MaZda 4.5, Technical University of Lodz, Institute of Electronics [28]) specially designed for texture analysis by Materka and co-workers as part of the European COST B11 and the following COST B 21 programs. For each MR image regions of interest (ROI) were manually placed symmetrically on the left and right hemispheres on each level of interest. For level 1 ROIs were drawn by hand in the area of mesencephalon (ROI size around 1200 pixels depending on the size of the mesencephalon), both left and right side. Circular ROIs (177 pixels) were placed both sides in WM (Figure 1a). For level 2 circular ROIs were placed both sides in WM (177 pixels) (Figure 1b). For level 3 three circular ROIs (177 pixels) were placed in both sides in WM from anterior to posterior (Figure 1c). Circular ROIs (68 pixels) were also placed on the splenium, body and rostrum of the corpus callosum (Figure 1d). The ROIs were carefully placed so they did not overlap any microhemorraghes, macroscopic hemosiderin deposits or hyperintensities, which were observed in few patients. The ROI drawing was done manually by person with special interest in developing quantitative radiology methods in clinical use.

The comparison of texture features was made between the left and right sides and between segments of CC to ascertain any changes in texture parameters between hemispheres or segments on patients and on controls.

After determining the ROIs we calculated texture features based on image histogram, the co-occurrence matrix, the run-length matrix, the absolute gradient and the autoregressive model and wavelets [28]. Run length matrix parameters were calculated in four directions: horizontal (0°), vertical (90°), 45° and 135° and co-occurrence matrix parameters were calculated in five distances (1, 2, 3, 4 and 5 pixels), four times for each distance (in directions θ = 0°, 45°, 90° and 135°). All of these texture features (See Additional file 1) were calculated for each ROI.

The grey level normalization of each ROI was performed using a method which normalizes image intensities in the range [μ-3σ, μ+3σ]. This method has been shown to give the best results in MRI texture classification among different normalization methods [29]. This was done to minimize the influence of contrast variation and brightness. To determine 10 texture features with the highest discriminative power for separation and classification we used feature selection method Fisher coefficient (F) provided by MaZda [28]. The Fisher criterion usually produces a set of features with a high discriminatory potential which are also highly correlated with each

Table 1: Sequences included in the MRI protocol for MTBI patients.

Sequence	TR	TE	TI	Slice/gap	matrix	FOV	Flip angle
sagittal T1w 3D magnetization prepared gradient echo	1910	3.1	1100	1.0/0	256 × 256	250	15
axial T2w Turbo Spin Echo	44860	96	0	5.0/1.5	293 × 448	230	
axial FLAIR	9000	109	2500	5.0/1.5	256 × 256	230	
axial T2*w HEMO	800	26	0	7.0/2.0	256 × 256	230	20
axial SE EPI 3 scan diff (b = 0, b = 500, b = 1000)	3400	89	0	5.0/1.5	192 × 192	230	
sagittal FLAIR	8860	116	2500	2.0/2.0	256 × 256	230	
axial SE MDDW 12dir (b = 0, b = 1000)	3600	96	0	5.0/1.5	128 × 128	230	
axial SWI 3D	15	49	40	2.0/0	177 × 256	230	15

TR = repetition time
TE = echo time
TI = inversion time
FOV = field of view

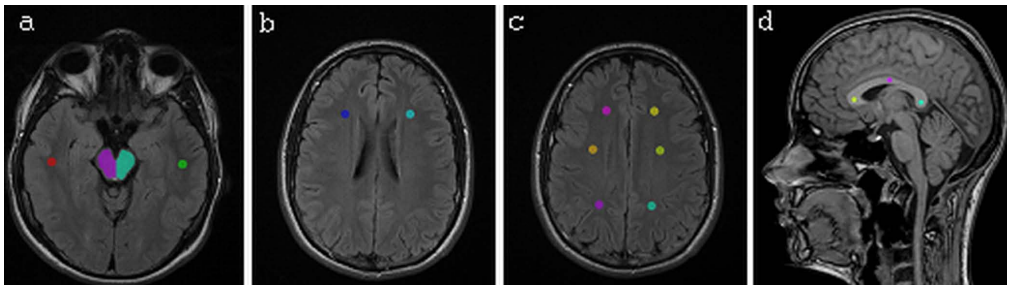

Figure 1 Regions of interest drawn on the each level of interest. Figure 1a: an axial FLAIR (T2w FLAIR) image in level 1. Figure 1b: an axial FLAIR (T2w FLAIR) image in level 2. Figure 1c: an axial FLAIR (T2w FLAIR) image in level 3. Figure 1d: sagittal T1w 3D magnetization prepared gradient echo (T1w MPR) in level 4. Regions of interest (ROIs) are drawn in the images.

other. The top 10 feature selections were made when comparing texture features between hemispheres of WM in different levels and features in the area of mesencephalon and features between segments of CC.

Data analysis

Statistical analyses were run for every texture feature. Differences in texture features between hemispheres in different tissues (the right vs. the left side of mesencephalon and WM) were analyzed by Wilcoxon Signed Ranks. The parameters in WM between three different levels and WM anterior-posterior (front, middle and back) on level 3, in the same hemisphere, were tested with the Friedman test. Texture parameters calculated from the segments of CC (rostrum, body and splenium) were also analyzed with the Friedman test. Similar tests were performed on the group of healthy controls. These analyses were performed using SPSS for Windows, version 14.0.2. (SPSS Inc., Illinois, USA). A p-value of under 0.05 was considered statistically significant.

Results

Analyses of mesencephalon

We tested all raw texture parameters to find out how many and which of the 277 parameters differed statistically between hemispheres. The number of texture parameters (n = 277) which were statistically significantly different ($p < 0.05$) analyzed with Wilcoxon test in the area of mesencephalon between hemispheres is presented in Table 2.

The parameters which differed statistically significantly were mainly based on the co-occurrence matrix. The patients had clearly more differences in texture features between hemispheres than the healthy controls. The healthy controls had no significantly differing run-length matrix based parameters unlike the patients.

The ten most discriminative texture features for separation of hemispheres in the area of mesencephalon as identified by calculation of Fisher coefficients, were mainly derived from the co-occurrence matrix in both patients and controls. The p-values for the most discriminative texture parameters on patients and on controls selected with the Fisher method are shown in Table 3.

Especially features derived from autoregressive model; Teta2, Teta3 and Teta4 ($p < 0.001$) were significantly different between hemispheres in patients and also in controls. Other parameters selected with the Fisher coefficient consisted mainly of parameters derived from the co-occurrence matrix. These were statistically different in patients but not in controls and vice versa.

Analyses of white matter

Again we tested all raw texture parameters to find out how many and which of the 277 parameters differed statistically between hemispheres in WM in different levels of interest. The number of texture parameters (n = 277) which were statistically significantly different ($p < 0.05$) analysed with Wilcoxon test in WM between hemispheres in patients and healthy controls are set out in Table 4.

In the level of corona radiata (level 2) there were clearly more significantly different parameters between hemispheres than in other levels in patients. In level 2 there were also clearly fewer texture differences in controls than in patients.

The ten most discriminative texture features for separation of WM in the left and right hemispheres varied clearly between the three levels. The features were mainly histogram-based or derived from the co-occurrence matrix. The p-values for the most discriminative texture parameters in patients and in controls selected with the Fisher method in level 2 are shown in Table 5.

The most discriminative texture parameters in WM on patients and on controls varied between levels and between patients and controls. Only a few parameters

Table 2: Numbers of parameters having statistically significant differences ($p < 0.05$) between hemispheres analyzed with Wilcoxon test.

	Mesencephalon	
Texture parameter groups	**Patients**	**Controls**
Histogram (n = 11)	7	3
GrM (n = 5)	1	0
COM (n = 220)	90	30
RLM (n = 20)	4	0
ARM (n = 5)	3	2
Wavelet (n = 16)	2	2
Total (n = 277)	**107**	**37**

The total number of evaluated texture parameters is 277. The total number of parameters having statistically significant differences between hemispheres in the area of mesencephalon is in bold face.
GrM: gradient matrix; COM: co-occurrence matrix; RLM: run-length matrix; ARM: autoregressive model; n: number parameters in each group.

were significantly different between hemispheres in both patients and controls.

The texture parameters of WM between different levels were analyzed with the Friedman test in order to find out whether the texture differed in the same hemisphere between levels. It was observed that many of the texture parameters of WM on level 1 were statistically significantly different from parameters on levels 2 and 3. Texture parameters in the same hemisphere of WM anterior-posterior (front, middle and back) on level 3 were also analyzed and it was observed that the texture parameters in the posterior region differed from the anterior and central regions in both hemispheres.

Analyses of the corpus callosum

We tested all raw texture parameters to find out how many and which of the 277 parameters differed statistically between segments of CC. The number of texture parameters (n = 277) which were statistically significantly different ($p < 0.05$) analyzed with Friedman test in the segments of CC is presented in Table 6.

Table 3: The ten most discriminating parameters according to the Fisher (*F*-) coefficient and corresponding Wilcoxon test p-values.

			Mesencephalon		
Most Discriminative Texture Parameters on Patients	**p-values (patients)**	**p-values (controls)**	**Most Discriminative Texture Parameters on Controls**	**p-values (controls)**	**p-values (patients)**
Teta4	<0.001*	0.105	S(4,-4)DifVarnc	0.002*	0.519
Teta3	<0.001*	0.020*	S(5,-5DifVarnc	0.004*	0.465
S(5,5)Entropy	<0.001*	0.105	Teta3	0.020*	<0.001*
S(5,5)AngScMom	<0.001*	0.020*	S(5,-5)DifEntrp	0.004*	0.413
S(4,4)AngScMom	<0.001*	0.432	Teta2	0.014*	<0.001*
S(4,4)Entropy	<0.001*	0.322	S(4,-4)DifEnrtp	0.002*	0.372
Teta2	<0.001*	0.014*	S(3,-3)DifVarnc	0.002*	0.160
S(1,-1)DifVarnc	<0.001*	0.375	WavEnLL_s-2	0.027*	0,472
S(1,1)DifVarnc	<0.001*	0.375	S(5,-5)Contrast	0.002*	0.833
S(3,3)AngScMom	<0.001*	0.492	S(4,-4)Contrast	0.002*	0.432

The ten most discriminating parameters according to the Fisher (*F*-) coefficient and their corresponding Wilcoxon test p-values are calculated between hemispheres in the area of mesencephalon for both patients and controls.
Teta, vectors of autoregressive model; AngScMom, angular second moment; SumAverg, sum average; DifEntrp, difference entropy; DiffVarnc, difference variance; WavEnLL, energy of wavelet coefficients in subband LL.
* p-values of under 0.05 are considered statistically significant

Table 4: Numbers of parameters having statistically significant differences ($p < 0.05$) between hemispheres analyzed with Wilcoxon test.

	White matter					
	WM Level 1		WM Level 2		WM Level 3	
Texture parameter groups	**Patients**	**Controls**	**Patients**	**Controls**	**Patients**	**Controls**
Histogram (n = 11)	8	9	9	9	8	6
GrM (n = 5)	0	0	0	0	0	0
COM (n = 220)	19	2	49	3	9	4
RLM (n = 20)	0	0	4	0	1	0
ARM (n = 5)	0	0	0	1	0	0
Wavelet (n = 16)	1	1	1	0	1	0
Total (n = 277)	**28**	**12**	**63**	**13**	**19**	**10**

The total number of evaluated texture parameters is 277. The total number of parameters having statistically significant differences between hemispheres in the cerebral white matter is in bold face.
GrM: gradient matrix; COM: co-occurrence matrix; RLM: run-length matrix; ARM: autoregressive model; n: number parameters in each group.

In the segments of CC the body of CC had statistically significantly differing from the other segments on patients. In healthy controls there were clearly fewer significantly different parameters.

The ten most discriminative texture features for the separation of segments of CC as identified by calculation of Fisher coefficients, were mainly derived from the co-occurrence matrix and wavelet based features in both patients and controls. The p-values for the most discriminative texture parameters in patients and in controls selected with the Fisher method are shown in Table 7.

The only texture features statistically significant in both patients and controls were two wavelet based features, otherwise the statistically significantly differing features differed between these two groups.

Discussion

The use of imaging to examine patients with MTBI has been investigated by a number of studies, and imaging abnormalities in CT, MRI and SPECT have all been associated with poor outcome on all modalities [30-33]. Although the imaging modalities have been developing fast in recent years, with many improvements especially in MRI techniques, such as diffusion-weighted MRI, DTI and new MRI sequences [34-36] it is still difficult to detect damaged lesions and make the diagnosis of MTBI on the basis of imaging findings. Some prior studies have demonstrated exclusive abnormalities on DWI, ADC, or DTI without overt structural damage seen in other sequences such as T1, T2 [34,37] The use of advanced imaging modalities [31,38,39] and different computer assisted detection (CAD) systems such as TA, which provides quantitative means of characterizing the properties of tissues in cases which tissue changes cannot be detected by direct inspection of the image may offer possible approaches on improving the prognostic capabilities of conventionally used MRI sequences.

We chose the MR images of MTBI patients for our study with the objective of detecting textural differences in different regions of cerebral tissue between the hemispheres. The purpose was to test the performance of TA to differentiate cerebral hemispheres and to characterize the changes caused by MTBI in cerebral tissue. Our study showed that there are significant differences in texture parameters in cerebral tissue between the hemispheres in MTBI patients and also differences between patients and healthy controls. We found texture differences between sides in the area of mesencephalon and between the hemispheres in WM, especially in the level of corona radiata and between different segments of CC. To the best of our knowledge there are so far no other studies of texture analysis of MTBI patients for comparison.

It has been established that MR images contain tissue-specific texture features which can be extracted by mathematical methods. It has been proven that TA can be used for classifying healthy and pathologic human cerebral tissue [14-16] and also distinguish different cerebral tissues. TA has also been used for distinguishing MS lesions from normal appearing - and normal white matter [40]. In light of our study we concur that TA can discriminate between different cerebral tissues and that different structures can also be distinguished from brain MR images. Traumatic brain injury is followed by activation of numerous proinflammatory mediators and glial cells. Both experimental and clinical data show activation of proinflammatory cytokines at the site of injury [41,42]. This together with an assumption of axonopathic changes in DTI might suggest inflammatory etiology of TA [43].

In our statistical tests on the raw parameters there were over a hundred parameters that were statistically signifi-

Table 5: The ten most discriminating parameters according to the Fisher (*F*-) coefficient and corresponding Wilcoxon test p-values.

White matter					
Most Discriminative Texture Parameters on Patients	**p-values (patients)**	**p-values (controls)**	**Most Discriminative Texture Parameters on Controls**	**p-values (controls)**	**p-values (patients)**
LEVEL 2					
S(4,4)Correlat	<0.001*	0.492	S(5,5)SumVarnc	0.002*	0.008*
S(4,4)Contrast	0.001*	0.557	S(5,5)Correlat	0.004*	0.008*
S(4,4)SumVarnc	<0.001*	0.695	S(4,4)InvDfMom	0.064	0.003*
S(4,4)InvDfMom	0.003*	0.064	WavEnLH_s-3	0.922	0.359
S(4,4)DifVarnc	0.002*	0.770	S(5,5)Contrast	0.010*	0.015*
S(5,5)Correlat	0.008*	0.004*	S(0,1)SumAverg	0.164	0.114
S(2,-2)AngScMom	<0.001*	0.396	S(1,-1)SumAverg	0.105	0.225
S(0,3)DifEntrp	0.002*	0.695	S(5,-5)SumVarnc	0.105	0.253
S(5,5)Contrast	0.015*	0.010*	S(5,-5)Correlat	0.105	0.603
S(5,5)SumVarnc	0.008*	0.002*	Teta1	0.064	0.274

The ten most discriminating parameters according to the Fisher (*F*-) coefficient and their corresponding Wilcoxon test p-values are calculated between hemispheres in the cerebral white matter in the level of corona radiata (level 2) for both patients and controls.
Correlat, correlation; DiffVarnc, difference variance; AngScMom, angular second moment; Teta, vectors of autoregressive model; SumAverg, sum average; InvDfMom, inverse difference moment; SumVarnc, sum variance; DifEntrp, difference entropy; WavEnLH, energy of wavelet coefficients in subband LH.
* p-values of under 0.05 are considered statistically significant

cantly different between the left and the right sides of the mesencephalon in patients. All the histogram-based percentiles, which give the highest grey-level value under which a given percentage of the pixels in the image are contained, were statistically significantly different ($p < 0.001$). Other texture parameters which were most often statistically significantly different consisted mainly of parameters derived from the co-occurrence matrix which gave the highest grey-level value under which a given percentage of the pixels in the image are contained. We observed that there were statistically differing run-length matrix-based parameters, giving information about the spatial variation of gray-level values, between hemispheres in patients but not in healthy controls. This may indicate that the presence of these texture parameters is related to the damage. Clearly there are not so many texture differences between sides in the area of mesencephalon in healthy controls than in MTBI patients.

The ten most discriminative texture features for separation of hemispheres in the area of mesencephalon as identified by calculation of Fisher coefficients, were mainly derived from autoregressive model and the co-occurrence matrix in both patients and controls. Features derived from the autoregressive model; Teta2, Teta3 ($p < 0.001$) were significantly different between hemispheres in patients and also in controls. Other selected parameters which were statistically different in patients were not different in controls and vice versa. The difference between texture parameters between patients and healthy controls may due to the fact that the injury of the patients has caused complexity in the structure of mesencephalon due to some axonal tearing.

In our study, the texture parameters of WM between hemispheres on different levels were analyzed with Wilcoxon test. Since texture properties are evaluated on a millimetre scale, they may capture the local coherence, direction, and density of fiber bundles, their myelinisation status, the density and direction of vessels supplying and draining WM. According to our study the parameters between WM hemispheres differed most on the level of corona radiata (level 2) in patients. There was not much difference between levels in healthy volunteers. The significantly differing parameters were mainly based on histogram and co-occurrence matrix. And again the run-length matrix-based parameters were statistically different in patients only. It is necessary to take into account that the human brain is asymmetric in structure and function and some of these significant differences in parameters between hemispheres are possibly attibutable to this since less difference was observed on healthy controls it can be assumed that most of the texture changes are caused by the injury.

The ten most discriminative texture features for the separation of hemispheres in the WM as identified by cal-

Table 6: Numbers of parameters having statistically significant differences ($p < 0.05$) between segments of CC analyzed with Friedman test.

	Corpus callosum					
	patients			controls		
Texture parameter groups	**Rostrum**	**Body**	**Splenium**	**Rostrum**	**Body**	**Splenium**
Histogram (n = 11)	3	6	1	1	1	0
GrM (n = 5)	0	0	0	0	0	0
COM (n = 220)	3	33	4	4	1	3
RLM (n = 20)	0	0	0	0	0	0
ARM (n = 5)	0	1	0	0	0	0
Wavelet (n = 16)	0	9	0	1	2	0
Total (n = 277)	**6**	**49**	**5**	**6**	**4**	**3**

The total number of evaluated texture parameters is 277. The total number of parameters having statistically significant differences between the segments of corpus callosum is in bold face.
GrM: gradient matrix; COM: co-occurrence matrix; RLM: run-length matrix; ARM: autoregressive model; n: number parameters in each group.

culation of Fisher coefficients, were mainly derived from the co-occurrence matrix in both patients and controls. Only a few parameters were significantly different between hemispheres in both patients and controls on each level.

Texture parameters of WM between different levels were also analyzed. It was observed that many texture parameters of WM on level 1 were statistically significantly different from parameters on levels 2 and 3, but there were not as many different parameters as between the left and the right hemisphere. Texture parameters between the areas of WM anterior-posterior (front, middle and back) on level 3 were analyzed and it was observed that mostly texture parameters in the posterior region differed from the anterior and the central regions in both hemispheres, which is in line with the fact that many times the trauma is located in the frontal or occipital lobe.

According to our results there are significant differences in texture parameters in the segments of CC and between healthy volunteers and MTBI patients. Our study showed that the texture of the body of CC was dif-

Table 7: The ten most discriminating parameters according to the Fisher (*F*-) coefficient and corresponding Wilcoxon test p-values.

	Corpus callosum				
Most Discriminative Texture Parameters on Patients	**p-values (patients)**	**p-values (controls)**	**Most Discriminative Texture Parameters on Controls**	**p-values (controls)**	**p-values (patients)**
WavEnLL_s-2	<0.001*	0.001*	WavEnLL_s-2	0.001*	<0.001*
WavEnLH_s-2	<0.001*	0.006*	WavEnLH_s-2	0.006*	<0.001*
S(5,0)SumOfSqs	0.001*	0.601	S(4,-4)SumAverg	0.030*	0.220
S(3,0)Contrast	<0.001*	0.368	S(5,-5)SumVarnc	0.007*	0.699
S(4,0)SumOfSqs	0.003*	0.316	S(2,-2)SumEntrp	0.710	0.847
S(4,0)Contrast	<0.001*	0.368	S(1,-1)SumOfSqs	0.368	0.110
S(1,0)DifVarnc	<0.001*	0.368	S(5,-5)SumAverg	0.012*	0.190
S(2,0)Contrast	<0.001*	0.316	S(0,1)SumOfSqs	0.135	0.073
S(1,0)Contrast	<0.001*	0.436	S(2,-2)SumOfSqs	0.368	0.404
S(0,1)SumVarnc	0.019*	0.436	S(1,0)SumOfSqs	0.046*	0.272

The ten most discriminating parameters, according to the Fisher (*F*-) coefficient and their corresponding Wilcoxon test p-values are calculated between segments of the corpus callosum for both patients and controls.
SumAverg, sum average; Sum Varnc, sum variance, SumEntrp, sum entropy; DiffVarnc, difference variance, SumOfSqs, sum of squares; WavEnLH, energy of wavelet coefficients in subband LH; WavEnLL, energy of wavelet coefficients in subband LL.
* p-values of under 0.05 are considered statistically significant

ferent in texture from the rostrum or splenium in patients. The CC is the largest fiber bundle in the human brain connecting two cerebral hemispheres with hundreds of millions of fibers. The fiber composition in the CC has been studied in [44,45] and it has been observed that there are least nerve fibers in the body of CC per unit area and Glial cells occupied more of the body of the CC than of the other segments. The different orientation or densities of the fibers may yield different textures so it could be assumed that the textural changes in the body of CC are caused by the different densities and number of the fibers in different regions of CC. However, since it was observed that in healthy controls the body of CC was not different in texture from the rostrum or splenium, we can presume that the texture differences between the body and other segments of CC in assume may be caused by the injury. Again the ten most discriminative parameters differed and there were only a few wavelet-based features which were significantly different in both groups.

Because our patient group all had normal MRI scans it proved to be very challenging to evaluate the texture changes possibly caused by the injury since we could not categorize the patients according to which part of the head the damage may have occurred in. Also, there are variations in brain structure between individuals making it difficult to detect and classify abnormal structural patterns caused by MTBI and making it difficult to place the ROIs in optimal places. We studied if we could detect differences in textures between the hemispheres in patients and controls. Based on this study the ten most discriminating parameters as identified by calculation of Fisher coefficients on each selected region might only be pertinent to the specific subset of patient tested in this current study. Therefore they are not to be generalized but they however give direction to which type of parameters may be applicable also to other subset of patients. Our results show that there are significant differences in texture parameters in cerebral tissue in the area of mesencephalon and also in the segments of CC and in WM on patients and not so much in healthy controls.

Conclusions

In conclusion, the study indicates that TA could be used to characterize the changes in cerebral tissue in MTBI patients. This study suggests that texture analysis with a variable set of texture features could in the future serve as an adjuvant diagnostic tool along with traditional MRI and DTI imaging for studying MTBI patients. However, to prove an established role of TA in MTBI further studies are needed, likewise comparison of the texture changes with other possible diagnostic findings.

Additional material

Additional file 1 Supplementary table. Texture parameters used in analysis.

Competing interests

The authors declare that they have no competing interests.

Authors' contributions

SS, PD, JÖ, HE designed and coordinated the whole MTBI project. KKH and LH designed this study and PD, SS and HE participated in its coordination. KKH performed the texture data collection and classification and drafted the manuscript. TL performed statistical analyses. MW performed the neuropsychological assessments. SL performed the neurological examinations and participated in the patient data collection. All authors participated in manuscript modifications, read and approved the final manuscript.

Acknowledgements

The authors thank Anne Vainionpää for her assistance with the image analysis. This study was supported by grants from the research funding of the Pirkanmaa Hospital District, Tampere University Hospital, the Jenny and Antti Wihuri foundation and the Instrumentarium Science Foundation.

Author Details

[1]Medical Imaging Center, Tampere University Hospital, Tampere, Finland, [2]Department of Biomedical Engineering, Tampere University of Technology, Tampere, Finland, [3]Tampere Medical School, University of Tampere, Tampere, Finland, [4]Department of Neurosciences and Rehabilitation, Tampere University Hospital, Tampere, Finland, [5]Department of Neurosurgery, Tampere University Hospital, Tampere, Finland, [6]Science Center, Pirkanmaa Hospital District, Tampere, Finland, [7]Tampere School of Public Health, University of Tampere, Tampere, Finland and [8]Department of Emergency Medicine Acuta, Tampere University Hospital, Tampere, Finland

Received: 2 November 2009 Accepted: 12 May 2010
Published: 12 May 2010

References

1. Cassidy JD, Carroll LJ, Peloso PM, Borg J, von Holst H, Holm L, Kraus J, Coronado VG: **Incidence, risk factors and prevention of mild traumatic brain injury: Results of the WHO collaborating centre task force on mild traumatic brain injury.** *J Rehab Med Suppl* 2004, **43:**28-60.
2. Yuan W, Holland SK, Schmithorst VJ, Walz NC, Cecil KM, Jones BV, Karunanayaka P, Michaud L, Wade SL: **Diffusion tensor MR imaging reveals persistent white matter alteration after traumatic brain injury experienced during early childhood.** *AJNR Am J Neuroradiol* 2007, **28:**1919-1925.
3. Belanger HG, Vanderploeg RD, Curtiss G, Warden DL: **Recent neuroimaging techniques in mild traumatic brain injury.** *J Neuropsychiatry Clin Neurosci* 2007, **19:**5-20.
4. Tuceryan M, Jain AK: **Texture analysis.** In *The Handbook of Pattern Recognition and Computer Vision* 2nd edition. Edited by: Chen CH, Pau LF, Wang PSP. New Jersey: World Scientific Publishing Co; 1998:207-248.
5. Castellano G, Bonilha L, Li LM, Cendes F: **Texture analysis of medical images.** *Clin Radiol* 2004, **59:**1061-1069.
6. Haralick R: **Statistical and structural approaches to texture.** *Proc IEEE* 1979, **67:**786-804.
7. Jirak D, Dezortova M, Taimr P, Hajek M: **Texture analysis of human liver.** *J Magn Reson Imaging* 2002, **15:**68-74.
8. Gibbs P, Turnbull LW: **Textural analysis of contrast-enhanced MR Images of the breast.** *Magn Reson Med* 2003, **50:**92-98.
9. Holli K, Lääperi A-L, Harrison L, Luukkaala T, Toivonen T, Ryymin P, Dastidar P, Soimakallio S, Eskola H: **Characterization of breast cancer types by texture analysis of magnetic resonance images.** *Academic Radiology* 2010, **17:**135-141.
10. Harrison L, Dastidar P, Eskola H, Järvenpää R, Pertovaara P, Luukkaala T, Kellokumpu-Lehtinen PL, Soimakallio S: **Texture analysis on MRI images of non-Hodgkin lymphoma.** *Comput Biol Med* 2008, **38:**519-524.
11. Harrison L, Luukkaala T, Pertovaara H, Saarinen T, Heinonen T, Järvenpää R, Soimakallio S, Kellokumpu-Lehtinen P, Eskola H, Dastidar P: **Non-Hodgkin**

lymphoma response evaluation with MRI texture classification. *Journal of Experimental & Clinical Cancer Research* 2009, **28:**87-100.
12. Herlidou S, Rolland Y, Bansard JY, Le Rumeur E, de Certaines JD: **Comparison of automated and visual texture analysis in MRI characterization of normal and diseased skeletal muscle.** *Magn Reson Imag* 1999, **17:**1393-1397.
13. Mahmoud-Ghoneim D, Cherel Y, Lemaire L, de Certaines JD, Meniere A: **Texture analysis of magnetic resonance images of rat muscles during atrophy and regeneration.** *Magn Reson Imaging* 2006, **24:**167-171.
14. Kjaer L, Ring P, Thomsen C, Henriksen O: **Texture analysis in quantitative MR imaging - tissue characterization of normal brain and intracranial tumours at 1.5T.** *Acta Radiol* 1995, **36:**127-135.
15. Herlidou-Meme S, Constans JM, Carsin B, Olivie D, Elia PA, Nadal-Desbarats L, Gondry C, Le Rumeur E, Idy-Perett I, de Certaines JD: **MRI texture analysis on texture test objects, normal brain and intracranial tumours.** *Magn Reson Imaging* 2003, **21:**989-993.
16. Lerski RA, Straughan K, Schad LR, Boyce D, Bluml S, Zuna I: **MR image texture analysis-an approach to tissue characterisation.** *J Magn Reson Imaging* 1993, **11:**873-887.
17. Schad LR, Blüml S, Zuna I: **MR tissue characterization of intracranial tumors by means of texture analysis.** *Magn Reson Imaging* 1993, **11:**889-896.
18. Mahmoud-Ghoneim D, Alkaabi MK, de Certaines JD, Goettsche FM: **The impact of image dynamic range on texture classification of brain white matter.** *BMC Med Imaging* 2008, **23:**8-18.
19. Freeborough PA, Fox NC: **MR image texture analysis applied to the diagnosis and tracking of Alzheimer's disease.** *IEEE Trans Med Imaging* 1998, **17:**475-479.
20. Bonilha L, Kobayashi E, Castellano G, Coelho G, Tinois E, Cendes F, Li LM: **Textural analysis of hippocampal sclerosis.** *Epilepsia* 2003, **44:**1546-1550.
21. Mahmoud-Ghoneim D, Toussaint G, Constans JM, de Certaines JD: **Three dimensional texture analysis in MRI: a preliminary evaluation in gliomas.** *Magn Reson Imaging* 2003, **21:**983-987.
22. Ganeshan B, Miles KA, Young RC, Chatwin CR, Gurling HMD, Critchley HD: **Three-dimensional textural analysis of brain images reveals distributed grey-matter abnormalities in schizophrenia.** *Eur Radiol* 2010, **20:**941-949.
23. Kovalev VA, Kruggel F, Gertz HJ, von Cramon Y: **Three dimensional texture analysis of MRI brain datasets.** *IEEE Trans Med Imaging* 2001, **20:**424-433.
24. Kovalev VA, Kruggel F: **Texture anisotropy of the brain's white matter as revealed by anatomical MRI.** *IEEE Trans Med Imaging* 2007, **5:**678-685.
25. Mahmoud-Ghoneim D, de Certaines JD, Herlidou S, Rolland Y, Maniere A: **Gender difference in MRI Texture Analysis of human adipose tissue.** *J Women's Imaging* 2001, **3:**105-107.
26. Carrol LJ, Cassidy JD, Holm L, Kraus J, Coronado VG: **Methodological Issues and Research Recommendations for Mild Traumatic Brain Injury: The WHO Collaborating Centre Task Force on Mild Traumatic Brain Injury.** *Journal of Rehabilitation Medicine Suppl* 2004, **43:**113-125.
27. Teasdale G, Jennett B: **Assessment of coma and impaired consciousness. A practical scale.** *Lancet* 1973, **11:**81-84.
28. Hajek M, Dezortova M, Materka A, Lerski R: *Texture analysis for magnetic resonance imaging* Prague: Med4publishing; 2006.
29. Collewet G, Strzelecki M, Mariette F: **Influence of MRI acquisition protocols and image intensity normalization methods on texture classification.** *J Magn Reson Imaging* 2003, **22:**81-91.
30. Uchino Y, Okimura Y, Tanaka M, Saeki N, Yamaura A: **Computed tomography and magnetic resonance imaging of mild head injury-is it appropriate to classify patients with Glasgow Coma Scale score of 13 to 15 as "mild injury"?** *Acta Neurochir* 2001, **143:**1031-1037.
31. Hofman PA, Stapert SZ, van Kroonenburgh MJ, Jolles J, de Kruijk J, Wilmink JT: **MR imaging, single-photon emission CT and neurocognitive performance after mild traumatic brain injury.** *Am J Neuroradiol* 2001, **22:**441-449.
32. Mitchener A, Wyper DJ, Patterson J, Hadley DM, Wilson JT, Scott LC, Jones M, Teasdale GM: **SPECT, CT, and MRI in head injury: acute abnormalities followed up at six months.** *J Neurol Neurosurg Psychiatry* 1997, **62:**633-636.
33. Levin HS, Williams DH, Eisenberg HM, High WM Jr, Guinto FC Jr: **Serial MRI and neurobehavioural findings after mild to moderate closed head injury.** *J Neurol Neurosurg Psychiatry* 1992, **55:**255-262.
34. Rutgers DR, Toulgoat F, Cazejust J, Fillard P, Lasjaunias P, Ducreux D: **White matter abnormalities in mild traumatic brain injury: a diffusion tensor imaging study.** *AJNR Am J Neuroradiol* 2008, **29:**514-519.
35. Posse S, Tedeschi R, Risinger R, Ogg R, Le Bihan D: **High speed 1H spectroscopic imaging in human brain by echo planar spatial-spectral encoding.** *Magn Reson Med* 1995, **33:**34-40.
36. Raucher A, Sedlacik J, Deistung A, Mentzel HJ, Reichenbach JR: **Susceptibility weighted imaging: data acquisition, image reconstruction and clinical applications.** *Z Med Phys* 2006, **16:**240-250.
37. Chu Z, Wilde EA, Hunter JV, McCauley SR, Bigler ED, Troyanskaya M, Yallampalli R, Chia JM, Levin HS: **Voxel-Based Analysis of Diffusion Tensor Imaging in Mild Traumatic Brain Injury in Adolescents.** *AJNR Am J Neuroradiol* 2009. doi:10.3174/ajnr.A1806
38. McGowan JC, Yang JH, Plotkin RC, Grossman RI, Umile EM, Cecil KM, Bagley LJ: **Magnetization transfer imaging in the detection of injury associated with mild head trauma.** *AJNR Am J Neuroradiol* 2000, **21:**875-880.
39. Sinson G, Bagley LJ, Cecil KM, Torchia M, McGowan JC, Lenkinski RE, McIntosh TK, Grossman RI: **Magnetization transfer imaging and proton MR spectroscopy in the evaluation of axonal injury: correlation with clinical outcome after traumatic brain injury.** *AJNR Am J Neuroradiol* 2001, **22:**143-151.
40. Zhang J, Tong L, Wang L, Li N: **Texture analysis of multiple sclerosis: a comparative study.** *Magnetic Resonance Imaging* 2008, **26:**1160-1166.
41. Harting MT, Jimenez F, Adams SD, Mercer DW, Cox CS Jr: **Acute, regional inflammatory response after traumatic brain injury: Implications for cellular therapy.** *Surgery* 2008, **144:**803-813.
42. Frugier T, Morganti-Kossmann C, O'Reilly D, McLean CA: **In situ detection of inflammatory mediators in post-mortem human brain tissue following traumatic injury.** *J Neurotrauma* 2010, **27:**497-507.
43. Kumar R, Husain M, Gupta RK, Hasan KM, Haris M, Agarwal Ak, Pandey CM, Narayana PA: **Serial changes in the white matter diffusion tensor imaging metrics in moderate traumatic brain injury and correlation with neuro-cognitive function.** *J Neurotrauma* 2009, **26:**481-495.
44. Aboitiz F, Scheibel AB, Fisher RS, Zaidel E: **Fiber composition of the human corpus callosum.** *Brain Res* 1992, **598:**143-153.
45. Rabi S, Madhavi C, Antonisamy B, Koshi R: **Quantitative analysis of the human corpus callosum under light microscopy.** *Eur J Anat* 2007, **11:**95-100.

Pre-publication history
The pre-publication history for this paper can be accessed here:
http://www.biomedcentral.com/1471-2342/10/8/prepub

doi: 10.1186/1471-2342-10-8
Cite this article as: Holli *et al.*, Texture analysis of MR images of patients with Mild Traumatic Brain Injury *BMC Medical Imaging* 2010, **10**:8

III

MRI Texture Analysis in Multiple Sclerosis: Toward a Clinical Analysis Protocol

Lara C. V. Harrison, MSc, MD, Minna Raunio, MD, Kirsi K. Holli, MSc, Tiina Luukkaala, MSc, Sami Savio, MSc, Irina Elovaara, MD, PhD, Seppo Soimakallio, MD, PhD, Hannu J. Eskola, PhD, Prasun Dastidar, MD, PhD

Rationale and Objectives: Magnetic resonance imaging (MRI)-based texture analysis has been shown to be effective in classifying multiple sclerosis lesions. Regarding the clinical use of texture analysis in multiple sclerosis, our intention was to show which parts of the analysis are sensitive to slight changes in textural data acquisition and which steps tolerate interference.

Materials and Methods: The MRI datasets of 38 multiple sclerosis patients were used in this study. Three imaging sequences were compared in quantitative analyses, including a comparison of anatomical levels of interest, variance between sequential slices and two methods of region of interest drawing. We focused on the classification of white matter and multiple sclerosis lesions in determining the discriminatory power of textural parameters. Analyses were run with MaZda software for texture analysis, and statistical tests were performed for raw parameters.

Results: MRI texture analysis based on statistical, autoregressive-model and wavelet-derived texture parameters provided an excellent distinction between the image regions corresponding to multiple sclerosis plaques and white matter or normal-appearing white matter with high accuracy (nonlinear discriminant analysis 96%–100%). There were no significant differences in the classification results between imaging sequences or between anatomical levels. Standardized regions of interest were tolerant of changes within an anatomical level when intra-tissue variance was tested.

Conclusion: The MRI texture analysis protocol with fixed imaging sequence and anatomical levels of interest shows promise as a robust quantitative clinical means for evaluating multiple sclerosis lesions.

Key Words: Magnetic resonance imaging (MRI); texture analysis (TA); multiple sclerosis (MS); tissue characterization.

Multiple sclerosis (MS) is the most common autoimmune disease of the central nervous system, with complex pathophysiology, including inflammation, demyelination, axonal degeneration, and neuronal loss. According to recent pathological evidence, these processes are not similarly represented in different patients, but may predominate selectively in individual patients, leading to heterogeneity in the expression of disease phenotypes. This diverse representation of different pathologies is also reflected in disease prognosis and response to therapies.

Diagnostic evaluation of MS with conventional magnetic resonance imaging (MRI) is generally based on the McDonald criteria (1,2). The development of modern imaging techniques for the early detection of brain inflammation and the characterization of tissue-specific injury is an important objective in MS research. The development of new imaging techniques is targeted especially at the identification of high-risk individuals in the early phase of MS disease and at the improved monitoring of disease activity. A better understanding of disease pathogenesis is also the basis for the further development of new and more effective therapies.

Quantitative MRI studies have shown that brain and focal lesion volume measures, magnetic transfer ratio and diffusion-weighted imaging–derived parameters can provide new information in detecting MS (3,4). Neurological diseases have been the focus of recent studies on texture analysis (TA) based on MRI. TA as a quantitative means of representing fine changes in tissues has been reported to be successful in studies of epilepsy (5–8), MS (9–13), brain tumors (14–16), amygdale activation (17), Alzheimer's disease (18,19), and cervical

Acad Radiol 2010; 17:696–707

From the Medical Imaging Center, Tampere University Hospital, Teiskontie 35, PO Box 2000, FIN-33521, Tampere, Finland (L.C.V.H., K.K.H., S. Savio, S. Soimakallio, H.J.E., P.D.); Tampere University Hospital, Tampere, Finland (L.C.V.H.); Tampere University Medical School, Tampere, Finland (L.C.V.H., M.R., I.E., S. Soimakallio, P.D.); Department of Biomedical Engineering, Tampere University of Technology, Tampere, Finland (L.C.V.H., K.K.H., S. Savio, H.J.E., P.D.); Science Center, Pirkanmaa Hospital District, Tampere, Finland (T.L.); Tampere School of Public Health, University of Tampere, Tampere, Finland (T.L.); Department of Neurology, Tampere University Hospital, Tampere, Finland (I.E.). Received July 22, 2009; accepted January 7, 2010. **Address correspondence to:** L.C.V.H. e-mail: lara.harrison@tut.fi

doi:10.1016/j.acra.2010.01.005

spondylotic myelopathy (20). Studies on MS TA have shown this method to be useful in detecting conventionally nonvisible microstructural changes in MS in the early stages of disease.

In a clinical context, constant innovation in imaging equipment and imaging sequences provides a challenging atmosphere in developing a robust multipurpose texture analysis protocol for neuroradiological quantitative analyses. Recent publications highlight various texture parameter sets in image analysis, whereas study protocol image acquisition settings differ. It appears that TA parameter subsets that distinguish subtle changes in tissues with the best classification results change relative to the imaging sequences (21). The foundation of a quantitative TA protocol consists of image acquisition and image processing, and it requires results obtained from fine structural changes between tissues through several manual, semiautomatic or automatic steps. In particular, nonstandardized manual phases of the process may cause immeasurable sources of error.

Regarding the clinical use of TA in MS diagnostics and follow-up, our intention was to determine which parts of the analysis are sensitive to small changes in a textural data analysis protocol and which steps tolerate interference in data acquisition. In this study, we focused specifically on the MRI protocols available in the majority of centers for clinical purposes. Therefore, a 1.5 T device and images acquired in normal clinical procedures were chosen to be used in this study.

We compared three imaging sequences with respect to TA classification results. Further, we analyzed two anatomical levels of interest for each sequence, and for two sequences we performed analyses of three sequential image slices to estimate the significance of image slice selection. In evaluating the TA method discrimination power, we used several standard size regions of interest (ROI) representing different tissues, pathological focal lesions, and diffuse-disease suspect tissue in the classification process. Additionally, we compared standard size and freehand-drawn ROIs of lesions from normal and normal-appearing brain tissue. The major goal of this study was to clarify the impact of different steps of analysis on TA classification and furthermore develop a robust quantitative MRI TA protocol for scientific and clinical use in MS evaluation and other neuroradiological purposes.

MATERIALS AND METHODS

Patients

MRI images of 38 patients participating in a prospective neuroinflammatory diseases research project were selected for this study. Because this study focused on normal clinical practice in MRI imaging of MS, the patient population represented average patients in our center being consecutively imaged for MS diagnosis and follow-up, showing some heterogeneity in age and subtypes in their disease. Imaging was performed between May 2006 and January 2007. There were 15 males and 23 females between ages 18 and 67 years (mean age 42, median 39), with different subtypes of MS: relapsing-remitting (n = 19), secondary progressive (n = 10), primary progressive (n = 4), progressive-relapsing (n = 2), and clinically isolated syndrome (n = 3). The diagnoses were based on revised McDonald's criteria (2). The Ethics Committee of the hospital approved the study and participants provided written informed consent.

MRI Acquisition

MRI was performed on a 1.5 T MRI device (Siemens, Avanto Syngo MR B15, Erlangen, Germany). The whole-brain MRI protocol included standardized axial T2-weighted Inversion Recovery Turbo Spin Echo (TIRM) sequence (repetition time 8500 ms, echo time 100 ms, TI 2500 ms, slice thickness 5 mm, zero gap between slices, pixel size 0.45 mm × 0.45 mm, echo train length 17, flip angle 150°); T1-weighted three-dimensional magnetization prepared gradient echo sequence (MPR) (repetition time 1160 ms, echo time 4.24 ms, TI 600 ms, slice thickness 0.9 mm, pixel size 0.45 mm × 0.45 mm, echo train length 1, flip angle 15°); and previous T1-weighted gradient echo sequence acquired with intravenous contrast agent gadoterate meglumine (DOTAREM 10 mL). The imaging artefacts were minimized with use of two filters. A prescan normalization filter was used for the correction of intensity inhomogeneity (heterogeneous brightness) in images. The data used for homogenization were acquired through a preliminary low-resolution measurement. An elliptical filter was used within the slice planes to improve the signal-to-noise ratio in the T2 TIRM sequence. The quality of image sets was evaluated by an experienced radiologist. The image sets were uniform and of good quality. The images were free of motion artefacts.

Texture Analysis

The texture analysis study protocol is illustrated in the flow chart (Fig 1). The protocol starts with image acquisition; in this study, we examined three imaging sequences from each patient. Two clinically important anatomical levels were defined, and one image slice was selected from each level and sequence. Further, for analysis of textural variation between sequential slices, sequential images were chosen from both anatomical levels of a subgroup of patients and image series. ROIs representing tissues and anatomical structures were set with two manual methods: standard-size ROI boxes and nonstandard size, freehand drawn ROIs. Texture features were calculated from the ROIs. All features calculated as well feature sets selected with different methods were fed as input for analyses of intra-tissue variability and classification of tissues.

Image series used in quantitative analyses were T2-weighted TIRM (T2 TIRM), native T1-weighted gradient echo (T1 MPR), and gadoterate meglumine–enhanced T1-weighted gradient echo sequence (T1 MPR+C). Images for analyses were selected from two anatomical levels: the corona radiata and centrum semiovale along with MS lesion and basal ganglia, where the nucleus

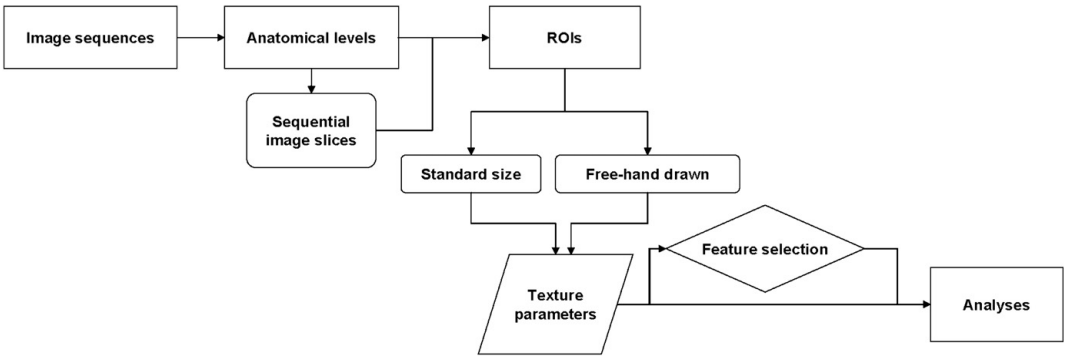

Figure 1. Texture analysis protocol.

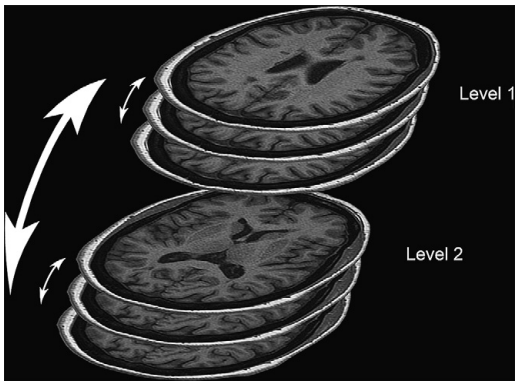

Figure 2. Two anatomical levels analyzed from all image series. Three sequential images from T1-weighted series from both levels were analyzed.

caudatus and lentiformis were simultaneously represented in the same image slice MS plaque also present (Fig 2). These levels are familiar in typical MS plaques.

Texture analysis applications MaZda (3.20) and B11 (3.4) (The Technical University of Lodz, Institute of Electronics (22–24)) were used for ROI setting, texture parameter calculation, and classification. Standard-size ROI boxes of 10 × 10 pixels were used for (a) white matter (WM) apart from lesions, (b) white matter near lesions (normal-appearing white matter, NAWM), (c) cerebrospinal fluid (CSF), (d) nucleus caudatus, (e) nucleus lentiformis and (f) MS plaque (MS plaque, 10 × 10 ROI). Standardized ROI boxes of 6 × 6 pixels were used for (a) cortex apart from lesions (gray matter, GM) and (b) cortex near lesion (normal-appearing gray matter, NAGM). One nonstandard size, freehand-drawn ROI was used for a MS plaque (MS plaque, freehand ROI) (Fig 3, Table 1).

MS subtype was not taken as a variable because of the small number of patients representing some of the subtypes. We leave the testing of emerging subtle changes between disease subtypes in plaque textural appearance to a separate study. The ROI drawing was done manually by a practiced licentiate of medicine, an engineer of medical technology with a special interest in developing quantitative radiology methods in clinical use. The software used did not provide any registration tool. Visual analysis based on anatomical landmarks was used when transferring ROIs among the imaging sequences. A specialized and experienced senior neuroradiologist double-checked the ROI setting by viewing the original images and the combination images with the ROIs superimposed.

A total of 280 texture parameters calculated were based on histogram, gradient, run-length matrix, cooccurrence matrix, autoregressive-model (AR-model), and wavelet parameters (24). Run-length matrix parameters were calculated in four directions: horizontal (0°), vertical (90°), 45°, and 135°. Cooccurrence matrix parameters were calculated in five distances, four times on each distance. Wavelet energy parameters were calculated on three scales, each with four frequency subband images. The image gray-level intensity normalization computation was run in the texture analysis application separately for each ROI, with method-limiting image intensities in the range μ-3σ, μ+3σ, where m is the mean gray-level value and σ the standard deviation (24,25).

Intra-tissue texture variation for all ROIs was analyzed between anatomical levels separately for each imaging sequence (n = 38). Variations in texture among three sequential image slices were evaluated within a T1-weighted image series of 23 patients chosen by random sampling from the 38 patients. The two aforementioned anatomical levels and all ROIs were analyzed. Because of image slice thickness, T2 TIRM images were not included the sequential image slice analysis: the anatomical image information changes significantly between sequential T2 TIRM 5-mm-thick images.

Texture classifications for two tissue combinations were performed for (a) WM vs. MS plaque (freehand ROI), (b) WM vs. MS plaque (10 × 10 ROI), (c) NAWM vs. MS plaque (freehand ROI), (d) NAWM vs. MS plaque (10 × 10 ROI), (e) WM vs. NAWM, and (f) nucleus caudatus vs. nucleus lentiformis (n = 38) (Table 2).

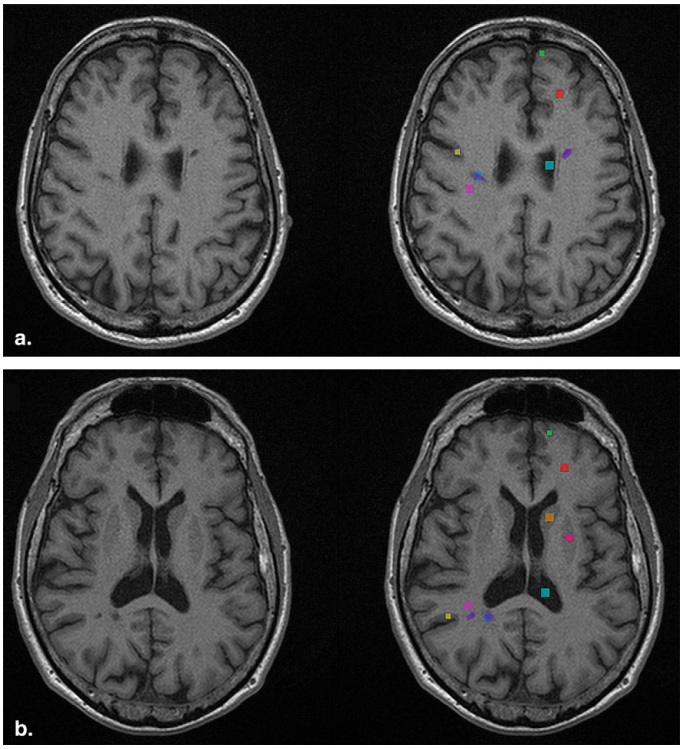

Figure 3. T1 magnetization prepared gradient echo sequence images representing anatomical levels used in the analyses. Plain images on left and images with regions of interest (ROIs) on right. Anatomical level 1: corona radiata and centrum semiovale with multiple sclerosis (MS) plaques **(a)**; level 2: basal ganglia **(b)**. ROIs presented in colors: red, white matter; pink, normal-appearing white matter; aquamarine, cerebrospinal fluid; orange, nucleus caudatus; darker pink, nucleus lentiformis; blue, MS plaque (10 × 10 ROI); green, cortex apart from lesions (gray matter); yellow, cortex near lesion (normal-appearing gray matter); violet, hand-drawn MS plaque (freehand ROI).

TABLE 1. Tissues Used as ROIs and Sizes of ROIs in Pixels

ROI	Size
White matter	10 × 10
Normal-appearing white matter	10 × 10
Cerebrospinal fluid	10 × 10
Normal-appearing gray matter apart lesion	6 × 6
Normal-appearing gray matter near lesion	6 × 6
Nucleus caudatus	10 × 10
Nucleus lentiformis	10 × 10
MS plaque, freehand ROI	Varying
MS plaque, standard size ROI	10 × 10

MS = multiple sclerosis; ROI = region of interest.

TABLE 2. Tissue Pairs Used in the Classification of Tissues

Tissue pairs used in classification
White matter/MS plaque, freehand ROI
White matter/MS plaque, 10 × 10 ROI
White matter/normal-appearing white matter
Normal appearing white matter/MS plaque, freehand ROI
Normal appearing white matter/MS plaque, 10 × 10 ROI
Nucleus caudatus/nucleus lentiformis

MS = multiple sclerosis; ROI = region of interest.

Two automated methods provided by MaZda, Fisher coefficient (Fisher), and classification error probability (POE) combined with average correlation coefficients (ACC), were used to identify 10 texture features giving the best discrimination between tissue pairs. Ten texture features were chosen with both methods separately for each combination of two ROIs, sequence and image level. In addition, 25 texture features recently reported to be efficient (13) were used (Table 3). The best 10 texture features selected with both automated methods as well as for the manually selected 25 features used in a recent study for each sequence/anatomical-level tissue pair combinations were analyzed by principal component analysis (PCA) and linear discriminant analysis, followed by nearest-neighbor classification with the leave-one-out-method for the most expressive features resulting from PCA and the most discriminating features from linear discriminant analysis. Nonlinear discriminant analysis (NDA) was run with included artificial neural network classification. The mathematical notations of parameter calculation, image intensity normalization, feature selection methods, and analyses are defined elsewhere (24,25).

TABLE 3. List of 25 Texture Analysis Parameters used in Manual Feature Selection

Parameters used in Manual Feature Selection

Parameter Group	Parameter Name
Cooccurrence matrix	Contrast S(0,1)
Cooccurrence matrix	Contrast S(1,0)
Cooccurrence matrix	Contrast S(1,1)
Cooccurrence matrix	Contrast S(1,-1)
Cooccurrence matrix	Difference variance S(0,1)
Cooccurrence matrix	Difference variance S(1,0)
Cooccurrence matrix	Difference variance S(1,1)
Cooccurrence matrix	Difference variance S(1,-1)
Cooccurrence matrix	Sum of squares S(0,1)
Cooccurrence matrix	Sum of squares S(1,0)
Cooccurrence matrix	Sum of squares S(1,1)
Cooccurrence matrix	Sum of squares S(1,-1)
Cooccurrence matrix	Sum variance S(0,1)
Cooccurrence matrix	Sum variance S(1,0)
Cooccurrence matrix	Sum variance S(1,1)
Cooccurrence matrix	Sum variance S(1,-1)
Run length matrix	Gray level nonuniformity, 135°
Run length matrix	Gray level nonuniformity, 45°
Run length matrix	Gray level nonuniformity, 0°
Run length matrix	Gray level nonuniformity, 90°
Gradient	Mean absolute gradient
Gradient	Variance of absolute gradient
Autoregressive model	Standard deviation
Wavelet	Energy, subband 1, HL
Wavelet	Energy, subband 2, HL

Because of the small sample size and skewed distributions, nonparametric statistical tests were used. The Wilcoxon signed rank test was used to evaluate the raw TA parameters used to describe the textural difference between tissues. The Wilcoxon signed rank test was used for all raw parameters when testing intra-tissue textural differences between imaging levels, and the Friedman test was used for intra-level analyses. A level of $P < .05$ was considered statistically significant. These analyses were performed using SPSS for Windows, version 16.0.2.

RESULTS

Intra-tissue Difference in Sequential Image Slices and between Anatomical Levels

The tissue textural variation between two anatomical levels of interest ($n = 38$) was analyzed separately for all three imaging series. Tests were performed for WM, NAWM, CSF, NAGM, and MS plaque (standard-size and freehand ROIs). The difference between levels was evaluated by the number of TA parameters with statistically significant differences. There were 280 TA parameters in total. The T1 MPR series proved to be uniform with a mean percentage difference of parameters of 6% in the Wilcoxon signed rank test. The T1 MPR with contrast agent and T2 TIRM series succeeded with a mean percentage difference of parameters of 10%. Within all series, freehand MS plaque ROI stood out with a mean percentage of 27% statistically different parameters, as opposed to the standard size MS ROI, with a mean percentage of 6% (Table 4).

Texture intra-level variation for three sequential image slices ($n = 23$) was analyzed for T1 MPR series with and without contrast agent. Tests were performed for WM, NAWM, CSF, NAGM, and MS plaque (standard size and freehand ROIs), in addition to which, nucleus caudatus and nucleus lentiformis were taken into the analyses on the level of basal ganglia. Slice-to-slice texture variation was evaluated as the proportion of parameters having a statistically significant difference in a total of 280 parameters in the Friedman test. The variation was small in both anatomical levels (mean percentages 5%–8%), and the presence of contrast agent did not show any advantage. Tissue-specific results were even, and MS freehand ROIs did not show differences as great as between levels (mean percentage 9%). However, NAGM appeared to change more than other tissues from slice to slice (mean percentage 10%) (Table 5).

Classification of Tissues

Classification was performed on six pairs of two-tissue combinations (Table 2). Classification with B11 analyses for WM-NAWM performed the best in NDA, with a correct classification percentage of 85% within T2 TIRM images at the anatomical-level basal ganglia and feature selection with POE+ACC. Nucleus caudatus–nucleus lentiformis classification was unsuccessful with a high rate of misclassification in all analysis combinations. All combinations of white matter and MS lesions (WM-MS plaque [10 × 10 ROI], WM-MS plaque [freehand ROI], NAWM-MS plaque [10 × 10 ROI], and NAWM-MS plaque [freehand ROI]) gave highly accurate classification results in all image types, anatomical levels, and feature selection methods (NDA 96%–100%).

On the whole, feature selection with POE+ACC resulted in the best classification; the Fisher method of selecting parameters was somewhat worse, and the manually selected group of parameters was inferior to both. T1 MPR with contrast agent sequence showed slightly better overall classification than without contrast agent and then the T2 TIRM series. However, all sequences achieved similar classification results, the best one varying somewhat between PCA, linear discriminant analysis, and NDA analyses. Separation of WM or NAWM from MS plaques proved slightly better when the ROI of the plaque was hand-drawn and white matter ROI was drawn apart from the MS lesion. A summary of

TABLE 4. Intra-tissue Differences between Anatomical Levels Calculated for Three Imaging Sequences

Imaging Sequence	T1 MPR		T1 MPR+C		T2 TIRM	
	n	% of Total	*n*	% of Total	*n*	% of Total
WM	9	3%	18	6%	35	12%
NAWM	3	1%	8	3%	7	2%
CSF	20	7%	28	10%	20	7%
NAGM apart lesion	18	6%	21	7%	26	9%
NAGM near lesion	7	2%	9	3%	10	4%
MS plaque, freehand ROI	46	16%	94	34%	85	30%
MS plaque, 10 × 10 ROI	13	5%	22	8%	13	5%

MPR = magnetization prepared gradient echo sequence; MPR+C = T1 MPR with contrast agent; WM = white matter; NAWM = normal-appearing white matter; CSF = cerebrospinal fluid NAGM = normal-appearing gray matter; MS = multiple sclerosis; ROI = region of interest.
The number and percentage of parameters having statistically significant difference in the Wilcoxon test ($P < .05$) are given in columns; the total number of parameters was 280. The total number of patients was 38.

TABLE 5. Intra-tissue Differences between Three Sequential Image Slices Calculated for T1-weighted Imaging Sequences T1 MPR and T1 MPR+C on Both Anatomical Levels with the Friedman Test

Imaging Sequence	T1 MPR				T1 MPR+C			
Imaging Level	1		2		1		2	
	n	% of Total	*n*	% of Total	*n*	% of Total	*n*	% of Total
WM	14	5%	20	7%	11	4%	15	5%
NAWM	18	7%	13	5%	26	9%	12	4%
CSF	3	1%	18	6%	17	6%	13	5%
NAGM apart lesion	22	8%	18	6%	18	6%	18	6%
NAGM near lesion	26	9%	26	9%	36	13%	21	8%
Nucleus caudatus			24	9%			18	6%
Nucleus lentiformis			11	4%			6	2%
MS plaque, freehand ROI	14	5%	38	14%	36	13%	15	5%
MS plaque, 10 × 10 ROI	17	6%	14	5%	20	7%	15	5%

MPR = magnetization prepared gradient echo sequence; MPR+C = T1 MPR with contrast agent; WM = white matter; NAWM = normal-appearing white matter; CSF = cerebrospinal fluid; NAGM = normal-appearing gray matter; MS = multiple sclerosis; ROI = region of interest.
Nucleus caudatus and nucleus lentiformis were visible only in level 2 and were thus left out of the analyses of level 1. The number and percentage of parameters having statistically significant differences ($P < .05$) are given in columns. The total number of texture parameters was 280. The total number of patients was 23.

classifications based on PCA and NDA for tissue pairs is presented in Tables 6a–c.

In different combinations of imaging sequences, anatomical level classification, and tissue pair classification, a total of 88 parameters was selected with automated methods POE+ACC and Fisher for discrimination of WM and MS lesion tissues. In the top 10 ranked parameters, the T1 MPR sequence had total of 63 automatically selected parameters, T1 MPR+C 55, and T2 TIRM a total of 47. The automated methods–based parameter group had 12 parameters in common with the manually selected group of parameters. The 10 best texture parameters for each image sequence are listed in Tables 7a–c, with the distribution median values and results of the Wilcoxon signed rank test *P* values showing statistically significant differences. Statistical differences between the raw parameters of tissue pair combinations tested were, in general, uniform. Distributions of the cooccurrence parameter sum average S(1,1) for WM, NAWM, MS 10 × 10 pixel, and freehand ROIs are shown in Figure 4 to demonstrate the separability of raw parameters between tissues, imaging levels, and sequences.

DISCUSSION

MRI texture analysis based on statistical, autoregressive-model, and wavelet-derived texture parameters yielded excellent classification of tissue-pair MS plaques and WM or NAWM with high accuracy (NDA 96%–100%), and this study strengthens the results reported in a recent study (13). Likewise, the texture parameter sets gave accurate classification in nearest-neighbor and artificial neural network analyses, and parameters assessed individually by the Wilcoxon signed rank test showed good discriminatory power of raw parameters between tissues. The WM, NAWM, and MS lesions examined with T2-weighted TIRM and T1-weighted MPR with and without contrast agent sequences

led to nearly identical classifications, the sequence with contrast agent being slightly superior to the others. Considering this, different imaging sequences may be selected for analysis without notable loss of accuracy, and invasive use of contrast agent is not necessary in analyses of these tissues to this extent. The additional value of combining parameter values from different sequences for single-classification analysis remains to be investigated.

In the classification of WM and NAWM we achieved up to 85% accurate classification. This corroborates the results of an earlier study (13). It should be considered whether the classification could be enhanced with some particular analysis protocol, and if not, whether this classification result of WM and NAWM is sufficient for automated classification for scientific purposes or can be used as a second opinion tool in a clinical setting.

The method did not succeed in distinguishing the tissue pair of nucleus lentiformis and nucleus caudatus, indicating that the texture parameters and image acquisition as performed were not sufficient for detecting the textural change between the tissues investigated.

There were no significant intra-tissue differences in slice-to-slice comparisons when standard size ROIs were used, indicating that image slice selection for analyses tolerates changes. Parameters describing tissues did not change considerably in slice-to-slice comparisons if the image slice was selected one or two slices cranially or caudally from the recommended slice, if slice thickness was 0.9 mm and if there was no spacing between slices. The difference between anatomical levels was also acceptably small, especially in T1-weighted MPR sequences without contrast agent. Variation was still found in the best discriminating features selected with automated methods, indicating changes between levels. In all comparisons, there were some small differences between imaging sequences. We recommend that tissue samples (ie, ROIs) be selected from fixed anatomical levels if possible,

TABLES 6A–C. Rate of Correct Classification of Tissue Pairs Independently Calculated for the Three Imaging Sequences T1 MPR (6a), T1 MPR+C (6b), and T2 TIRM (6c)

Table 6a

T1 MPR

Imaging Level	Level 1			Level 2		
Feature Selection	F	P	M	F	P	M
WM vs. MS freehand ROI						
PCA	94% (72/76)	98% (75/76)	85% (65/76)	90% (69/76)	97% (74/76)	85% (65/76)
NDA	100% (76/76)	100% (76/76)	100% (76/76)	98% (75/76)	100% (76/76)	98% (75/76)
WM vs. MS 10 × 10 ROI						
PCA	94% (72/76)	96% (73/76)	78% (60/76)	81% (61/75)	94% (71/75)	81% (61/75)
NDA	100% (76/76)	100% (76/76)	98% (75/76)	97% (73/75)	100% (75/75)	98% (74/75)
NAWM vs. MS freehand ROI						
PCA	92% (70/76)	98% (75/76)	86% (66/76)	98% (75/76)	97% (74/76)	85% (65/76)
NDA	100% (76/76)	100% (76/76)	100% (76/76)	100% (76/76)	100% (76/76)	100% (76/76)
NAWM vs. MS 10 × 10 ROI						
PCA	90% (69/76)	90% (69/76)	81% (62/76)	93% (70/75)	97% (73/75)	85% (64/75)
NDA	98% (75/76)	98% (75/76)	98% (75/76)	100% (75/75)	100% (75/75)	97% (73/75)

Table 6b

T1 MPR+C

Imaging Level	Level 1			Level 2		
Feature Selection	F	P	M	F	P	M
WM vs. MS freehand ROI						
PCA	97% (73/75)	100% (75/75)	93% (70/75)	96% (73/76)	96% (73/76)	93% (71/76)
NDA	100% (75/75)	100% (75/75)	100% (75/75)	100% (76/76)	100% (76/76)	98% (75/76)
WM vs. MS 10 × 10 ROI						
PCA	92% (70/76)	94% (72/76)	82% (63/76)	96% (73/76)	97% (74/76)	77% (59/76)
NDA	100% (76/76)	100% (76/76)	96% (73/76)	100% (76/76)	100% (76/76)	98% (75/76)
NAWM vs. MS freehand ROI						
PCA	93% (70/75)	98% (74/75)	90% (68/75)	90% (69/76)	96% (73/76)	88% (67/76)
NDA	96% (72/75)	100% (75/75)	100% (75/75)	98% (75/76)	97% (74/76)	98% (75/76)
NAWM vs. MS 10 × 10 ROI						
PCA	94% (72/76)	92% (70/76)	81% (62/76)	100% (76/76)	98% (75/76)	82% (63/76)
NDA	100% (76/76)	100% (76/76)	96% (73/76)	100% (76/76)	100% (76/76)	98% (75/76)

TABLES 6A–C. (*continued*) Rate of Correct Classification of Tissue Pairs Independently Calculated for the Three Imaging Sequences T1 MPR (6a), T1 MPR+C (6b), and T2 TIRM (6c)

Table 6c						
T2 TIRM						
Imaging Level	**Level 1**			**Level 2**		
Feature Selection	**F**	**P**	**M**	**F**	**P**	**M**
WM vs. MS freehand ROI						
PCA	100% (76/76)	100% (76/76)	89% (68/76)	98% (74/75)	100% (75/75)	96% (72/75)
NDA	100% (76/76)	100% (76/76)	100% (76/76)	100% (75/75)	100% (75/75)	100% (75/75)
WM vs. MS 10 × 10 ROI						
PCA	85% (65/76)	86% (66/76)	80% (61/76)	88% (66/75)	97% (73/75)	86% (65/75)
NDA	97% (74/76)	98% (75/76)	96% (73/76)	97% (73/75)	100% (75/75)	98% (74/75)
NAWM vs. MS freehand ROI						
PCA	98% (75/76)	100% (76/76)	93% (71/76)	100% (76/76)	100% (76/76)	89% (68/76)
NDA	100% (76/76)	100% (76/76)	100% (76/76)	100% (76/76)	100% (76/76)	100% (76/76)
NAWM vs. MS 10 × 10 ROI						
PCA	77% (59/76)	81% (81/76)	68% (52/76)	86% (66/76)	89% (68/76)	69% (53/76)
NDA	96% (73/76)	96% (73/76)	98% (75/76)	97% (74/76)	98% (75/76)	98% (75/76)

Results are presented for two anatomical imaging levels: corona radiata and centrum semiovale and basal ganglia, for three feature reduction methods: Fisher (F), POE+ACC (P), and manual (M). Classifications were based on 1-NN for features of principal component analysis (PCA) and on ANN for nonlinear discriminant analysis (NDA) features. Data are percentages of correct classification. Data in parentheses are the number of region of interest (ROI) samples correctly classified and the total number of ROI samples in the analysis in question used to calculate percentages. The total number of patients was 38.

MPR = magnetization prepared gradient echo sequence; MPR+C = T1 MPR with contrast agent; WM = white matter; NAWM = normal-appearing white matter; CSF = cerebrospinal fluid NAGM = normal-appearing gray matter; MS = multiple sclerosis; ROI = region of interest.

though some acceptable slice-to-slice variation still remains even with the use of anatomical landmarks for slice selection.

The ROI setting with standard-size vs. freehand ROIs was tested with one tissue sample, MS plaque. There were distinct differences between the hand-drawn and standard ROIs of MS plaques in intra-tissue texture parameter comparison. Standardized ROI on a lesion gave slightly weaker classification from WM than hand-drawn ROI; naturally, a standard-size ROI box may overlap some NAWM neighboring a MS plaque. Compared to hand-drawn ROIs, the advantages of standardized ROIs include increased tolerance for slice selection and reproducibility. The advantages and disadvantages of ROI-drawing methods on lesions should be taken into consideration when establishing the analysis protocol.

When automated feature reduction methods were compared, the POE+ACC method was found to select parameters giving better separation between tissue pairs. It should be noted that feature selections that were run independently for each tissue pair combination led to superior classification results compared to the fixed feature group used in another study (13). The best discriminating texture parameters showed a change between the imaging sequences and tissue pairs of interest; automated methods recommended 88 parameters out of a total of 280 for analyses. Future studies should examine whether there are sensitive sets of features robust to changing imaging sequences and tissues in the neuroradiological context.

In MRI, the images may suffer from artefacts of different origin, such as image thermal noise, image background nonuniformity from magnetic field inhomogeneities, and nonstandardness of image gray-scale intensity. High image quality and minimization of image artefacts are important, especially in quantitative analyses. There are numerous methods to correct intensity inhomogeneity artefacts, but this problem is still not completely solved (26). Several reports have shown effective methods for image intensity standardization (27–29). The clinical images obtainable in our normal clinical procedures, including elliptical and prescan filtering to improve the image quality, also appeared to lead to accurate classification of WM and MS lesions. If extended artefact-correcting methods or a combination of methods was used, the texture analysis results would probably have shown even better discrimination between tissues.

Our texture analysis protocol is suitable for the classification of MS plaques from WM and NAWM. Using one image sequence in the protocol would meet the goal; all sequences tested were suitable for TA purposes. However, this situation may change due study design–specific issues; for example, the study focuses on expected differences in the contrast enhancement of lesions or lesions visible in different types of sequences. According to the requirements of the case in question, more than one sequence should be considered when establishing a protocol and selecting imaging sequences to analyze. As was shown here, both anatomical levels used in the analyses resulted in equal classification. When constructing the analysis protocol, it does not seem necessary to select more than one anatomical level of interest. The ROI drawing

TABLES 7 A–C. The 10 Best Texture Parameters for White Matter and MS Classification Given Individually for Imaging Sequences T1 MPR (7a), T1 MPR+C (7b), and T2 TIRM (7c)

Table 7a

T1 MPR	Tissues	WM		NAWM		MS, Freehand ROI		MS, 10 × 10 ROI	
	Imaging Level	1	2	1	2	1	2	1	2
Parameter Group, Name		Md	Md	Md	Md	Md	Md	Md	Md
Autoregressive model	Standard deviation	0.42	0.40	0.40	0.41	0.22	0.23	0.26	0.25
Histogram	MinNorm	293	299	304	295	158	158	183	177
Histogram	Variance	176	185	203	192	1102	1209	819	754
Gradient	Mean absolute gradient	1088	1095	1091	1082	732	781	887	813
Cooccurrence matrix	Contrast S(1,0)	988	932	877	860	410	448	588	529
Wavelet	Energy, subband 2, LL	17,629	17,369	17,683	17,087	29,582	26,829	27,055	23,209
Co-occurrence matrix	Sum entropy S(3,0)	1.65	1.62	1.66	1.64	2.17	2.06	1.73	1.75
Co-occurrence matrix	Contrast S(0,1)	945	874	929	940	409	419	541	479
Co-occurrence matrix	Sum entropy S(2,0)	1.70	1.71	1.72	1.72	2.22	2.11	1.79	1.80
Co-occurrence matrix	Contrast S(2,0)	31,110	2840	2813	2618	1263	1448	1936	1595

Table 7b

T1 MPR+C	Tissues	WM		NAWM		MS, Freehand ROI		MS, 10 × 10 ROI	
	Imaging Level	1	2	1	2	1	2	1	2
Parameter Group, Name		Md	Md	Md	Md	Md	Md	Md	Md
Histogram	MinNorm	297	299	310	295	162	162	167	170
Autoregressive model	Standard deviation	0.43	0.39	0.40	0.39	0.24	0.21	0.27	0.21
Gradient	Mean absolute gradient	1144	1109	1073	1075	772	775	895	835
Histogram	Variance	183	179	185	184	1231	1422	730	749
Run length matrix	Gray level nonuniformity, 90°	2.88	2.94	2.89	2.95	5.11	3.58	2.00	1.94
Wavelet	Energy, subband 2, LL	17,076	16,812	18,352	18,651	27,477	27,614	25,828	24,621
Co-occurrence matrix	Sum average S(1,1)	255	254	254	254	246	246	245	245
Co-occurrence matrix	Sum entropy S(2,2)	1.63	1.64	1.64	1.63	2.22	2.09	1.71	1.71
Co-occurrence matrix	Sum entropy S(1,0)	1.77	1.76	1.78	1.77	2.29	2.18	1.84	1.85
Run length matrix	Gray level nonuniformity, 45°	2.85	3.00	2.85	2.93	5.14	3.55	2.04	2.06

Table 7c

T2 TIRM	Tissues	WM		NAWM		MS, Freehand ROI		MS, 10 × 10 ROI	
	Imaging Level	1	2	1	2	1	2	1	2
Parameter Group, Name		Md	Md	Md	Md	Md	Md	Md	Md
Co-occurrence matrix	Sum average S(1,0)	254	254	253	254	263	265	261	262
Co-occurrence matrix	Sum average S(1,1)	254	255	253	252	265	266	268	268

Autoregressive model	Standard deviation	0.41	0.42	0.38	0.34	0.15	0.18	0.23	0.19
Co-occurrence matrix	Sum average S(1,-1)	254	255	253	253	265	267	266	268
Histogram	Variance	165	162	193	221	2507	2073	906	1164
Co-occurrence matrix	Sum average S(2,0)	253	255	254	254	268	269	264	267
Run length matrix	Gray level nonuniformity, 135°	2.94	3.00	2.84	2.84	5.67	4.20	1.89	1.92
Co-occurrence matrix	Sum average S(0,2)	253	256	254	253	269	267	264	263
Co-occurrence matrix	Sum average S(0,1)	254	255	254	253	264	263	261	260
Co-occurrence matrix	Contrast S(1,-1)	1307	1532	1275	1283	439	612	957	777

Texture feature distribution median values (Md) are given in columns for white matter (WM), normal-appearing white matter (NAWM), MS 10 × 10 and freehand regions of interest (ROIs). Statistical differences between the tissue pairs WM vs. MS freehand ROI, WM vs. MS 10 × 10 ROI, NAWM vs. MS freehand ROI, and NAWM vs. MS 10 × 10 ROI for imaging levels 1 and 2 was calculated with the Wilcoxon signed rank test. The results were uniform and are given in *P* values. Statistical differences between tissue pairs was highly significant ($P < .0001$) in all comparisons except those mentioned in the table footnotes. The total number of patients was 38.

MPR = magnetization prepared gradient echo sequence; MPR+C = T1 MPR with contrast agent; WM = white matter; NAWM = normal-appearing white matter; CSF = cerebrospinal fluid NAGM = normal-appearing gray matter; MS = multiple sclerosis; ROI = region of interest.

Table 7b

1) Gray level nonuniformity, 90°: WM vs. MS freehand ROI, level 2: $P = .0140$; NAWM vs. MS freehand ROI; level 2: $P = .0411$.

2) Gray level nonuniformity, 45°: WM vs. MS freehand ROI, level 2: $P = .0150$; NAWM vs. MS freehand ROI; level 2: $P = .0326$.

Table 7c

1) Gray level nonuniformity, 135°: WM vs. MS freehand ROI, level 2: $P = .0090$.

2) Contrast S(1,-1): NAWM vs. MS 10 × 10 ROI, level 1: $P = .0032$.

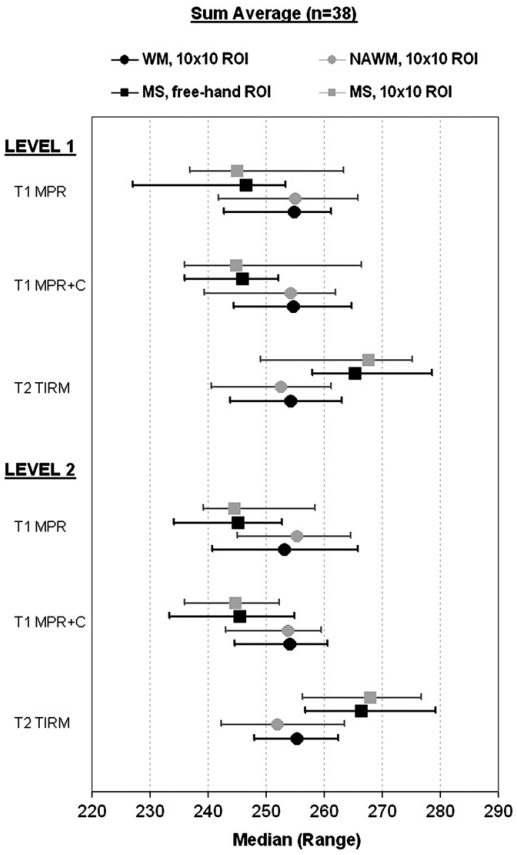

Figure 4. Distribution of the cooccurrence parameter sum average S(1,1) for white matter (WM), normal-appearing white matter (NAWM), and standard-size and freehand regions of interest (ROIs) of multiple sclerosis (MS) lesions. Median values shown with range for imaging sequences T1 magnetization prepared gradient echo sequence (MPR), T1 MPR with contrast agent (T1 MPR+C), and T2 TIRM for two levels of interest. Total number of patients was 38.

method should be considered for each individual study. The automated feature selection method POE+ACC, provided by MaZda, led to better separation between tissues than the other two methods, but all methods used were effective.

Regarding a clinical analysis protocol in MRI-based MS texture analysis, we evaluated the effects of imaging sequence, anatomical level of interest, slice-to-slice variation, ROI drawing method, and feature selection method. Statistical, autoregressive-model, and wavelet-derived texture parameters are suitable for the classification of white matter and MS lesions. All imaging sequences used in this study performed the classifications equally well; different types of sequences can be used for the analyses. ROIs should be selected from fixed anatomical levels to minimize TA parameter variation. Using anatomical landmarks for slice selection still leaves some acceptable slice-to-slice variation. Standard size ROI boxes were shown to tolerate changes in image slice selection. Standard ROIs vs. free-hand ROIs should be considered according to the requirements of the study. Case-specific selection of the texture parameters to analyze outperformed the discriminatory power of the fixed parameter group by a small margin. These results are important in protocol determination and should always be considered regarding the case in question when striving for a robust and reproducible protocol in the clinical setting.

Appropriate MRI texture analyses (ie, analyses of NAWM and NAGM) in MS patients can, along with routine MRI analyses (ie, analyses of plaques and atrophy), increase the extent of pathological lesions detected (total lesion load). This kind of combination analysis, when performed longitudinally, can adequately quantify the lesion load after treatment, thereby helping to monitor treatment effects. MRI texture analyses of lesions in MS can also help in specifying the types of MS (clinically isolated syndrome, primary progressive MS, progressive-relapsing MS, relapsing-remitting MS, secondary progressive MS) based on the differences in analyses between the groups. In conclusion, we believe that a robust and reproducible MRI TA protocol based on statistical, autoregressive-model and wavelet-derived texture parameters can provide a new and better clinical method for the early diagnosis and monitoring of quantitative disease progression and of the effectiveness of various treatment protocols in multiple sclerosis.

ACKNOWLEDGMENT

We thank MSc Maija Rossi; MSc Pertti Ryymin, Chief Physicist; and Ms Marjut Keskivinkka from the Medical Imaging Centre, Tampere University Hospital, for their cooperation in this broad project. We thank Ms Arja Hilander and Ms Anu Kuhanen for the measurements at the Tampere University Hospital.

REFERENCES

1. McDonald WI, Compston A, Edan G, et al. Recommended diagnostic criteria for multiple sclerosis: guidelines from the international panel on the diagnosis of multiple sclerosis. Ann Neurol 2001; 50:121–127.
2. Polman CH, Reingold SC, Edan G, et al. Diagnostic criteria for multiple sclerosis: 2005 revisions to the "McDonald criteria." Ann Neurol 2005; 58:840–846.
3. Rovira À, León A. MR in the diagnosis and monitoring of multiple sclerosis: an overview. Eur J Radiol 2008; 67:409–414.
4. Bakshi R, Thompson AJ, Rocca MA, et al. MRI in multiple sclerosis: current status and future prospects. Lancet Neurol 2008; 7:615–625.
5. Bonilha L, Kobayashi E, Castellano G, et al. Texture analysis of hippocampal sclerosis. Epilepsia 2003; 44:1546–1550.
6. Bernasconi A, Antel SB, Collins DL, et al. Texture analysis and morphological processing of magnetic resonance imaging assist detection of focal cortical dysplasia in extra-temporal partial epilepsy. Ann Neurol 2001; 49:770–775.
7. Antel SB, Collins DL, Bernasconi N, et al. Automated detection of focal cortical dysplasia lesions using computational models of their MRI characteristics and texture analysis. NeuroImage 2003; 19:1748–1759.
8. Sankar T, Bernasconi N, Kim H, et al. Temporal lobe epilepsy: differential pattern of damage in temporopolar cortex and white matter. Hum Brain Mapp 2008; 29:931–944.
9. Mathias JM, Tofts PS, Losseff NA. Texture analysis of spinal cord pathology in multiple sclerosis. Magn Reson Med 1999; 42:929–935.

10. Yu O, Mauss Y, Zollner G, et al. Distinct patterns of active and non-active plaques using texture analysis on brain NMR images in multiple sclerosis patients: preliminary results. Magn Reson Imaging 1999; 17:1261–1267.
11. Theocharakis P, Glueer C, Kostopoulos S, et al. Pattern recognition system for the discrimination of multiple sclerosis from cerebral microangiopathy lesions based on texture analysis of magnetic resonance images. Magn Reson Imaging 2009; 27:417–422.
12. Loizou CP, Pattichis CS, Seimenis I, et al. Quantitative analysis of brain white matter lesions in multiple sclerosis subjects: preliminary findings. The 5th International Conference on Information Technology and Applications in Biomedicine (ITAB) 2008;58–61.
13. Zhang J, Tong L, Wang L, et al. Texture analysis of multiple sclerosis: a comparative study. Magn Reson Imaging 2008; 26:1160–1166.
14. Herlidou-Meme S, Constans JM, Carsin B, et al. MRI texture analysis on texture test objects, normal brain and intracranial tumors. Magn Reson Imaging 2003; 21:989–993.
15. Mahmoud-Ghoneim D, Toussaint G, Constans J, et al. Three dimensional texture analysis in MRI: a preliminary evaluation in gliomas. Magn Reson Imaging 2003; 21:983–987.
16. Georgiadis P, Cavouras D, Kalatzis I, et al. Enhancing the discrimination accuracy between metastases, gliomas and meningiomas on brain MRI by volumetric textural features and ensemble pattern recognition methods. Magn Reson Imaging 2009; 27:120–130.
17. Yu O, Parizel N, Pain L, et al. Texture analysis of brain MRI evidences the amygdala activation by nociceptive stimuli under deep anesthesia in the propofol–formalin rat model. Magn Reson Imaging 2007; 25: 144–146.
18. Freeborough PA, Fox NC. MR image texture analysis applied to the diagnosis and tracking of Alzheimer's disease. IEEE Trans Med Imaging 1998; 17:475–479.
19. Torabi M. Discrimination between Alzheimer's disease and control group in MR-images based on texture analysis using artificial neural network. International Conference on Biomedical and Pharmaceutical Engineering (ICBPE) 2006;79–83.
20. Boniatis I, Panayiotakis G, Klironomos G, et al. Texture analysis of spinal cord signal in pre- and post-operative T2-weighted magnetic resonance images of patients with cervical spondylotic myelopathy. IEEE International Workshop on Imaging Systems and Techniques (IST) 2008;353–356.
21. Mayerhoefer ME, Breitenseher M, Amann G, et al. Are signal intensity and homogeneity useful parameters for distinguishing between benign and malignant soft tissue masses on MR images? Objective evaluation by means of texture analysis. Magn Reson Imaging 2008; 26:1316–1322.
22. Szczypinski PM, Strzelecki M, Materka A. Mazda—a software for texture analysis. International Symposium on Information Technology Convergence (ISITC) 2007;245–249.
23. Szczypiński PM, Strzelecki M, Materka A, et al. MaZda—A software package for image texture analysis. Comput Methods Programs Biomed 2009; 94:66–76.
24. Hajek M, Dezortova M, Materka A, et al. Texture analysis for magnetic resonance imaging. Prague: Czech Republic: Med4publishing s.r.o, 2006.
25. Materka A, Strzelecki M, Szczypiń ski P, MaZda manual, 2006. Available at http://www.eletel.p.lodz.pl/mazda/download/mazda_manual.pdf. Accessed on October 5, 2009.
26. Vovk U, Pernus F, Likar B. A review of methods for correction of intensity inhomogeneity in MRI. IEEE Trans Med Imaging 2007; 26:405–421.
27. Nyúl LG, Udupa JK. On standardizing the MR image intensity scale. Magn Res Med 1999; 42:1072–1081.
28. Madabhushi A, Udupa JK. Interplay between intensity standardization and inhomogeneity correction in MR images. IEEE Trans Med Imaging 2005; 24:561–576.
29. Zhuge Y, Udupa JK, Liu J, et al. Image background inhomogeneity correction in MRI via intensity standardization. Comp Med Imaging Graph 2009; 33:7–16.